Design and Optimization of High Frequency Microstrip Patch Antenna using Metamaterial

A Thesis Submitted in Partial Fulfillment For the Degree of

Doctor of Philosophy

In the subject Electronics and Telecommunication

In the Faculty of Engineering

Goa University



By

Satarkar Pandharinath Ramnath

Goa College of Engineering, Farmagudi

Goa University

Sept-2023

Declaration

I, **Satarkar Pandharinath Ramnath** hereby declare that this thesis represents work which has been carried out by me and that it has not been submitted, either in part or full, to any other University or Institution for the award of any research degree.

Place: Taleigao Plateau **Satarkar Pandharinath Ramnath**

Date:

Certificate

I hereby certify that the above Declaration of the candidate, **Satarkar Pandharinath Ramnath** is true and the work was carried out under my supervision.

Dr. Rajesh B. Lohani

Professor, Electronics and Telecommunication Department,

Former Principal, Goa Engineering College (Govt. of Goa),

Farmagudi-Ponda-Goa, 403401.

Acknowledgement

First and foremost I would like to thank the almighty God for his blessings and for providing me the opportunity and strength to complete this research work.

I am extremely grateful to my Guide, Prof. Dr. Rajesh B. Lohani, Prof. Electronics and Telecommunication Engineering department and former Principal of Goa College of Engineering, Farmagudi. His continuous guidance valuable support and patience inspired me to work consistently during my PhD work. His immense knowledge and plentiful experience have encouraged me in all the time of my academic research and daily life.

I extend my heartiest thanks to Principal of Goa college of Engineering Dr.Krupashankar M.S. for his support.

I would like to express my deepest gratitude to the other members of DRC Prof. Dr. R. K. Prasad, Prof. Dr. H.G. Virani, Prof. Dr. Ameeta Sinai Amonkar, Prof. Dr. Nitesh Guinde for their valuable guidance, suggestions and motivation throughout my research work.

I extend my heartiest thanks to Assoc. Prof. Dr. Samarth Borkar, Assoc. Prof. Dr. Shajahan Kutty, Asst. Prof. Chetan Dessai, Asst. Prof. Milind Fernandes, Asst. Prof. Devendra Sutar Asst Prof. John Colaco for their suggestion and support.

I would like to extend my sincere thanks to Prof. Dr. V.N. Shet, Shri Ketan Naik, Prof. Dr. Rajesh Prabhugaonkar, Prof. Dr. Anant Naik for their help and support.

I sincerely thank my organization Goa College of Engineering (Goa University), I would like to extend my sincere thanks to former Director of NIT Prof. Gopal Muguraya, HOD ECE dpt Prof.G R Prashant, Prof.Mallikarjun NIT Goa for their support and valuable guidance.

I also thank my colleague Mr. Jaya Gaitonde, Mrs. Remya Pillai for their support.

I am deeply indebted to former CM State of Goa, President of Ponda Education society and presently Minister for Civil Supplies and Agriculture Govt. of Goa Shri Ravi S. Naik, Principal of PES RSN HSS Mr. V.R. Raiker Principal of PES Ravi S.Naik College of Arts and Science Dr. Vikas Pisurlekar Vice Principal Shri G.P.P Khanolkar for their encouragement and Support.

Finally, I would like to express my gratitude to my parents, my wife my Son Other members of family relatives friends and well-wishers. Without their tremendous understanding and encouragement in the past few years, it would be impossible for me to complete my study.

Abstract

Electromagnetic Metamaterial is an artificial material that is made up of different types of structural designs on dielectric substrates. In this thesis a broad and elite investigation is being carried out by designing and simulating a metamaterial cell comprising a square split ring resonator with a copper wire strip etched on the ground plane to discover its some unusual parameters such as double negativity of cell which are naturally not found in other materials of nature. A course of action of these unit cells in a grouping shapes metamaterial. Also different types of metamaterial cells such as square split ring resonator, circular split ring resonator, circular complimentary split ring resonator, have been designed to resonate at frequency 2.8 GHz,3.5 GHz, 5.8 GHz, 10 GHz,12 GHz, 26 GHz and 28 GHz. Lower frequency cells were designed using FR4 substrate with 4.4 dielectric constant. Higher frequency cells are designed using RT Duroid 5880 substrate with a 2.2, dielectric constants.A square split ring resonator cell have been mathematically modelled and used to design the microstrip patch antenna. These metamaterial cells show exceptionally great applications in the design of microstrip patch antennas by improving their characteristics such as bandwidth, return loss, and gain. The proposed microstrip line feed edge port excited, Co-axial feed rectangular, Circular patch antennas and metamaterial loaded bio-inspired planar microstrip patch antennas such as hibiscus leaf and kaju leaf shape antennas have been designed. These antennas are also designed with metamaterials to resonate at above frequencies. These antennas with different resonance frequencies are useful for various WiMAX applications, 5G applications and other wireless applications. The parameters of conventional antenna and metamaterial loaded antennas were compared. The patch antenna loaded with square split ring resonatorhaving resonance frequency 3.5 GHz used for WiMAX application. The proposed patch antenna have been simulated, fabricated tested analysed, and reported for performance comparison of its parameters.

Introduction/Motivation

With the introduction of the Internet system and cellular technology, the demand for and popularity of mobile terminals (laptops, cell phones, etc.) skyrocketed, propelling the telecommunications industry to new heights. The digital information system and wireless communication technology are playing important role in the development of society. Various wireless services, such as Wi-Fi, Bluetooth, GPS, NFC, 4G, and 5G systems that operate in multiple frequency bands, necessitate the use of portable devices for broadband applications. The rapid increase in the system of wireless communication demands a base station and portable terminal equipped with the best antenna. The portable terminals should satisfy some important characteristics such as miniaturization, system integration, and multiband or broadband operation. Due to some important features mentioned in section 5.2, microstrip antennas are well suitable for the application of wireless communication.

Although research on 'synthetic' materials for microwave applications began in 1948.Metamaterials have only recently emerged as a breakthrough in the realm of electromagnetic [1],[2]. Metamaterials have piqued people's curiosity because of their unusual responses to electromagnetic radiation. These materials are created by structuring precise metallic inclusions onto a host dielectric substrate. The structural design of metamaterial cells is responsible for the properties of the cell and not the chemical composition of their constituents[3]. The metamaterial concept was presented by Victor Veselago in 1968 who stated that the Poynting vector of a monochromatic plane wave is anti-parallel to its phase velocity in a medium having dielectric permittivity (ϵ) and magnetic permeability (μ), to be negative at the same time. He named these materials "Left-Handed Materials" (LHM). In 1999, J.B. Pendry proposed the artificial negative permeability medium by an arrangement of an array of small metallic structures called split-ring resonators (SRR) [4],[5],[6].Rectangular rings having equal sides are called square split-ring resonators (SSRR)[7]. The cells which are having electric per-

mittivity and magnetic permeability close to zero, But less than zero are called zero Index metamaterials[8],[9]. It is made up of a periodic array of metallic resonant elements. The wavelength is very much higher than the lattice constant of metamaterial cell. Surface waves propagate within the substrate and are scattered at bends and surface discontinuities, such as dielectric and ground plane truncation, degrading the antenna pattern and polarisation characteristics [10]. Using metamaterials, surface waves can be eliminated while maintaining large bandwidths. If the impedance of the antenna does not match the impedance of the transmission line, the signals will be reflected, resulting in high return loss and poor communication. The antenna impedance should be matched with the transmission line impedance to avoid the problem of return loss [11], [12],[13]. A patch antenna is designed on a a dielectric substrate such as RT duroid 5880 with dielectric constant 2.2. The thickness of this dielectric substrate is 0.5 mm or 0.25 mm, so that it is lightweight and easy to design and fabricate. It can be designed in different ways on dielectric substrate. If we use a substrate of higher thickness efficiency can be increased, however, as the height increases, surface waves are introduced which usually are not desirable because they extract power from the total available for direct radiation (space waves). Surface waves are eliminated using metamaterials. To increase the bandwidth of patch antenna arrays can be used. Bandwidth also can be increased by loading metamaterial on a microstrip patch antenna.[14],[15],[16]. The proposed double negative and mu negative metamaterial cells are designed and tested using MATLAB software. Metamaterial cells are mathematically modelled [17],[18]. Also parameters of mu negative metamaterial cell are extracted using full-wave simulator HFSS. Data files (.csv files) of S_{11} and S_{21} are then exported and applied MATLAB script to obtain the curve of complex permeability [19], [20]. The authors have designed and simulated an edge port-fed rectangular patch antenna and circular patch antenna for a 5G application and WiMAX application using FEKO software.It is a wireless technology based on IEEE 802.16 standard that provides fast data

over a widespread area. The WiMAX stands for Worldwide Interoperability for Microwave Access, and it is a point to multipoint wireless networking technology. It works in three layers, physical layer, MAC layer, and convergence layer. RT duroid 5880 and FR4 substrates are used for designing metamaterial based antenna for WiMAX and 5G application respectively, The metamaterial-based rectangular microstrip patch antenna (RMPA) is simulated and bandwidth, return loss, gain and VSWR are measured.Impedance matching is noted on smith chart. Optimization is done by using FEKO software [21],[22] ,[23].For further advances and suitability, for the construction of antennas, the researchers concentrated on using bio-inspired geometrical shapes. The most important one is bioinspired plant geometries, which employ shape of plant parts such as leaves, fruits, and flowers to create antennas for various frequencies. The study of microstrip antennas based on models inspired by leaves (leaf-shaped antennas) has piqued researchers' curiosity due to promising outcomes. The hibiscus leaf and kaju leaf shape patch antennas are designed and simulated [24], [25], [26]. These antennas are loaded with metamaterials for improvement of their performance. The lattice constant of metamaterial should be very much smaller compared to the wavelength A conventional antenna and a proposed novel edge port fed bio-inspired microstrip patch antenna (BMPA) with resonance frequency 5.8 GHz and a ground plane of the substrate are loaded with square split-ring resonators are simulated, analyzed and comparison of parameters such as bandwidth, return loss, gain and VSWR is presented [27], [28],[29]. This patch antenna is designed on FR-4 substrate with permittivity value equal to 4.4 and thickness equal to 1.6 mm. FR-4 material is cheaper and easily available. Surface wave propagation is decreased by a metamaterial-loaded substrate, which improves antenna performance. This patch antenna with improved parameters can be used for WiMAX applications.The bandwidth required for the band with a center frequency of 5.8 GHz is 300 MHz [30],[31]. And the proposed patch antenna finds its suitability for this application with a bandwidth higher than required.

Contents

1 Literature Survey with Gap Analysis **1**

1.1 Application of Metamaterials for the Microwave Antenna Realisations 1

1.2 Survey on Microstrip Patch Antenna using Metamaterial. 2

1.3 Impedance and Gain improvement of Microstrip Antenna using Metamaterials. 3

1.4 Microstrip Patch Antenna loaded with Complementary SRR . . . 4

1.5 MSA-T: Enabling affordable, All-Electronic Beam Steering satcom user terminals 5

1.6 High Gain Patch Antenna realized by using Negative Permeability Electromagnetic Metamaterials 5

1.7 Metamaterials: Fundamentals and Applications in the Microwave and Optical regimes 6

1.8 Nature Inspired Sunflower Shaped Microstrip Antenna for Wideband Performance 7

1.9 Gap analysis 7

2 Objectives, Methodology and Novelty / Main contributions of research **12**

2.1 Objectives 12

2.2 Methodology 12

2.3 Novelty / Main contributions of research 14

3 Introduction to metamaterials **15**

3.1 History of Metamaterials 15

3.2 Fundamental theory and background of metamaterials 16

3.3 Analysis of metamaterials using transmission line 21

3.3.1 Retrieval methods of parameters of metamaterials 24

4 Classification of metamaterials **26**

4.1 Electromagnetic Metamaterials 27

4.1.1 Double negative metamaterials 28

4.1.2 Single negative metamaterials 31

4.1.3 Electromagnetic Bandgap Metamaterials 31

4.1.4 Bi-isotropic and bianisotropic metamaterials 32

4.1.5 Chiral metamaterials 33

4.1.6 Terahertz Metamaterials 33

4.1.7 Photonic Metamaterials 34

4.1.8 Tunable Metamaterials 34

4.1.9 Frequency Selective Surface (FSS) based Metamaterials . 34

5 Theory and design of microstrip patch antenna **36**

5.1 Introduction 36

5.2 Advantages and Disadvantages of Microstrip Patch Antenna . . . 39

5.3 Basic principle of operation 40

5.4 Resonant Frequency 41

5.5 Feed technique 42

5.5.1 Coaxial Probe Feed 42

5.5.2 Microstrip-line feed 43

5.5.3 Proximity-coupled Microstrip-line feed 44

5.5.4 Aperture-coupled feed 45

5.6 Method of Analysis 46

5.7 Antenna parameters 48

6 Design and development of metamaterial based microstrip patch antenna 51

6.1 Design and development of Metamaterial based patch antenna for 5G application 51

6.1.1 Metamaterials, Double negative or Left-Handed metamaterials 52

6.1.2 Design of square split ring resonator cell 54

6.1.3 Parameters of SSRR Metamaterial Cell 54

6.1.4 Method to find parameters of metamaterial cell of complex Structure 55

6.1.5 Edge Port fed Rectangular Microstrip patch Antenna (RMPA) Design on Substrate without Metamaterial 56

6.1.6 Application of Metamaterial in designing edge port fed rectangular microstrip patch antenna. 58

6.1.7 Application of metamaterial in designing edge port fed Circular Microstrip Patch Antenna (CMPA). 61

6.1.8 Simulation results 66

6.2 Patch antenna design using complementary split ring resonator . 68

6.2.1 Metamaterials 68

6.2.2 Double negative metamaterial 69

6.2.3 Application of metamaterials in designing circular patch antenna 70

6.2.4 Circular patch antenna design on circular substrate without Metamaterial 70

6.2.5 Circular patch antenna design with Metamaterials 72

6.2.6 Simulation Results 73

6.3 Design and development of coaxial feed circular patch antenna on a metamaterial substrate 74
6.3.1 μ (mu)negative metamaterial structures 74
6.3.2 Circular patch antenna design without Metamaterial and with coaxial feed at resonance frequency 10GHz (used in Wireless communication and tested on software FEKO . . 75
6.3.3 Patch antenna design with Metamaterial and with coaxial feed at resonance frequency 10GHz (Tested on software FEKO) 76
6.3.4 Simulation Results 77
6.4 Design and Extraction of Parameters of Metamaterial cell and its Application to enhance the performance of Patch Antenna 78
6.4.1 Double negative metamaterial 78
6.4.2 Design of SSRR (Double negative metamaterial cell . . . 79
6.4.3 Parameters of SSRR 80
6.4.4 Single negative Metamaterial cell 81
6.4.5 Rectangular microstrip patch antenna (RMPA) design on the substrate without Metamaterial 82
6.4.6 Parameters of RMPA 83
6.4.7 Rectangular microstrip patch antenna (RMPA) design on a substrate with metamaterial 85
6.4.8 Parameters of RMPA with metamaterial substrate 86
6.4.9 Simulation Results 88
6.5 Capacitive Coupled Circular Patch Antenna for band suppression and Gain improvement by loading Circular Slot on Coupling . . . 88
6.5.1 CCCCPA design on a rectangular substrate without slot on coupling at resonance frequency 6 GHz (used in Wireless communication and tested on software FEKO 89

6.5.2 Parameters of CCCCPA 90
6.5.3 CCCPA design on a Rectangular substrate with slot on Coupling at Resonance frequency 6 GHz 91
6.5.4 Simulation Results 93
6.6 Characterization of patch Antenna with Rectangular slot for 5G Application 93
6.6.1 Design of antenna 94
6.6.2 Parameters of RMPA without slot 95
6.6.3 Rectangular microstrip patch antenna.(RMPA) design with rectangular slot at 26 GHz resonating frequency 95
6.6.4 Parameters of RMPA with slot 96
6.6.5 Simulation Results 97

7 Design of Microstrip Patch Antenna using Mathematical Modeled Metamaterial Cell 98

7.1 Characterization of microstrip patch antenna using mathematically modelled metamaterial cell 98
7.1.1 Double negative or left-handed metamaterials 99
7.1.2 Design of mu negative metamaterial cell on RT/Duroid 5880 substrate 99
7.1.3 Method to find Parameters of SSRR Metamaterial 101
7.1.4 RMPA design on the substrate without metamaterial at 26 GHz resonance frequency 102
7.1.5 Rectangular microstrip patch antenna (RMPA) design with a modeled metamaterial at 26 GHz resonating frequency . 104
7.1.6 Simulation Results 107
7.2 Mathematical Modelling of Metamaterial Cell and its Application in Design of Microstrip Patch Antenna 108

7.2.1 Mathematical modelling of mu negative metamaterial cells with two rings and structured on Rogers RT/Duroid 5880 108
7.2.2 Method to find Parameters of SSRR Metamaterial 109
7.2.3 Application of modelled metamaterial in designing Rectangular microstrip patch antenna. (RMPA) 111
7.2.4 Rectangular Microstrip Patch Antenna (RMPA) design with Metamaterial at 28 GHz Resonating Frequency . . . 113
7.2.5 Simulation results 116
7.3 Mathematical Modelling of Metamaterial Cell on Various Dielectric Substrates and comparison with Numerical simulations . . . 117
7.3.1 Introduction 117
7.3.2 Design of mu negative metamaterial Cell on RT/Duroid 5880 substrate 117
7.3.3 Method to find parameters of SSRR metamaterial cell . . 118
7.3.4 Simulated results 118

8 Design and development of metamaterial based bioinspired patch antenna 122

8.1 Introduction 122
8.2 Circular Microstrip Patch Antenna 124
8.2.1 Circular microstrip patch antenna(CMPA) 124
8.3 Metamaterial Design 126
8.3.1 Double negative metamaterials 126
8.3.2 Design of the SSRR Cell 126
8.3.3 Parameters of the SSRR Metamaterial Cell 126
8.3.4 Single negative metamaterial cell 128
8.4 Hibiscus leaf shape Microstrip Patch Antenna 128

8.4.1 Design of Hibiscus leaf shape Microstrip patch Antenna (HLMPA) for WIMAX and other Wireless Applications . 128
8.4.2 Different parameters of HLMPA 129
8.4.3 Design of metamaterial-loaded HLMPA (MHLMPA) for WIMAX and other wireless applications 132
8.4.4 Different parameters of MHLMPA 133
8.5 Kaju leaf shape Microstrip Patch Antenna 135
8.5.1 Design of geometrical structure of Kaju leaf shape Microstrip Patch Antenna 135
8.5.2 Different parameters of KLMPA 136
8.5.3 Design of metamaterial-loaded KLMPA (MKLMPA) for wireless application 137
8.5.4 Different parameters of MKLMPA 138
8.6 Results and Discussion 140

9 Design simulation and fabrication of metamaterial based rectangular microstrip patch antenna 142

9.1 Introduction 142
9.2 Lefthanded and Mu negative Metamaterial Design 143
9.2.1 Double Negative Metamaterials 143
9.2.2 Design of SSRR Cell 143
9.2.3 Parameters of SSRR Metamaterial Cell 143
9.2.4 Single Negative Metamaterial cell 145
9.3 Metamaterial based Rectangular Microstrip Patch Antenna . . . 145
9.3.1 RMPA Design on Substrate without Metamaterial 146
9.3.2 Rectangular Microstrip Patch Antenna (RMPA) Design on Metamaterial Substrate 147

9.4 Fabrication and experimental parameters of metamaterial-based rectangular microstrip patch antenna 150
9.4.1 Experimental Parameters of Metamaterial loaded Rectangular Microstrip Patch Antenna.(RMPA) from Vector Network Analyser(VNA) 150
9.5 Results and Discussion 153

10 Conclusions And Future Scope **155**
10.1 Conclusions 155
10.2 Future Scope 157

REFERENCES **158**

PUBLICATIONS **171**

List of Figures

3.1 Lattice constant d of metamaterial cell and wavelength relation . 16
3.2 Schematic structures 17
3.3 Wire structure 19
3.4 Metamaterial cells 19
3.5 Ideal homogeneous incremented line model for composite Right/Left-handed metamaterial. 21
3.6 Equivalent circuit of a periodic RH-TL 23
3.7 Schematic of the propagation mechanism. 24

4.1 Material classification. 26
4.2 Scatering of wave incident on DPS-DNG interface 30

5.1 Antenna as transitional device 36
5.2 structure of a microstrip patch antenna 37
5.3 Different shapes of microstrip patch antenna 38
5.4 Coaxial Probe Feed 43
5.5 Microstrip-Line Feed 44
5.6 Proximity-coupled Microstrip-line feed 44
5.7 Aperture-Coupled Feed 45
5.8 Microstrip line field 47
5.9 Different shapes of microstrip patch antenna 48

6.1 Square split-ring resonators (SSRR) 53
6.2 Equivalent circuit for SSRR 53

6.3 S_{11} and S_{21} of SSRR cell. 54
6.4 Real and imaginary values of μ of SSRR cell 54
6.5 Design of edge-fed RMPA without metamaterial 56
6.6 Reflection coefficient v/s frequency of RMPA without metamaterials 57
6.7 Smith chart showing impedance matching at 26GHz. 58
6.8 3D view of far-field of an RMPA without metamaterials at 26 GHZ 58
6.9 Design of metamaterial-loaded RMPA. 59
6.10 Reflection coefficient v/s frequency of metamaterial loaded RMPA 59
6.11 Smith chart. 60
6.12 3D view of the far-field of RMPA with metamaterials at 26 GHz resonance frequency 60
6.13 3D view of far field of RMPA with metamaterials at 25 GHz . . 60
6.14 3D view of far field of RMPA with metamaterials at 27 GHz . . . 60
6.15 Design of CMPA. 63
6.16 Reflection coefficient v/s frequency graph of CMPA without metamaterial 63
6.17 Smith chart showing impedance matching of CMPA. 63
6.18 VSWR v/s Frequency of CMPA 63
6.19 3D view of the far-field of a CMPA without metamaterials at 25 GHz resonance frequency 63
6.20 3D view of the far-field of a CMPA at 26 GHz resonance frequency 63
6.21 CMPA with metamaterial 64
6.22 Reflection coefficient v/s Frequency of CMPA with metamaterial 64
6.23 Smith chart showing impedance matching of CMPA with metamaterial 65
6.24 VSWR v/s Frequency of CMPA with metamaterial 65
6.25 3D view of the far-field of a CMPA at 26GHz resonance frequency 65
6.26 3D view of the far-field of a CMPA at 25 GHz resonance frequency 65

6.27 Directivity of antenna. 66
6.28 3D view of theta gain of of a CMPA at 26 GHz frequency 66
6.29 Complementary split ring resonators (CSRR) 69
6.30 coaxial feed circular patch antenna on circular substrate 71
6.31 Reflection coefficient v/s frequency of CPA without metamaterial 71
6.32 CPA on circular substrate with Metamaterial 73
6.33 Reflection coefficient v/s frequency of CPA with metamaterials . 73
6.34 Circular patch antenna without Metamaterial 75
6.35 Circular antenna parameters) 76
6.36 Parameters of metamaterial loaded circular antenna 77
6.37 Square split-ring resonators (SSRR) with a metal strip 79
6.38 Parameters of metamaterial cell. 80
6.39 refractive index of SSRR 81
6.40 Real and imaginary values of Mu of SSRR 82
6.41 Microstrip patch antenna 83
6.42 Reflection coefficint V/S Frequency graph 84
6.43 smith chart showing impedance matching at 2.8GHz 84
6.44 3D view of far-field of patch antenna without metamaterial at 2.8GHz 85
6.45 RMPA with six cells of SSRR on its ground plane 86
6.46 Reflection coefficient v/s frequency of RMPA with metamaterial 86
6.47 3D view of the far-field patch antenna with metamaterial loaded and at 2.8GHz 87
6.48 Graph of VSWR v/s frequency of metamaterial loaded RMPA. . 87
6.49 CCCCPA on rectangular substrate without slot 90
6.50 Freq v/s Reflection coefficient and gain (without slot) 90
6.51 CCCCPA design on a rectangular substrate with a slot on coupling 91
6.52 Freq v/s Reflection coefficient and Gain of CCCCPA(with semi-circular slot) 92

6.53 3D view of far field of CCCCPA 6 GHz 92
6.54 Equivalent circuit model of the proposed CCCCPA with slot . . . 92
6.55 Edge fed RMPA on RT duroid substrate 94
6.56 Parameters of antenna 95
6.57 RMPA with rectangular slot on patch. 96
6.58 Parameters of antenna 96

7.1 square split ring resonator 100
7.2 Graph of k v/s K(k) and K(k') 101
7.3 SSRR parameters 102
7.4 Design of edge-fed RMPA without metamaterial. 103
7.5 Reflection coefficient v/s freq of RMPA without metamaterials . 104
7.6 3D far-field radiating pattern at 26 GHz 104
7.7 Design of edge-fed RMPA with metamaterial. 105
7.8 Reflection coefficient v/s freq of RMPA with metamaterials . . . 106
7.9 3D view of the far-field of a RMPA at 26GHz resonance frequency 106
7.10 3D view of the far-field of a RMPA at 25GHz 106
7.11 Impedance matching of RMPA at 26GHz 106
7.12 VSWR of RMPA with metamaterial 106
7.13 Square split-ring resonators (SSRR) metamaterial cell 109
7.14 Metamaterial cell simulation in the waveguide 109
7.15 SSRR parameters 110
7.16 Design of edge fed RMPA without metamaterial 111
7.17 Reflection coefficient v/s freq of RMPA without metamaterials . 112
7.18 Far field radiating pattern and total gain at 28 GHz 112
7.19 smith chart with impedance matching 112
7.20 3D view of far field and surface current 113
7.21 Design of edge fed RMPA with metamaterial 113

7.22 Reflection coefficient v/s freq.ofRMPA with metamaterial 114
7.23 Far field radiation pattern of antenna with metamaterial 115
7.24 3D far field radiation pattern 115
7.25 VSWR 115
7.26 impedance matchingat 28 GHz 115
7.27 Square split-ring resonators (SSRR) metamaterial 118
7.28 SSRR parameters 119
7.29 SSRR parameters 119
7.30 SSRR parameters 120

8.1 Circular MPA 125
8.2 Reflection coefficient v/s frequency of CMPA 125
8.3 Hibiscus and Kaju leaves 125
8.4 split-ring resonators (SSRR) 126
8.5 S_{11} and S_{21} of SSRR cell 127
8.6 Permittivity and permeability of SSRR 127
8.7 Refractive index and impedance of double negative SSRR 127
8.8 Mu of SSRR at frequency 5.8 GHz. 127
8.9 Hibiscus leaf microstrip patch antenna 129
8.10 Hibiscus leaf antenna parameters-1 130
8.11 Hibiscus leaf antenna parameters-2 131
8.12 Hibiscus leaf antenna parameters-3 131
8.13 3D view of the far-field of HLMPA. 132
8.14 Metamaterial loaded HLMPA(MHLMP) 132
8.15 MHLMPA antenna parameters 134
8.16 MHLMPA antenna parameters 134
8.17 KLMPA 136
8.18 KLMPA antenna parameters-1 136

8.19 KLMPA antenna parameters-2 137
8.20 Metamaterial loaded Kaju leaf microstrip patch antenna 138
8.21 Reflection coefficient v/s frequency of KHLMPA 139
8.22 MKHLMPA antenna parameters -1 139
8.23 MKHLMPA antenna parameters -2 140
8.24 Total surface current distribution at 5.8 GHz. 140

9.1 Square split ring resonators with strip (SSRR) 143
9.2 Parameters of antenna 144
9.3 Refractive index and impedance of SSRR 144
9.4 mu of SSRR at frequency 3.5 GHz 145
9.5 RMPA without metamaterial substrate 146
9.6 Reflection coefficient v/s frequency of RMPA without metamaterial 147
9.7 Gain of patch antenna without metamaterial 147
9.8 Smith chart showing impedance matching of RMPA at 3.5 GHz . 147
9.9 SSRR cells on ground plane of RMPA. 148
9.10 Reflection coefficient v/s frequency of RMPA with metamaterial 149
9.11 Smith chart showing impedance matching of RMPA with metamaterial at 3.5 GHz. 149
9.12 Parameters of antenna 149
9.13 Far field E-plane radiation patterns for a metamaterial loaded RMPA. 150
9.14 Reflection coefficient v/s frequency of RMPA with metamaterial obtained from VNA 151
9.15 Reflection coefficient v/s frequency of metamaterial loaded RMPA generated using .csv file obtained from VNA 151
9.16 Smith chart showing impedance matching obtained from VNA . . 152

9.17 Fabricated top and bottom view of RMPA 152
9.18 Figures used for fabrication .gbr file 153

List of Tables

5.1 Advantages and disadvantages of feeding methods 46

6.1 Design of RMPA without metamaterial 58
6.2 Design of Edge port fed RMPA with metamaterial 59
6.3 Design of Edge port fed CMPA without metamaterial 62
6.4 Design of Edge port fed CMPA with metamaterial 64
6.5 Different parameters of RMPA. 66
6.6 Different parameters of CMPA. 67
6.7 Different parameters of circular patch antenna 77
6.8 Different parameters of SSRR. 81
6.9 Design of RMPA without metamaterial 83
6.10 Design of RMPA with metamaterial 85
6.11 Different parameters of RMPA. 88
6.12 Dimensions of RMPA 94
6.13 Dimensions of RMPA with slot 96

7.1 Comparison of calculated and simulated resonance frequency of SSRR with Rogers RT/Duroid dielectric materials 102
7.2 Design of RMPA without metamaterial 103
7.3 Design of RMPA with metamaterial 105
7.4 Different parameters of RMPA. 108
7.5 Comparison of calculated and simulated resonance frequencies of SSRR with Rogers RT/Duroid dielectric materials 110

7.6 Design of RMPA without metamaterial 111
7.7 Design of RMPA with metamaterial 114
7.8 Different parameters of RMPA. 116
7.9 Comparison of calculated and simulated resonance frequencies of SSRR with various dielectric materials 121

8.1 Design of HLMPA 129
8.2 Different parameters of HLMPA. 132
8.3 Design of MHLMPA 133
8.4 Different parameters of MHLMPA. 135
8.5 Design of KLMPA 135
8.6 Different parameters of KLMPA. 137
8.7 Design of MKLMPA 138
8.8 Different parameters of MKLMPA. 140
8.9 The comparison of the parameters of HLMPA(HL), MHLMPAM(MH), KLMPA(KL), and MKLMPA(MK) 141

9.1 Design of RMPA 146
9.2 Design of RMPA with metamaterial 148
9.3 Different parameters of RMPA. 154

Chapter 1

Literature Survey with Gap Analysis

1.1 Application of Metamaterials for the Microwave Antenna Realisations

In the first decade of the twenty-first century, scientists have become very interested in artificial structures whose electromagnetic (EM) characteristics depend on the geometry of the structure units rather than the chemical composition. These electromagnetic structures, also known as metamaterials (MTM), exhibit a wide range of incredibly strange properties, such as extremely high effective permittivity and permeability values, phase and group velocity antiparallelism, etc. It has been proposed to use left handed metamaterials (LHMTM), which concurrently have negative permittivity and permeability as well as a negative refractive index, to make a variety of microwave components with cutting-edge features and compact sizes. Numerous MTM applications have been developed. They include conical-beam radiators, resonant antennas, and new leacky wave antenna with full-space scanning fan/pencil-beam. conical-beam radiators, As one of the potential LHMTM-based applications, graded refractive index profile (GRINMTM) with the composite right left handed (RH/LH) structures have been studied intensively both experimentally and theoretically in recent years [32].

1.2 Survey on Microstrip Patch Antenna using Metamaterial.

There are various ways to increase the bandwidth of a microstrip patch. the usage of numerous resonators placed in the same plane, multilayer designs with numerous resonators stacked vertically, impedance matching networks, and lowering the Q factor of the patch by increasing substrate height and lowering dielectric constant are few examples. The use of multi-resonator systems has drawbacks, including larger area requirements and variability in radiation patterns. Wide band impedance matching network applications present a problem due to the larger substrate area required for the matching network's inclusion. The simplest direct technique to increase the bandwidth of the microstrip element is to employ a thick, low dielectric constant substrate. This always leads to unacceptably high feed inductance, surface wave generation, or spurious feed radiation. Therefore, picking a substrate with a suitable thickness is crucial, and expanding the methods will broaden the bandwidth. The most well-liked and efficient of them are: a) covering the surface of the printed element with slots of the right shape. b) the edge of the microstrip patch is texturized with small or large slits. However, these methods also have the disadvantages, which leads to the formation of complex structures.The study of metamaterials has recently attracted more theoretical and experimental interest. Metamaterials (MTM) are manufactured materials with characteristics that may not exist in nature. In the latter half of the 1960s, metamaterial was first developed.The fundamental characteristics of common materials found in nature, also referred to as Double Positive (DPS) materials, are positive permeability and permittivity. Due to the property of negative mu and epsilon, metamaterials are referred to as Double Negative (DNG) materials. V. G. Veselago observed that the plane wave's Poynting vector is antiparallel to the direction of the phase velocity, which is different from how plane

waves generally propagate in natural media. He used the term "left-handed" to describe a chemical while keeping in mind that it is a synonym for "substance with negative group velocity. Even though metamaterial does not exist in nature, fascinating phenomena for these substances, such as Cherenkov radiation, the reversal of the Snell Law, and Doppler effects, were theoretically predicted. Metamaterials are also referred to as negative index materials (NIM) because of their negative index of refraction. Given that the left-hand rule connects the electric field (E), magnetic field (H), and propagation vector (K), a composite medium made of conducting, non-magnetic materials can produce a left-handed frequency band. In the metamaterial structure, negative permeability is produced by split ring resonators (SRRs), whilst negative permittivity is produced via thin wire components Each of the two concentric rings that make up the distinctive pattern known as SRR has a split. The structure is referred to as a resonator because it exhibits a specific magnetic resonance at a particular frequency. Split ring resonators have the capacity to generate an effective negative permeability across a certain frequency range[33].

1.3 Impedance and Gain improvement of Microstrip Antenna using Metamaterials.

Typically, a conducting ground plane is used to support a substrate-mounted conventional microstrip patch antenna. In the investigation, a rectangular patch antenna mounted on the substrate has a planar left-handed material pattern designed to improve its horizontal radiation and increase its working bandwidth through coupling with the conducting ground that is backed to the substrate and has a different pattern. The suggested small metamaterial antenna has a permittivity of 2.2 and is printed on an F4BM-2 substrate with a thickness of 0.8 mm. To achieve 50- characteristic impedance from 3.85 to 16.15 GHz, the microstrip feedline's width is fixed at 2.40 mm. Four isosceles triangles in the upper layer

are connected at their apexes by a square frame, and four narrow metal strips are radially attached to the outer frame in the unit cell from the connected portion. On the lower layer are square metal patches with regular gaps.One parameter at a time is changed while the other ones are fixed to investigate the suggested antenna. To establish the ideal settings and completely comprehend how the antenna's construction behaves, the antenna was analyzed using Ansoft simulation software high-frequency structure simulator (HFSS)[34].

1.4 Microstrip Patch Antenna loaded with Complementary SRR

Metamaterial based microstrip patch antennas loaded with complementary split-ring resonators (CSRRs) is designed and characteristics are reported. The ground plane of the suggested antenna uses CSRRs to modify the substrate's effective medium properties. Experimental findings supported the simulation results. The experimental results show that the CSRR loaded patch antenna reduces in size while maintaining the same bandwidth. On a glass epoxy FR-4 substrate, the radiation characteristics of a circular patch antenna with a U-slot are measured, and they are contrasted with those of a conventional circular patch antenna made under the same condition. In addition to having a significantly wider bandwidth, the updated antenna resonates at two separate frequencies. The return loss and VSWR are measured for a simple circular patch antenna and a circular patch antenna with a U-shaped slot.The designed antennas have been described.The radiation pattern, VSWR, transmission coefficient, and reflection coefficient are all presented. All of the designs have the same 1.6 mm substrate thickness, 4.4 dielectric constant, and 0.02 loss tangent [35].

1.5 MSA-T: Enabling affordable, All-Electronic Beam Steering satcom user terminals

A new type of antenna technology called Metamaterial Surface Antenna Technology (MSA-T) was created by Intellectual Ventures. It allows a radio signal to be directed in a specific direction without the need for expensive parts or moving pieces. New devices are made for people to use with advanced satellites. These satellites will help people who work in transportation like planes, ships, and cars. This will be the first time we use MSA-T technology. It can be used in places where it's important to have simple installation. The MSA-T's antenna is made similarly to printed circuit boards and can be made very easily. This is different from the large, heavy and difficult to make antennas we use presently. MSA-T allows for cheaper and lighter user devices that are only a few kilograms and can be as thin as 2-3 centimetres. To give the customer enough internet speed, MSA-T can use additional modules that send and receive information. MSA-T versions can make antenna pieces that bend to match the shape of an object, such as the body of an airplane[36].

1.6 High Gain Patch Antenna realized by using Negative Permeability Electromagnetic Metamaterials

It is discussed how to make a high gain patch antenna that operates at 5-5.5 GHz using electromagnetic metamaterials with negative permeability. The suggested metamaterial cell is investigated and analysed using numerical methods. We noticed that the reference microstrip antenna's working frequency band overlaps with the negative permeability provided by the suggested metamaterial construction from 5 GHz to 5.5 GHz. Periodically placing a few of the suggested metamaterial cells on the substrate surrounding the patch antenna increases the gain of the antenna at the operational frequency by around 2.5 dBi, but the reference

antenna's operating bandwidth is unaffected[37].

1.7 Metamaterials: Fundamentals and Applications in the Microwave and Optical regimes

Metamaterials are artificial structures of conducting materials such as copper on dielectric substrate and have peculiar electromagnetic properties, from radio and microwave frequencies up to optical frequencies. Although the field of metamaterials, which has its roots in the history of artificial dielectrics, is only a little over ten years old today, it has already sparked a great deal of interest among scientists all over the world. Classical electromagnetism suddenly assumed a new and fascinating perspective, demonstrating that there are fascinating phenomena still undiscovered and applications for them still to be developed. All of this richness is specifically connected to the idea of the macroscale constitutive characteristics, including permittivity and permeability. What would be conceivable if we could create materials whose constitutive parameters could be customised? When we consider the fact that material parameters can typically be anisotropic tensors that can also be spatially inhomogeneous (changing from point to point), the variety of these possibilities becomes more apparent. Additionally, they are capable of achieving values that were previously unthinkable and even combining a material's magnetic and electric responses. some of the most eminent experts in the area describe how to design metamaterials with exotic new functions, how to physically construct them, and how to use them in microwave and optical applications[38].

1.8 Nature Inspired Sunflower Shaped Microstrip Antenna for Wideband Performance

Analysis and synthesis of a high frequency nature-inspired broadband micro-strip patch antenna is designed and simulated. It is based on the sunflower structure with particular type of the spirals which are frequently found in nature. The reason behind using sunflower structure is to explore the properties of wideband performance, uniform and stable distribution of electromagnetic energy obtained in natural structure, successfully translated to antenna technology and to provide a frame work for solving the optimization problems related to antenna application in satellite communication A mathematical concept that is capable of defining many complex shapes found in nature is the key of this new design. The proposed antenna has simple geometric structure so it satisfies the requirements of satellite communication in form of the reduced lobe level and stable radiation pattern. The design is using computer simulation technology microwave Studio and the geometry of proposed antenna offers impedance bandwidth of more than 5.44 GHz (12 GHz to 17.44 GHz) in the Ku Band. A simple construction, broad bandwidth, adjustable and moderate gain are some of the key features of this design. Sunflower based micro strip patch antenna structure shows a non-uniformly spaced, direct radiating array which is responsible for reducing complexity and cost compared with conventional antenna [39].

1.9 Gap analysis

• Design and development of left handed and mu negative split ring resonator and complimentary split ring resonator metamaterial cells with circular and square shape.

• Design and development of coaxial feed and microstrip line feed metamaterial loaded patch antenna for enhancing the bandwidth of antenna.

• Design and development of metamaterial loaded various types of patch antenna for high gain application.

• High gain-bandwidth product caters to long haul 5G communication.

• To observe high gain in rectangular slot based microstrip patch antenna.

• Mathematical modeling of metamaterial cell to resonate at 26 GHz and 28 GHz.

• Design and simulation of multiband bioinspired conventional and metamaterial loaded microstrip patch antenna design with peculiar hibiscus leaf shape and kaju leaf shape, comparison of their parameters.

• Application of different types of metamaterial cells for miniaturising patch antenna.

The fourth generation (4G) antennas are under continuous development stage for achieving multiple frequency bands with compact design.In the recent years high data rate in 4G and 5G communication technology has attracted many personal wireless application for industrial and scientific area. To support channel capacity in the operating frequency of 4G and 5G electrically small antennas are needed in the customer premises equipment and handheld receivers.To meet the requirements various microwave techniques like metamaterial loaded antennas,bioinspired metamaterial loaded antennas are reported.

Metamaterial cell square split ring resonator (SSRR) consisting of two ring is designed on RT Duroid 5880 substrate with a permittivity value equal to 2.2 and thickness equal to 0.5 mm.The resonating frequency of cell is 26 GHz. The negative mu appears in the frequencies between 24.8 GHz to 28 GHz. Edge-fed rectangular microstrip patch antenna (RMPA) and edge fed circular patch antenna with metamaterial cells loaded on the ground plane of the antenna.The antennas resonates at 26 GHz frequency which is used for 5G communication.The bandwidth and gain of both the antennas are increased compare to conventional antennas.

Complementary circular split ring resonator is designed to resonate at 12 GHZ is loaded on ground plane of Circular patch antenna which considerably increases

its bandwidth. The left handed metamaterial cell is designed with SSRR and copper strip of width 0.6 mm on ground plane of FR-4 substrate with a permittivity value equal to 4.4 and thickness equal to 1.6 mm. The dimensions of cell are 8 mm by 8 mm. The cell resonates at 2.8 GHz. The real part of permittivity and permeability of SSRR are negative. The negative permittivity and permeability exist between 2.6 GHz to 3.2 GHz frequency.The mu negative cell is designed with resonant frequency equal to 2.8 GHz. The rectangular microstrip patch antenna is designed loading mu negative metamaterial cells on ground plane of patch antenna.The antenna is simulated and the bandwidth and gain reporded are equal to 113 MHz and 3.5 dBi. The single negative metamaterial cell is mathematically modelled and simulated, It consists of a square split ring resonator with two rings. The Rogers RT/Duroid substrate with dielectric constant 2.2 is used in this design. The cell is designed to resonate at 26 GHz frequency.The calculated resonance frequency is almost equal to ssimulated resonance frequency. For a specific range of frequencies that is 24.5 GHz to 28 GHz this metamaterial cell depicts negative values of permeability.A square split ring resonator cell is mathematically modeled, These metamaterial cells are used to design the microstrip patch antenna.The bandwidth and gain of antenna are equal to 1.93 and 9dBi respectively.The bandwidth and gain are higher compare to convantional antenna. The single negative metamaterial cell is mathematically modelled and simulated, It consists of a square split ring resonator with two rings having slots at 180 degrees to each other. The Rogers RT/Duroid substrate with dielectric constant 2.2 is used in this design. The cell is designed to resonate at 28 GHz frequency.The calculated resonance frequency is almost equal to ssimulated resonance frequency. For a specific range of frequencies this metamaterial cell depicts negative values of permeability.This mathematically modeled metamaterial cells are loaded on the surface of patch.The bandwidth and gain of antenna are equal to 2.14 and 8 dBi respectively.The bandwidth and gain are higher compare to convantional antenna. Mathematically modeling and simulating a single negative metamaterial cell com-

prising of a square split ring resonator with two rings.Various dielectric substrates like FR4, Rogers RT/Duroid5880 and Roger RT/Duroid 6006 are used for modeling metamaterial cells with same structure and dimensions. This metamaterial cell depicts negative values of permeability for a specific range of frequencies. The resonant frequency predicted analytically is found to be extremely close to the frequency obtained by modeling metamaterial structure. The S parameters are extracted using simulating software. The method used to extract the S parameters is one using perfect electric and perfect magnetic (PE-PM) boundary conditions.Resonance frequencies of the cells with Rogers RT/Duroid 5880, FR4 and Rogers RT/Duroid 6006 substrate are 5.8 GHz,4.9 GHz and 4.4 GHz respectively.

The Planar antennas can be printed on different types of dielectric substrates with minimum cost and processing. One fundamental factor that makes planar antennas so desirable and important is their easy way of integration with microwave or millimeter- wave circuit components.Some novel architectures and techniques of designing the metamaterial loaded bio inspired planar microstrip patch antennas such as hibiscus leaf and Kaju leaf shape antennas are discussed. Conventional hibiscus leaf shape antenna is multiband antenna which resonates at 5.8 GHz ,10 GHz and 13.4 GHz with bandwidth 267.7 MHZ,280.5 MHz,450.8 MHz.Metamaterial loaded hibiscus leaf shape antenna resonates at 5.8 GHz and 11 GHz.The bandwidth obtained is 750 MHZ and 2.25 GHz respectively. Conventional kaju leaf shape antenna is multiband antenna which resonates at 5.8 GHz ,9.67 GHz with bandwidth 313.9 MHZ,390 MHz respectively.Metamaterial loaded kaju leaf shape antenna resonates at 5.8 GHz and 9.18 GHz.The bandwidth obtained is 404 MHZ and 480.5 MHz respectively.

A conventional antenna and a proposed novel coaxial feed rectangular microstrip patch antenna (RMPA) with resonance frequency 3.5GHz and a ground plane of substrate is loaded with square split ring resonators , This patch antenna is designed on FR-4 substrate with permittivity value equal to 4.4 and thickness equal

to 1.6 mm.The proposed rectangular microstrip patch antenna is fabricated to obtain experimental parameters.The Bandwidths of proposed conventional patch antenna metamaterial loaded patch antenna and fabricated patch antenna are 122.9 MHz, 274.2 MHz and 210.2 MHz respectively.And the cnventional antenna gain is 2.74 dBi and metamaterial loaded antenna Gain is 5 dBi.

The Microstrip patch antenna (MPA) is loaded with metamaterial cells that increases the effective wavelength of the antenna, and thus lowers the resonant frequency of the radiating mode. This in turn, leads to a substantial reduction in its size as compared to the conventional half-wavelength MPA.All the metamaterial loaded patch antennas are reduced in size.

Chapter 2

Objectives, Methodology and Novelty / Main contributions of research

2.1 Objectives

The objectives of this research are:

- I) Metamaterial cell design and optimization at resonance frequency using MATLAB.
- II) To miniaturize microstrip patch antenna using Metamaterials.
- III) To enhance the band width of antenna.
- IV) Improvement of power handling capacity of antenna. Simulation of antenna using HFSS software and fabrication

2.2 Methodology

- The metamaterial cell comprising of Square split ring resonator (SSRR) with copper strip on a ground plane of the substrate,and metamaterial cells comprising of only square split ring resonator (SSRR), are designed and simulated using MATLAB software to find parameters of cell such as S_{11}, S_{21}, Permittivity, Permeability. The CST platform is invoked through the MATLAB script file. The complementary split ring resonator (CSRR) was

designed and simulated to load it on circular microstrip antenna.[40]. The effective parameters of SSRR can be found out using second method in which, We have to find out the transmission and reflection coefficient of the cell by simulating cell using HFSS/FEKO based on numerical algorithms, such as (FDTD) and Finite Element Method (FEM). Equations given below are used to calculate impedance and refractive index respectively, from the transmission coefficient (S_{21}) and reflection coefficient (S_{11}). And further to calculate complex permeability and permittivity. Both the coefficients S_{11} and S_{21} are exported to MATLAB to extract real and imaginary curves of permeability using the following equations.

$$Z_{eff} = \pm\sqrt{\frac{(1+S_{11})^2 - S_{21}^2}{(1-S_{11})^2 - S_{21}^2}} \tag{2.1}$$

$$\eta_{eff} = \pm\frac{1}{kod}[[In(e^{i\eta_{eff}kod})] + 2m\pi - i[In(e^{i\eta_{eff}kod})]] \tag{2.2}$$

$$e^{i\eta_{eff}kod} = \frac{S_{21}}{(1 - S_{11}[(Z_{eff}-1)/(Z_{eff}+1)])} \tag{2.3}$$

where d is the thickness of homogenous slab or substrate,Z_{eff} is a complex wave impedance and $k_0 = 2\pi c/\lambda$, m is a branch due to periodicity of sign function. Z_{eff} and η_{eff} from the above equation. Real part of the impedance is positive and an imaginary part of the refractive index is negative. Further $\epsilon_{r,eff}$ and $\mu_{r,eff}$ can be obtained according to ,$\epsilon_{r,eff}$= η_{eff}/Z_{eff} and $\mu_{r,eff} = \eta_{eff}\ Z_{eff}$. This method is mainly used to find parameters of complex structures[19]. Also metamaterial cells on various substrate are mathematically modelled, simulated and their resonance frequency are compared. Conventional rectangular microstrip patch antenna (RMPA), Circular microstrip patch antenna (CMPA) and metamaterial loaded patch antennas are designed and optimised by FEKO software, for this purpose the genetic algorithm method is selected, Objectives or goals are marked as reflection coefficient, efficiency and impedance. Variables selected are length of patch, width of patch, microstrip feed length and resonance frequency for RMPA.

2.3 Novelty / Main contributions of research

The main contributions and observations of this research are as follows:

- The novel idea is to place seven cells of metamaterial on the substrate ground in an English letter U shape pattern to obtain very good impedance matching, improved bandwidth and gain compare to conventional patch antenna. Edge port feeding has been used in this antenna. Excitation of surface wave becomes easy when a material with higher dielectric constants and thicker material is used. Metamaterial cells reduce surface wave propagation thereby reducing the surface wave quality factor and increasing the bandwidth of the RMPA.

- The bioinspired structure of the shape of hibiscus leaf and kaju leaf has been designed. The circular patch was designed to determine the approximate length of the major axis of the hibiscus leaf microstrip patch antenna (HLMPA). Then the resultant circular microstrip patch antenna CMPA is perturbed to acquire the proposed HLMPA structure. These antennas are then loaded with metamaterial cells. The dimensions of an antenna are optimized using FEKO. Both antennas are multi-band. The Hibiscus leaf microstrip patch antenna resonate at 5.8 GHz, 10 GHz,13.4 GHz, and Kaju leaf shape microstrip patch antenna (KLMPA) resonates at 5.8 GHz and 9.67 GHz, both antennas have considerable bandwidth and gain which can be used for WiMAX and other wireless applications.

- Two Complementary circular split ring resonator are loaded on ground plane of circular patch antenna to miniaturise antenna and to increase the band width of an antenna.

Chapter 3

Introduction to metamaterials

3.1 History of Metamaterials

Metamaterial, an artificially structured material that exhibits extraordinary electromagnetic properties not available or not easily obtainable in nature. Since the early 2000s, metamaterials have emerged as a rapidly growing interdisciplinary area, involving physics, electrical engineering, materials science, optics, and nanoscience. The properties of metamaterials are tailored by manipulating their internal physical structure. This makes them remarkably different from natural materials, whose properties are mainly determined by their chemical constituents and bonds. The primary reason for the intensive interest in metamaterials is their unusual effect on light propagating through them. In 1898 J.C. Bose showed the possibility of existence of artificial material by conducting microwave experiment on twisted structure. Later, the physicist victor Veselgo (1968) presented theoretical investigation and Pendry in 1996 used an artificial wired medium whose permittivity is negative to realize artificial electric plasma, followed by this, in 1999 he used split-ring resonators (SRR) to realise magnetic plasma. whose permeability is negative. [41],[42].Smith had realized gradient refractive index medium to bend electromagnetic waves [5]. Metamaterial opened a new exciting world for the scholars[43]. Since a metamaterial is a material which is having negative permittivity and permeability, it is also having negative index

of refraction.Negative refraction was determined by a Snell's law. The metamaterials which are having electric permittivity and magnetic permeability close to zero, But less than zero are called as zero Index metamaterials.The zero index metamaterials are playing important role in a high directivity antennas.

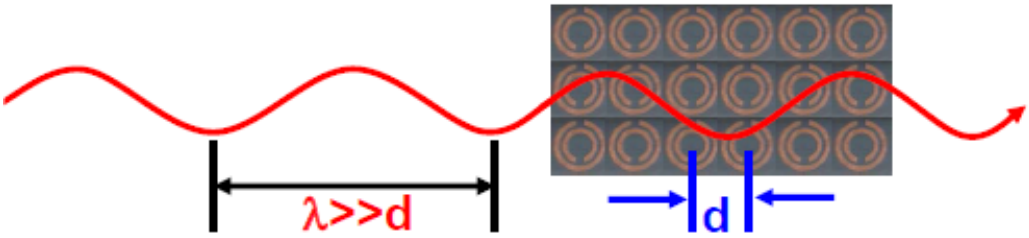


Figure 3.1: Lattice constant d of metamaterial cell and wavelength relation

Metamaterial is made up of periodic array of metallic resonant element. Size of element and unit cells are small relative to wavelength. Lattice constants of metamaterials are much smaller than the wavelength of the incident radiation as shown in (Fig.3.1) [44].Electromagnetic waves bend in the gradient refrective index medium, Smith in 2004 proposed this theory.The split ring resonator which gives negative permeability acts just like an artificial magnetic dipole. The gap between both the rings i.e inner and outer ring acts as a capacitor while the rings themselves act as an inductor, resulting in an LC resonant circuit. Just below resonance, the magnetic dipole due to the split rings will lag the H field by roughly 180 degree resulting in negative permeability. Negative permittivity is obtained by the array of thin wire which is made of materials like aluminium , copper, silver, and gold. The value of permittivity and permeability can be verified "theoretically" with the help of mathematics.

3.2 Fundamental theory and background of metamaterials

Left-handed materials are those that exhibit both negative permittivity and permeability. The wave vector and the two field vectors of a plane wave form a left handed triplet as seen inFig.3.2.Energy will be sent by the electromagnetic wave

in the direction opposite to the phase velocity [45]. Backward wave media are those in which the scalar product is negative or the energy velocity direction is the opposite of the phase velocity direction . The material with simultaneously nega-



(a) Plane wave in a backward wave medium. (b) Plane wave in a isotropic medium

Figure 3.2: Schematic structures

tive permittivity and permeability are called as left handed metamaterials which possesses many properties investigated by Vesalgo. Maxwell's equations given to understand metamaterial. They are artificial materials that show negative refractive index. These parameters are not found in natural materials. Equations3.1 and 3.2 are two Maxwells equation. Where ϵ_r and μ_r are relative permittivity and permeability respectively and Equation 3.3 and 3.4 shows electric and magnetic field intensities.[1],[46].

$$\nabla \times E = -\mu_0 \mu_r \frac{\partial H}{\partial t} \tag{3.1}$$

$$\nabla \times H = -\epsilon_0 \epsilon_r \frac{\partial E}{\partial t} \tag{3.2}$$

$$D = \epsilon_E = \epsilon_0 \epsilon_r E \tag{3.3}$$

$$B = \mu H = \mu_0 \mu_r H \tag{3.4}$$

$$\eta = \pm \sqrt{|\epsilon_r||\mu_r|} \tag{3.5}$$

Further it can be simplified as $k \times E = \mu\omega H$ and

$k \times H = -\mu\omega E$

D and B are electric and magnetic field densities respectively. ϵ_0 and μ_0 are permittivity permeability of vaccume . It is observed that k,E,H vector forms the

right handed triplet when it propagates through medium with eps and mu grater then zero. These vectors form left-handed triplets when it propagates through medium with ϵ and μ less than zero. The refractive index is having a negative sign, so that the causality is conserved. Due to the aforementioned facts, these materials are known as left handed material. The Drude–Lorentz model describes the material properties in classical electromagnetic. The frequency-dependent permittivity and permeability are shown in equation 3.6 and3.7. These equations are symmetrical because of the symmetrical nature of EM wave

$$\epsilon_r(\omega) = 1 - \frac{\omega_{p,e}^2}{\omega^2 - \omega_{o,e}^2 + i\gamma_e\omega} \tag{3.6}$$

$$\mu_r(\omega) = 1 - \frac{\omega_{p,m}^2}{\omega^2 - \omega_{o,m}^2 + i\gamma_m\omega} \tag{3.7}$$

Plasma frequency denoted by ω_p ,ω_0 is the resonance frequency, and damping factor γ which are in connection to material losses. e and m represent electric and magnetic responses respectively. The microwave range to optical range properties of materials are realised by above equations. For noble metals $\omega_{p,e}$ is at visible or UV frequency and $\omega_{0,e} = 0$ under the free electron approximation [1]. This shows that below plasma frequency permittivity of metals is always negative. Naturally existing materials are not available with negative permeability. When we cross GHz frequency magnetic response reduces which is due to magnetic polarisation. In the optical region,mu equal to 1 for all natural materials. Metamaterial consists of periodically distributed structural elements, whose spacing and size is much smaller than the wavelength of EM wave. The great aspect of metamaterial is that the permittivity and permeability can be controlled by proper design structure. Pendry proposed metal with low plasma frequency. Thin metallic wires are used for structure which are arranged in three dimensional lattice of very thin wires as depicted in (Fig.3.3)Two effects are possible from this structure. One effect is that the effective electron density is reduced. Second, the effective electron mass is increased because of the self-inductance of the wire structure. Calculations show

that the effective relative permittivity of the system obeys the Drude–Lorentz model.

$$\epsilon_{eff} = 1 - \frac{\omega_{peff}^2}{\omega^2 - j\gamma\omega} \tag{3.8}$$

$$\omega_{peff}^2 = \frac{2\pi c^2}{d^2 ln(d/r)} \tag{3.9}$$

$$\gamma_{eff} = \frac{\epsilon_0 d^2 \omega_p^2}{\pi r^2 \sigma} \tag{3.10}$$

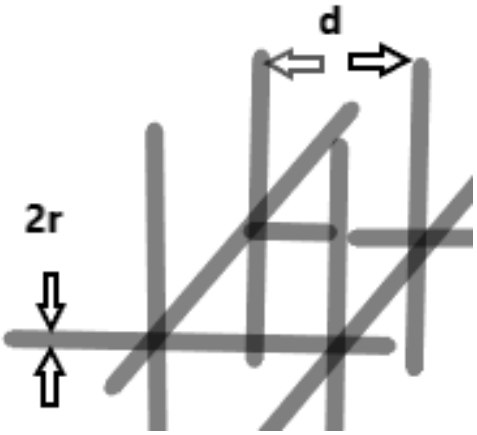
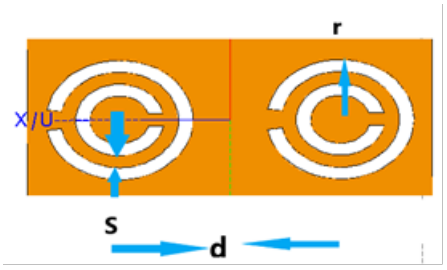
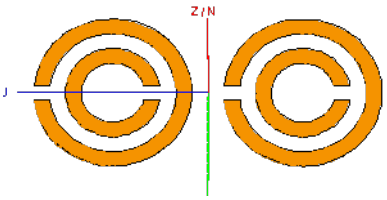


Figure 3.3: Wire structure

where σ is the conductivity of metal (typically in the order of $10^7/ohms/m$). Considering the wire radius $r = 1.2 \times 10^{-6}m$, lattice constant $d = 3.8 \times 10^{-3}m$, ω_{peff} is the effective plasma frequency, now using the equation effective plasma frequency can be obtained.



(a) Complementary split ring resonators (CSRR),with outer radius r



(b) Split ring resonator (SRR)

Figure 3.4: Metamaterial cells

Complementary split ring resonators (CSRRs) shown in Fig.3.4a and split ring resonator (SRR) depicted in Fig.3.4b are one of the original designs for strong artificial magnetism. Each SRR consists of concentric split rings that may be two or three with the gap in the opposite directions. From the point of view of equivalent circuits, an SRR can be considered as an LC circuit with the natural resonant frequency given by $\omega_0 = \sqrt{1/LC}$ with L and C denoting the inductance and capacitance of the SRR structure, respectively. Within a certain frequency region centred at the vicinity ofω_0 the magnetic flux is produced at SRR or CSSR The strong circulating current are induced resulting in an effective magnetic moment. This magnetic moment is in phase or out of phase with respect to the external magnetic field. A negative value permeability $\mu_{r,eff}$ can be obtained as a result of magnetic moments. Detailed derivations show that the effective relative magnetic permeability of an SRR array is given by equation3.11.

$$\mu_{reff}(\omega) = 1 - \frac{F\omega^2}{\omega^2 - \omega_0^2 + i\Gamma} \tag{3.11}$$

$$F = \frac{\pi r^2}{d^2} \tag{3.12}$$

ω_0 represents the resonance frequency,F is a filling ratio of SRR

$$\omega_0 = \sqrt{\frac{3SC^2}{\pi^2 r^3}} \tag{3.13}$$

Γ is a damping term $\Gamma = \frac{2}{r\sigma\mu_0}$ Complementary Split Rings (CSRR) Structures complementary to double split rings were designed by applying the Babinet principle to the split rings . In this way structures with apertures in metal surface are obtained. These complementary split rings (CSRR) create negative epsilon instead of μ in a narrow range near the resonance frequency. As an example, we take the following parameters of SRRs: $d = 4.5 \times 10^{-3}$ m,$r = 1.5 \times 10^{-3}$ m, and $S = 1 \times 10^{-4}$ The resulting resonance is $f_0 = \omega_0/2\pi$ GHz. It should be noted that this frequency corresponds to a free-space wavelength of 2.2 cm, about one order of magnitude larger than the lattice constant d. Very often, it is difficult

to analytically derive the effective parameters of certain metamaterials, due to the complexity of the structure. Alternatively, we can obtain the effective parameters from numerical simulations. The first step of the retrieval procedure is to calculate the transmission and reflection coefficient of the composite metamaterials, based on numerical algorithms, such as Finite-Difference Time-Domain (FDTD) and Finite Element Method (FEM). Some commercial softwares, including COMSOL Multiphysics and ANSOFT HFSS, CST microwave studio, FEKO are widely used. The refractive index and impedance are related to the transmission coefficient S_{21} and reflection coefficient S_{11} as shown in section 2.2.

3.3 Analysis of metamaterials using transmission line

If the homogenous medium is considered then metamaterials are operated in the fundamental mode. This defines the effective value of ϵ and μ. Because of the homogeneity of metamaterials, they can also be viewed as one dimensional (1D) transmission line (TL). If conventional TL is compared, Homogeneous TL for wave propagation in the z-direction has an incremental length $\Delta Z \rightarrow 0$ However, the only restriction of the incremental length is $\Delta z << \lambda_g$ or$\Delta z < \lambda_{g/4}$, where Δz is equal to the average unit-cell size and $\lambda_{g/4}$ is the guided wavelength [47] [48] . The ideal incremental homogeneous line model for a composite

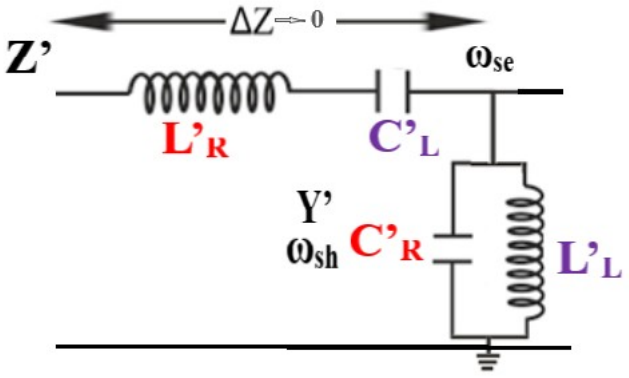


Figure 3.5: Ideal homogeneous incremented line model for composite Right/Left-handed metamaterial.

Right/Left-handed metamaterial is depicted in (Fig.3.5) [49]. It is possible to

think of the circuit as a combination of the Left-Handed (LH) and Right-Handed (RH) models (CRLH) of the transmission line. The impedance per unit-length for metamaterial transmission line (MTM-TL) with ϵ_{reff} and μ_{eff}, is defined as$Z^{'} = Z/\Delta Z$ and admittance per unit-length is defined as$Y^{'} = Y/\Delta Y$. The $L_R(H.m)$ and $C_L(F/m)$ stand for series right-handed inductance and series left handed capacitance respectively . The $L_L(H.m)$ and $C_R(F/m)$ stand for parallel left-handed inductance and parallel right-handed capacitance, respectively. The complex propagation constant$\gamma$is written as equation 3.14 [50] [51].

$$\gamma = \alpha + j\beta = \sqrt{Z'Y'} \tag{3.14}$$

$$Z^{'} = j\left(\omega L_R - \frac{1}{\omega C_L}\right) = j\frac{\left(\frac{\omega}{\omega_s}\right)^2 - 1}{\omega C_L} \tag{3.15}$$

$$Y^{'} = j\left(\omega C_R - \frac{1}{\omega L_L}\right) = j\frac{\left(\frac{\omega}{\omega_p}\right)^2 - 1}{\omega L_L} \tag{3.16}$$

$$Z^{'} = \pm\sqrt{\frac{(1+S_{11})^2 - (S_{21})^2}{(1-S_{11})^2 - (S_{21})^2}} \tag{3.17}$$

$$Y^{,} = \pm\sqrt{\frac{(1+S_{11})^2 - (S_{21})^2}{(1-S_{11})^2 - (S_{21})^2}} \tag{3.18}$$

Where ω_p and ω_s are resonant frequency corresponding to parallel and the series branch of the circuit respectively and defined as $\omega_s = \frac{1}{\sqrt{(L_R C_L)}}$ and $\omega_(p) = \frac{1}{\sqrt{(L_L C_R)}}$. The resonance factor$K(s/rad2)$ is given as the sum of $L_R C_L$ and $L_L C_R$. Therefore, expression of *gamma* can be written as

$$\gamma = jS(\omega).\sqrt{(\frac{\omega}{\omega_R})^2 + (\frac{\omega_L}{\omega})^2 - K\omega_L^2} \tag{3.19}$$

$$\tag{3.20}$$

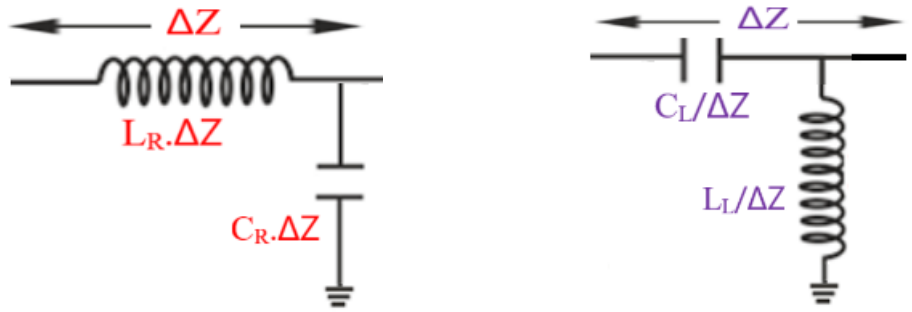
$$\gamma = \pm\sqrt{\frac{(1+S_{11})^2 - (S_{21})^2}{(1-S_{11})^2 - (S_{21})^2}} \tag{3.21}$$

where$\omega_R$andω_L are right-handed and left-handed frequencies in rad/(m.sec) and defined as$\omega R = \frac{1}{\sqrt{L_R C_R}}$ and $\omega_L = \frac{1}{\sqrt{L_L C_L}}$ s(w) is a signed function expressed as s(w) is a signed function expressed as

$$S(\omega) = -1; \omega < min(\omega_s, \omega_p)\, Left - handed \tag{3.22}$$

$$S(\omega) = +1; \omega > min(\omega_s, \omega_p)\, Right - handed \tag{3.23}$$

CRLH-TL is reduced to RH-TL if$C_L and L_L$are open-circuited. Similar to how CRLH-TL transforms into solely LH-TL when LR and CR are short-circuited, fig.3.6b By taking into account phase velocity (vp) and group velocity (vg), the can be understood. when $\omega > max(\omega_s, \omega_p)$ $vp = vg$ exhibits parallel behaviour, indicating that(β) will be positive . In contrast If the frequency $\omega < min\omega_s, \omega_p)$ then the relationship $vp = -vg$ is antiparallel. As a result, the LH-TL phase constant(β) will be negative.



(a) Equivalent circuit of a periodic RH-TL with an infinitesimal incremental length (ΔZ)

(b) Dual configuration of RH-TL

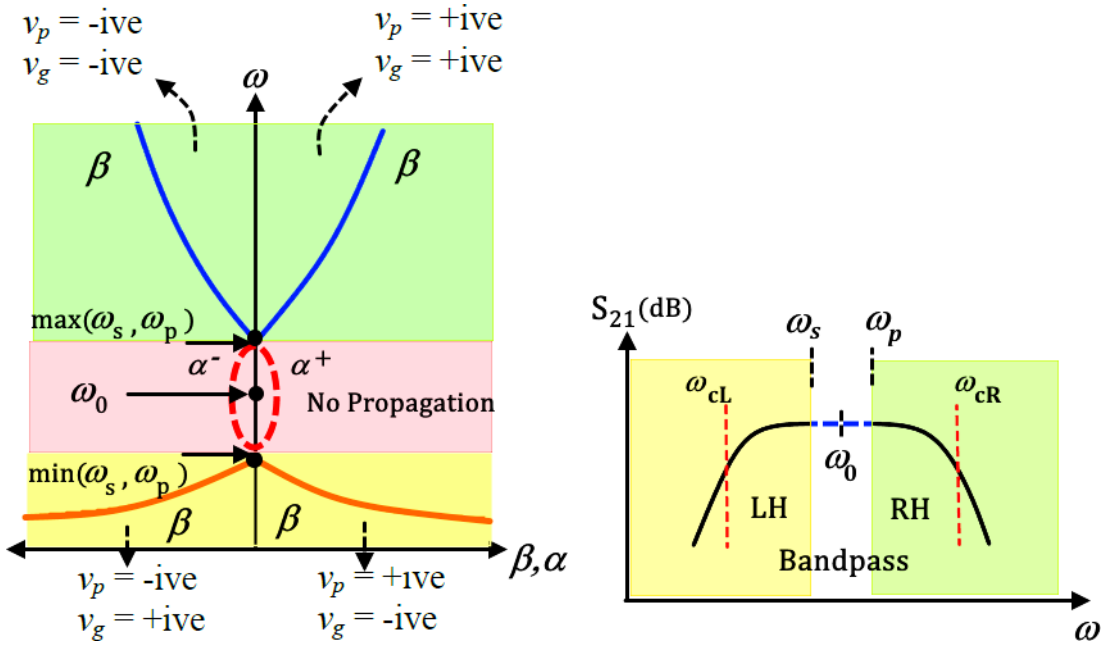
Figure 3.6: Equivalent circuit of a periodic RH-TL

The presence of RH and LH circuit components causes the CRLH-TL circuit to have a bandpass response, according to a later interpretation. The RH-TL components produce a low-pass response at low frequencies, while the remaining circuit components function as high-pass filtering.The expression of the vp is shown in the equation 3.25. [52] [53].

$$v_p = \frac{\omega}{\beta} = S(\omega) \frac{\omega}{\sqrt{\left(\frac{\omega}{\omega_R}\right)^2 + \left(\frac{\omega_L}{\omega}\right)^2 - k\omega_L^2}} \tag{3.24}$$

$$v_g = \frac{\sqrt{\left(\frac{\omega}{\omega_R}\right)^2 + \left(\frac{\omega_L}{\omega}\right)^2} - k\omega_L^2}{(\omega/\omega_R^2) - (\omega_L^2/\omega^3)} \tag{3.25}$$

The presence of RH and LH circuit components causes the CRLH-TL circuit to



(a) Equivalent circuit of a periodic RH-TL with an infinitesimal incremental length (ΔZ)

(b) Dual configuration of RH-TL

Figure 3.7: Schematic of the propagation mechanism.

have a bandpass response, according to a later interpretation [47]. The RH-TL components produce a low-pass response at low frequencies, while the remaining circuit components function as high-pass filtering.[54] [55] [56]

3.3.1 Retrieval methods of parameters of metamaterials

The response of metamaterial is attributed by the effective material medium quantities, i.e. permittivity and permeability. However, retrieval of constitutive effective material medium parameters may not be possible directly. In these methods, permittivity and permeability are obtained and the behavior of most of the metamaterials is anisotropic. A proper electric or magnetic tensor is a necessary requirement and only after exciting the metamaterial by a plane wave with suitable electric and magnetic polarizations, negative refractive index is possible. In most of the case, the near-field information of metamaterial structure is un-

available. Some of the popular extraction techniques involve simulation of metamaterial cell to obtain scattering parameters ($S_{11} and S_{21}$). In this method,[54] homogeneous model of metamaterial is considered. The effective impedance and its refractive index are expressed using S-parameters. Equation3.26 and Equation3.29 are used to calculate refractive index and impedance, from transmission coefficient(S_{21}) and reflection coefficient (S_{11}) [19].Equation 3.27 is also can be used to calculate refractive index.

$$Z_{eff} = \pm\sqrt{\frac{(1+S_{11})^2 - S_{21}^2}{(1-S_{11})^2 - S_{21}^2}} \tag{3.26}$$

$$\eta_{eff} = \pm\frac{1}{kod}[[In(e^{i\eta_{eff}kod})] + 2m\pi - i[In(e^{i\eta_{eff}kod})]] \tag{3.27}$$

$$e^{i\eta_{eff}kod} = \frac{S_{21}}{(1 - S_{11}[(Z_{eff}-1)/(Z_{eff}+1)])} \tag{3.28}$$

$$\eta_{eff} = \frac{1}{kd}cos^{-1}[\frac{1}{2S_{11}}(1 - S_{11}^2 + s_{21}^2)] \tag{3.29}$$

where d is the thickness of homogenous slab or substrate,Z_{eff} is a complex wave impedance and $k_0 = 2\pi c/\lambda$. By using Equation 3.26 and Equation 3.29 ,permittivity and permeability are calculated as $\epsilon = n/z$ and $\mu = n.z$ In reality, solving Equation3.26 gives multiple branches of inverse cosine and creates difficulty in determining the material medium parameters. In addition to this when the metamaterial unit-cell is inhomogeneous, and then Equation 3.26 and Equation 3.29 led to an ambiguous solution. This is because asymmetry in the model along the direction of propagation results in the variation of S_{11} and S_{21} profile and retrieval method becomes even more difficult. However, if the asymmetric unit-cell is in infinite repetition, the unique index value can be extracted.

Chapter 4

Classification of metamaterials

Electromagnetic field is determined by the properties of the materials involved. These properties define the macroscopic parameters permittivityϵ and permeability μ of materials. It is well known that the response of a system to the presence of an electromagnetic field is determined to a large extent by the properties of the materials involved We describe these properties by defining the macroscopic parameters permittivity and permeability mu of these materials. This allows for the classification of a medium, this class of materials has been presented in(Fig.4.1) [44] . A medium with both permittivity and permeability greater than zero ($\epsilon>$ 0, μ >0) will be designated a double positive (DPS) medium. Most naturally occurring media (e.g., dielectrics) fall under this designation.[57].

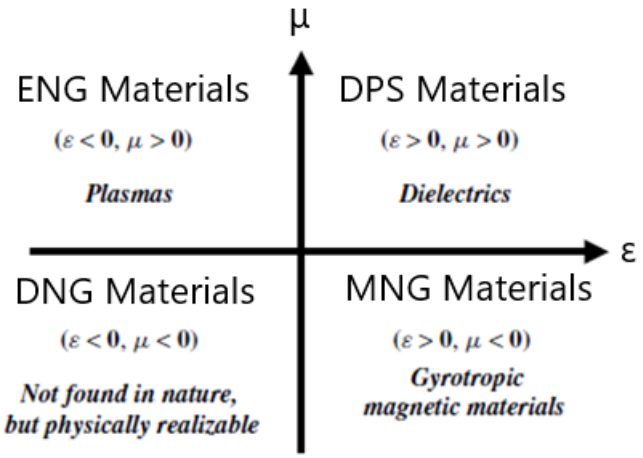


Figure 4.1: Material classification.

A medium with permittivity less than zero and permeability greater than zero ($\epsilon<$ 0, μ >0) will be designated an epsilon-negative (ENG) medium. This prop-

erty is seen in many plasmas in specific frequency regimes. Noble metals, such as silver and gold, for instance, exhibit this behaviour in the visible and infrared (IR) frequency ranges. A mu negative (MNG) medium is one that has a permittivity more than 0 and a permeability less than 0 ($\epsilon > 0, \mu < 0$). Some gyrotropic materials show this property in specific frequency ranges. Artificial materials with DNG, ENG, and MNG characteristics have been created. A medium will be referred to as a DNG medium if its permittivity and permeability are both less than zero ($\epsilon < 0$, $\mu < 0$)

4.1 Electromagnetic Metamaterials

Metamaterials have become a new sub discipline within physics and electromagnetism (especially optics and photonics).They are used for microwave and optical applications such as new types of beam steerers, modulators, band-pass filters, lenses, and antenna radomes, microwave couplers . Metamaterials consist of structures. A metamaterial affects electromagnetic waves by having structural features smaller than the wavelength of electromagnetic radiation it interacts with. It is the greatest potential of metamaterials to create a structure with a negative refractive index, since this property is not found in any non-synthetic material. Almost all materials encountered in optics, such as glass or water, have positive values for both permittivity and permeability . However, many metals (such as silver and gold) have negative permittivity at visible wavelengths. Although the optical properties of a transparent material are fully specified by the parameters ϵ and μ, refractive index n is used in practice. All known non-metamaterial transparent materials possess positive ϵ and μ. By convention the positive square root is used for η. However, some artificial metamaterials have($\epsilon < 0$, $\mu < 0$). Because the product of ϵ μ is positive,η is real. Under such circumstances, it is necessary to take the negative square root for η. Physicist Victor Veselago proved that such substances can transmit light.

4.1.1 Double negative metamaterials

The discovery that Jagadis Chandra Bose, an Indian physicist, conducted the first microwave experiment on twisted structures—geometries that were essentially artificial chiral elements by today's terminology—in 1898 marks the beginning of attempts to explore the concept of "artificial" materials. In order to create "artificial" chiral media, Lindman embedded several tiny wire helices with random orientations into a host medium in 1914. By stacking conducting spheres, strips, and successfully controlling the artificial media's effective refractive index, Kock created lightweight microwave lenses in 1948. Since then, a lot of researchers throughout the world have been studying artificial complex materials. In recent years new concepts in synthesis and novel fabrication techniques have allowed the construction of structures and composite materials that mimic known material responses or that qualitatively have new, physically realizable functions that do not occur or may not be readily available in nature. These metamaterials can in principle be synthesized by embedding various constituents/inclusions with novel geometric shapes and forms in some host media. Various types of electromagnetic composite media, such as double-negative (DNG) mate- rials, chiral materials, omega media, wire media, bianisotropic media, linear and nonlinear media, and local media, to name a few, have been studied by various research groups worldwide [44]. It is common knowledge that electromagnetic waves interact with inclusions in particulate composite media to produce electric and magnetic moments. These moments then have an impact on the macroscopic effective permittivity and permeability of the bulk composite "medium." Since artificially created inclusions can be used to create metamaterials, the designer has a wide range of independent parameters (or degrees of freedom) to work with in order to create a metamaterial with specific electromagnetic properties. These parameters include the characteristics of the host materials, the size, shape, and composition of the inclusions, as well as the density, arrangement, and alignment

of these inclusions. All of these design factors may be crucial. can play a key role in the final outcome of the synthesis process. Among these, the geometry (or shape) of the inclusions is one that can provide a variety of new possibilities for metamaterials processing. Recently, the idea of complex materials in which both the permittivity and the permeability possess negative real values at certain frequencies has received considerable attention. In 1967, Veselago theoretically investigated plane-wave propagation in a material whose permittivity and permeability were assumed to be simultaneously negative. His theoretical study showed that for a monochromatic uniform plane wave in such a medium the direction of the Poynting vector is antiparallel to the direction of the phase velocity, contrary to the case of plane- wave propagation in conventional simple media. In recent years, Smith, Schultz, and their group constructed such a composite medium for the microwave regime and demonstrated experimentally the presence of anomalous refraction in this medium .

For metamaterials with negative permittivity and permeability, several names and terminologies have been suggested, such as "left-handed" media ; media with negative refractive index "backward-wave media" and "double-negative (DNG)" metamaterials , to name a few. Many research groups all over the world are now studying various aspects of this class of metamaterials, and several ideas and suggestions for future appli- cations of these materials have been proposed.[58],[16]. It is well known that the response of a system to the presence of an electromagnetic field is determined to a large extent by the properties of the materials involved. We describe these properties by defining the macroscopic parameters permittivity ϵ and permeability μ of these materials. This allows for the classification of a medium as follows. A medium with both permittivity and per- meability less than zero($\epsilon < 0$, $\mu < 0$) will be designated a DNG medium. To date, this class of materials has only been demonstrated with artificial constructs. This medium classification can be graphically illustrated. While one often describes a material by some constant (frequency- independent) value of the permittivity and perme-

ability, all material properties are frequency dependent. A number of material models have been developed to explain the frequency response of various materials. The wave impedance of the medium in which an electromagnetic wave is propagating causes the magnetic field of an electromagnetic wave to be smaller than its electric field, so one typically focuses attention on how the electron motion in the presence of the nucleus and, consequently, the fundamental dipole moment of this system are changed by the electric field.

In double negative metamaterials (DNG), the index of refraction is negative because both permittivity and permeability are negative. The term "negative index metamaterials" (NIM) is another name for DNGs. DNGs are also referred to as "left-handed media", "media with a negative refractive index", and "backward-wave media".[44]

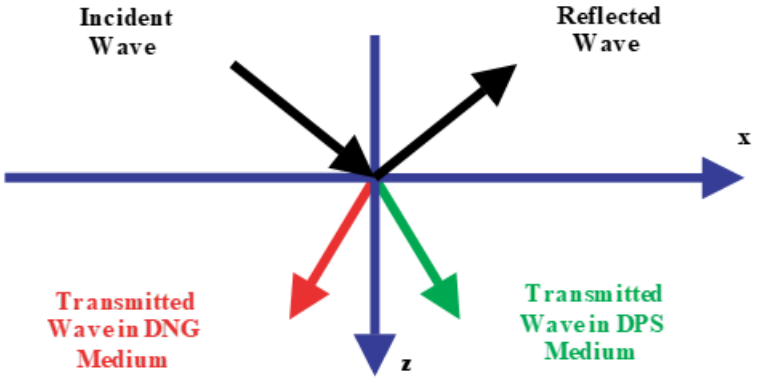


Figure 4.2: Scatering of wave incident on DPS-DNG interface

The phenomenon of negative refraction is studied on basis of the scattering of a wave that is obliquely incident on a DPS– DNG interface as shown in(Fig.4.2). Enforcing the electromagnetic boundary conditions at the interface, one obtains the law of reflection. It should be noted that Snell's law states that if a medium's index of refraction is negative, the refracted angle should similarly become "negative." The refracted angle is on the same side of the contact as the incident angle, indicating that the refraction is anomalous.

4.1.2 Single negative metamaterials

In single negative (SNG) metamaterials either permittivity or permeability are negative, but not both. These are ENG metamaterials and MNG metamaterials discussed below. Interesting experiments have been conducted by combining two SNG layers into one metamaterial. These effectively create another form of DNG metamaterial. A slab of ENG material and slab of MNG material have been joined to conduct wave reflection experiments. This resulted in the exhibition of properties such as resonances, anomalous tunneling, transparency, and zero reflection. Like DNG metamaterials, SNGs are dispersive, so their permittivityϵ permeability μ, and refraction index n, will alter with changes in frequency [44].

4.1.3 Electromagnetic Bandgap Metamaterials

The propagation of light is controlled by electromagnetic bandgap metamaterials.Either photonic crystals (PC), a form of metamaterial, or left-handed materials (LHM), a different class, are used to achieve this. Both belong to a brand-new class of artificially created structures that are used to direct and control the movement of electromagnetic waves (light). Photonic crystals (PCs) and photonic bandgap (PBG) materials are a novel class of artificially produced structures that have the capacity to regulate and modify the propagation of electromagnetic (EM) waves. Electromagnetic bandgap (EBG) materials are these materials. A well-designed photonic crystal can stop light from travelling in some directions, allow it to go in only a few, or only in a specific area. They can be built in one, two, or three dimensions (1D, 2D, and 3D), and they can be made of metallic or dielectric materials.PCs' photonic band structure is the source of their capacity to regulate the transmission of light. When compared to the idea of electronic band structure, the concept of photonic band structure emerges. We anticipate a similar arrangement of energy bands, separated by bandgaps, to arise when electromagnetic waves propagate in a medium in which the dielectric constant varies

regularly in space. This is similar to how electron waves travelling through the periodic potential of a crystal are organised. Photonic bandgap materials or PCs are the structures which show such a phenomenon, that is, produce a forbidden frequency gap in which all propagating states are prohibited. The investigation of these materials is a topic of intensive studies by many groups, both theoretically and experimentally. The periodicity alone does not ensure the existence of a full PBG in the EM instance, but the PBG property of PCs makes them the EM analogue of the electronic semiconductor crystals. However, a significant advantage of PCs is that, unlike semiconductors, where the periodicity is fixed, the periodicity in PCs may be altered at will, altering the PBG's frequency range. These structures have recently been constructed in the far-infrared range, and their prospective uses are still being researched. However, creating composite materials with spectral gaps at frequencies up to the optical region is the biggest scientific difficulty in the field of PCs. The first prescription for a periodic dielectric structure with a full PBG rather than a pseudogap was provided by Ho, Chan, and Soukoulis. The proposed structure consisted of a periodic lattice-like diamond made of dielectric spheres. It was discovered that PBGs exist for both air spheres in a dielectric and dielectric spheres in air over a broad range of filling ratios and for refractive index contracts between spheres and host as low as 1.98. However, this diamond dielectric structure is not easy to fabricate, especially in the micrometer- and submicrometer-length scales for infrared or optical devices [44][16].

4.1.4 Bi-isotropic and bianisotropic metamaterials

Metamaterials classification into double and single negative is normally done based on the assumption that the metamaterials electric and magnetic responses described by the parameters epsilon and mu. However in electromagnetic metamaterials, the electric field that causes magnetic polarization, and the magnetic field induces an electrical polarization, That is magnetoelectric coupling. This

media are denoted as being biisotropic. Media which are exhibit magnetoelectric coupling, and which are also anisotropic, are called as bianisotropic metamaterials. [59],[16].

4.1.5 Chiral metamaterials

If there is no translational or rotational change that enables an object's mirror image to be superimposed onto the original one, that thing is said to be chiral. The use of chiral media and systems is widespread, as Lord Kelvin noted. Examples of things that are visibly chiral include our hands, screws, snail shells, and so on. At the molecular level, there are also a number of chiral substances, such as sugars and amino acids. But as the fatal misuse of the drug thalidomide shows, the chirality of a medium is often ignored. From an optics perspective, there are two basic causes for this: First, chirality often results in a weaker optical reaction than achiral response, and second, a medium can contain an equal number of elements with opposite handednesses, known as a racemic mixture, rendering it optically inactive. Circular dichroism and optical activity are two typical (but distinct) forms of chiral media's optical response. As mentioned previously, optical activity relates to the rotation of the plane of polarisation of a linearly polarised light beam, while circular dichroism denotes the difference in absorption of light with left or right circular polarisation . The rotation angle is used to describe optical activity. it is convenient to use the ellipticity, which is a function of the relative difference in transmission. Here we should note that optical rotatory dispersion, the unequal rotation of the plane of polarization of light of different wavelengths, is different from optical activity.[60]

4.1.6 Terahertz Metamaterials

Terahertz metamaterials are metamaterials which interact at terahertz frequencies. For research or applications of the terahertz range for metamaterials and other materials, the frequency range is usually defined as 0.1 to 10 THz. This

corresponds to the wavelengths between 3 mm (EHF band) and 0.03 mm (long-wavelength edge of far-infrared light).[61]

4.1.7 Photonic Metamaterials

A subwavelength, periodic structure created artificially and intended to interact with optical frequencies is known as a photonic metamaterial. The photonic metamaterial can be distinguished from photonic band gap structures by its sub-wavelength period.[62]

4.1.8 Tunable Metamaterials

A tunable metamaterial is a metamaterial which has the capability to arbitrarily adjust frequency changes in the refractive index [63].

4.1.9 Frequency Selective Surface (FSS) based Metamaterials

. FSS-based metamaterials have taken the place of the fixed frequency metamaterial. Intriguing roles are played by frequency-selective surfaces (FSSs) printed on grounded stratified dielectric media in the variety of electromagnetic bandgap (EBG) structures that have lately been produced. It is possible to create artificial magnetic conductors (AMCs) or surfaces with "soft" and/or "hard" equivalent boundary conditions by using this type of construction. These surfaces fall into the category of artificial or metamaterial surfaces. Additional applications concentrate on obtaining a stop band for surface wave (SW) propagation along the contact. Consequent benefits are the suppression of SW coupling the reduction of diffraction lobes, the improvement of planar antenna efficiency, the development of compact antennas and resonators, and the suppression of parallel-plate waveguide modes. A simple and intuitive way to design an FSS-based metamaterial resorts to a model based on equivalent LC circuits based on quasi-static concepts. The LC model describes the dominant physics at low frequencies. The LC characteristics are more and more dependent on wave polarisation and phasing as the

frequency increases, rendering basic, quasi-static notions inadequate. This introduces the need for a more rigorous network derivation which extracts from the full-wave analysis the minimum number of wavenumber- dependent parameters for an analytical synthesis of the surface impedance. Along this line, this chapter illustrates first an integral equation method for the analysis of FSS-based metamaterials and then a general process to rigorously derive equivalent networks for designing reflection and dispersion properties [64]

Chapter 5

Theory and design of microstrip patch antenna

5.1 Introduction

According to Webster's Dictionary, an antenna is "a usually metallic device (as a rod or wire) for radiating or receiving radio waves." According to the IEEE Standard Definitions of Terms for Antennas (IEEE Std 145- 1983), an antenna or aerial is "a means for radiating or receiving radio waves." It is, in other words, the structural link between a directing mechanism and open space. Electromagnetic

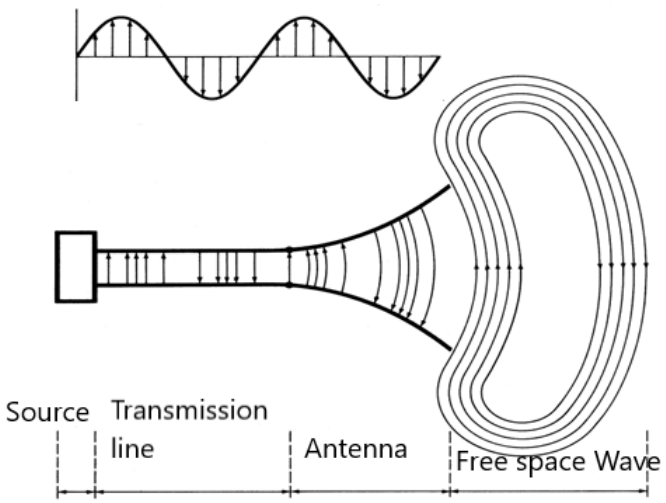


Figure 5.1: Antenna as transitional device

energy is transferred from the transmitting source to the antenna or from the antenna to the receiver via a guiding device or transmission line. It can take the

form of a hollow pipe (waveguide) or a coaxial line.In the first situation, we have a sending antenna, and in the second, a receiving antenna. Microstrip antennas appeal because they are lightweight, affordable, and conformable. These antennas are compatible with printed strip-line feed networks and active devices.Since the middle of the 1950s, it has been known that micro strip formations exhibit radiation properties. When conformal antennas were necessary for missiles in the early 1970s, this type of antenna utilisation got its start. Circular and rectangular micro strip resonant patches have been employed successfully in many array topologies. The recent developments in microstrip antennas have been greatly influenced by the present revolution in electronic circuit miniaturisation brought about by large scale integration breakthroughs.Because traditional antennas are typically a large and expensive part of an electronic system, micro strip antennas based on photolithographic technology are seen as a technical achievement. A microstrip Patch antenna, as depicted in(Fig.5.2), comprises of a radiating patch on one side of a dielectric substrate and a ground plane on the other. The patch can take any form and is typically constructed of conductive materials like copper or gold [65].

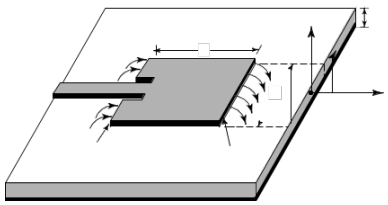


Figure 5.2: structure of a microstrip patch antenna

High-performance aircraft, as well as many other governmental and commercial applications where size, weight, cost, performance, ease of installation, and aerodynamic profile are limits, may need low-profile antennas. Already have similar requirements, such as mobile radio and wireless communications. These requirements can be met by using microstrip antennas. Low profile, conformability to planar and nonplanar surfaces, ease of fabrication using current printed-circuit technology, mechanical robustness when mounted on rigid surfaces, compatibil-

ity with Monolithic Microwave Integrated Circuit (MMIC) designs, and great versatility in terms of resonant frequency, polarisation, pattern, and impedance depending on the patch shape and mode chosen are some of the qualities of these antennas.Building adaptive elements with changeable resonant frequency, impedance, polarisation, and pattern is possible by inserting loads like pins and varactor diodes between the patch and ground plane.The patch is typically square, circular, rectangular, triangular, elliptical, or some other common shape as indicated in order to facilitate analysis and performance prediction.Shapes are shown in (fig.5.3). For a rectangular shape patch, the length L of the patch is usually $0.333\lambda_0 < L < 0.5\lambda_0$, where λ_0 is the free-space wavelength. A very thin patch is used such that $t < \lambda_0$ (where t is the patch thickness) The dielectric substrate height h is usually $0.003\lambda_0 \leq h \leq 0.05\lambda_0$.The microstrip patch is designed so its pattern maximum is normal to the patch (broadside radiator). The length L of the element for a rectangular patch is typically $\lambda_0/3 < L < \lambda_0/2$. Microstrip antennas can be designed using a variety of substrates [65] [66]. Microstrip antennas are often integrated with other microwave circuitry, a compromise has to be reached between good antenna performance and circuit design. Often microstrip antennas are also referred to as patch antenna.

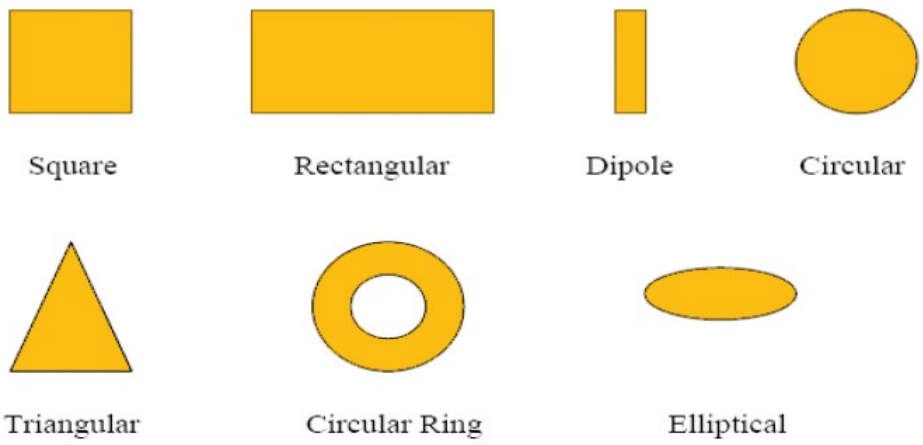


Figure 5.3: Different shapes of microstrip patch antenna

Square, rectangular, dipole (strip), and circular are the most common because of ease of analysis and fabrication, and their attractive radiation characteristics,

especially low cross-polarization

5.2 Advantages and Disadvantages of Microstrip Patch Antenna

Microstrip patch antennas are increasing in popularity for use in wireless applications due to their low-profile structure. Therefore they are extremely compatible for embedded antennas in handheld wireless devices such as cellular phones,Bluetooth etc. The telemetry and communication antennas on missiles need to be thin and conformal and are often in the form of microstrip patch antennas. Some of their principal advantages are given below:

- Light weight and low volume.
- Low profile planar configuration.
- Low fabrication cost.
- Supports both, linear as well as circular polarization.
- Can be easily integrated with microwave integrated circuits
- Capable of dual and triple frequency operations.
- Mechanically robust when mounted on rigid surfaces.
- Can be designed for dual or multi-frequency operations.

Microstrip patch antennas suffer from more drawbacks as compared to conventional antennas. Some of their major disadvantages discussed by Garg are given below:[67] In its basic form, The microstrip antenna has a narrow impedance bandwidth, However, various bandwidth-widening techniques have been developed. Up to 50 percent bandwidth have been achieved.It is typically true that larger bandwidth requires giving up more physical volume of the antenna. The microstrip antenna has a comparatively limited RF power handling capability because of the close proximity of its radiating patch to its ground plane. Due to its short length—roughly one half wave—a single patch element often has very low loss, while microstrip arrays typically suffer from higher ohmic losses than

arrays of other types of antennas with comparable aperture sizes. The dielectric substrate and the metal conductor of the power splitting circuit and microstrip line feed network are where this ohmic loss primarily occurs.

5.3 Basic principle of operation

A metal patch makes a resonant cavity, with the patch serving as the cavity's top, the ground plane as the cavity's bottom, and the patch's edges as the cavity's sides. The patch's edges essentially serve as an open-circuit boundary condition. Therefore, the patch functions as a cavity with ideal "magnetic conductors" on the sides and an ideal "electric conductor" on the top and bottom surfaces. This helps with patch antenna analysis. The electric field is largely z-directed and independent of the z coordinate inside the patch cavity. Hence, the patch cavity modes are described by a double index (m, n). For the (m, n) cavity mode of the rectangular patch the electric field has the form

$$E_z(x, y) = A_{mn} cos(\frac{m\pi x}{L}) cos(\frac{n\pi y}{w}) \tag{5.1}$$

Where L is the patch length and W is the patch width. The patch is usually operated in the(1, 0) mode, the field is largely constant in the y direction, and L is the resonant dimension. In this mode, the patch can be thought of as a wide microstrip line with a width W and a resonant length L that is roughly half a wavelength in the dielectric. This mode also results in the surface current on the bottom of the metal patch being x-directed, and is given by. The electric field is strongest at the two "radiating" edges of the patch, x = 0 and x = L, while the current is strongest at the patch's centre, x = L/2. Since the bandwidth is related to the width, the width W is typically selected to be greater than the length (W = 1.5 L is typical) in order to maximise the bandwidth. (The width should be kept less than twice the length, however, to avoid excitation of the (0,2) mode.) At first glance, it might appear that the microstrip antenna will not be an effective radiator when the substrate is electrically thin, since the patch current

in will be effectively shorted by the close proximity to the ground plane. If the modal amplitude A10 were constant, the strength of the radiated field would in fact be proportional to h. However, the Q of the cavity increases as h decreases (the radiation Q is inversely proportional to h). Hence, the amplitude A_{10} of the modal field at resonance is inversely proportional to h. Hence, the strength of the radiated field from a resonant patch is essentially independent of h, if losses are ignored. The resonant input resistance will likewise be nearly independent of h. This explains why a patch antenna can be an effective radiator even for very thin substrates, although the bandwidth will be small.

5.4 Resonant Frequency

The simplest is the transmission-line model, As will be demonstrated using the cavity model, a rectangular microstrip antenna may be thought of as an array of two radiating narrow apertures (slots), each of which is of width W and height h, separated by a distance L. In essence, the two slots of the transmission-line type of the microstrip antenna are separated by the low-impedance transmission line of length L.

Effects of a patch antenna's fringing edge. The patch has limited dimensions along its length and width, and the fields at its edges have fringing. This is displayed for the microstrip antenna's two radiating slots along its length. The width is exactly the same. The patch's dimensions and substrate height both influence the fringing. For the principal E-plane (xy-plane) fringing is a function of the ratio of the length of the patch L to the height h of the substrate (L/h) and the dielectric constant *epsilon* of the substrate. Since for microstrip antennas L/ h $>$ 1, fringing is reduced; however, it must be taken into account because it influences the resonant frequency of the antenna. The same applies for the width. The typical electric field lines are nonhomogeneous line of two dielectrics; typically the substrate and air. As can be seen, most of the electric field lines

reside in the substrate and parts of some lines exist in air. As W/ h » 1 and ϵ_r » 1, the electric field lines concentrate mostly in the substrate. Since some of the waves travel in the substrate and some in air, an effective dielectric constant ϵ_{reff} is introduced to account for fringing and the wave propagation in the line. The patch of the microstrip antenna seems electrically larger than its true size because of the fringing effect.The width-to-height ratio (W/h) and the effective dielectric constant ϵ_{reff} have been used to expand the patch's dimensions along its length for the major E-plane by a distance called ΔL The resonant frequency of the microstrip antenna is a function of its length for the predominantTM_{10} mode. The width of RMPA, effective permittivity and fringing length ΔL are shown in Equations. h=height of the substrate, W=width of rectangular patch L=length of RMPA C_0 = Speed of electromagnetic wave [65]

$$W = \frac{C_0}{2f_r}\sqrt{\frac{2}{\epsilon_r + 1}} \tag{5.2}$$

$$\epsilon_{reff} = \frac{\epsilon_r + 1}{2} + \frac{\epsilon_r - 1}{2}(1 + \frac{12h}{W})^{-1/2} \tag{5.3}$$

$$\Delta l = h\,(0.412)\,\frac{(\epsilon_{reff} + 0.3)\left(\frac{w}{h} + 0.264\right)}{(\epsilon_{reff} - 0.258)\left(\frac{w}{h} + 0.8\right)} \tag{5.4}$$

$$L_eff = \frac{C_0}{2f_r\sqrt{\omega_{reff}}} \tag{5.5}$$

Substrate width $= w + 6h$

Substrate length $= L + 6h$

5.5 Feed technique

We briefly describe here four feeding methods for the microstrip patch antenna. [65] [68]

5.5.1 Coaxial Probe Feed

The geometry of coaxial feed method is shown in (Fig.5.4). The coaxial probe usually has a characteristic impedance of 50 ohms. The input impedance of the

patch antenna varies with the feed location. Thus the location of the probe should be at a 50 ohm point of the patch to achieve impedance matching. There are a number of terms associated with the coaxial probe. Type N, TNC, or BNC connectors are for VHF, UHF, or lower microwave frequencies. OSM or OSSM connectors can be used throughout the microwave frequencies.The Omni Spectra Corporation version of SMA connector is known as OSM connector. OSSM connector,The OSSM connector was promoted by Omni Spectra. It is a microminiature version of the SMA. It is a 50-ohm connector system with performance from DC to 26.5 GHz with a flexible coaxial cable and up to 40 GHz when assembled with a semi-rigid cable. OS-50 or K-connector are for millimeter wave frequencies.

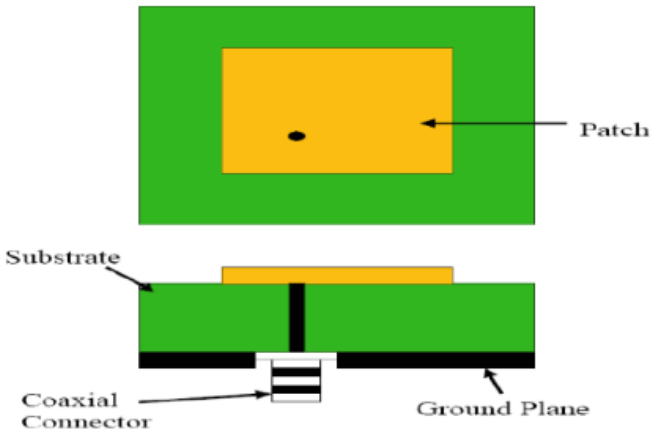


Figure 5.4: Coaxial Probe Feed

5.5.2 Microstrip-line feed

A microstrip patch can be connected directly to a microstrip transmission line, as shown in (Fig.5.5). At the edge of a patch, the impedance is generally much higher than 50 ohms (e.g. 220 ohms).The geometry of a direct microstrip feed microstrip patch antenna top view is shown in (Fig.5.5). For impedance matching, sections of quarter-wavelength transformers can be used to transform a large input impedance to a 50 ohms line. The input impedance is smaller at points away from the edge. Thus another method of matching the antenna impedance is to extend the microstrip line into the patch. An array of patch elements and

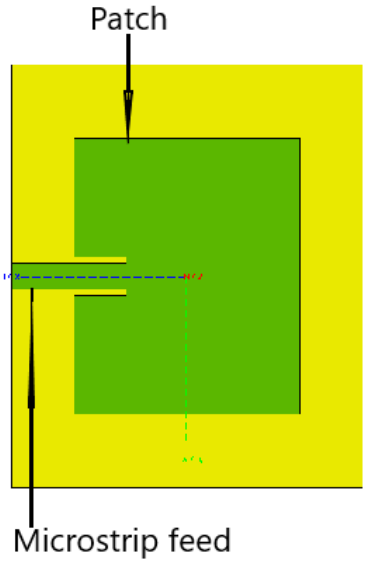


Figure 5.5: Microstrip-Line Feed

associated microstrip power division lines can all be created and chemically etched on the same substrate using the microstrip-line feed approach for a reasonably low fabrication cost per element. However, the transmission line leakage radiation may be sufficiently enough to increase the sidelobe or cross-polarized levels of the array radiation.

5.5.3 Proximity-coupled Microstrip-line feed

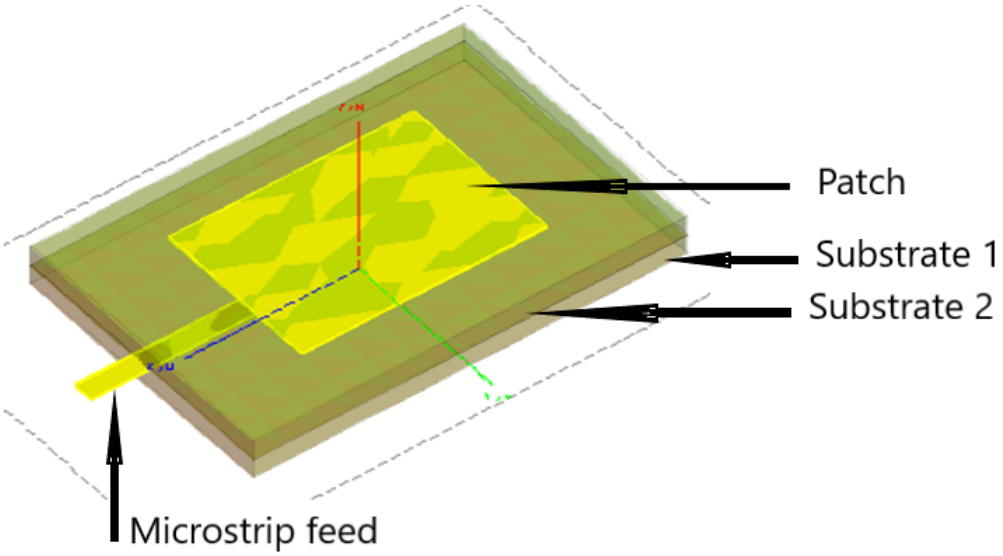


Figure 5.6: Proximity-coupled Microstrip-line feed

Cross-polarized radiation is produced by higher order modes that are generated by coaxial feed patch antennas and microstrip patch antennas.The adoption

of non-contacting feeds helps solve these issues.Through proximity coupling, an open-ended microstrip line can be used to feed a patch antenna as shown in Fig.5.6.The open end of a 100-ohm line can be placed underneath the patch at its 100 ohm location. An open-ended microstrip line can also be placed in parallel and very close to the edge of a patch, to achieve excitation through fringe-field coupling, as shown in figure Both these noncontacting methods avoid any soldering connection, which in some cases, could achieve better mechanical reliability. As shown in diagram two substrates and microstrip line feed is between both substrate.[65] [68]

5.5.4 Aperture-coupled feed

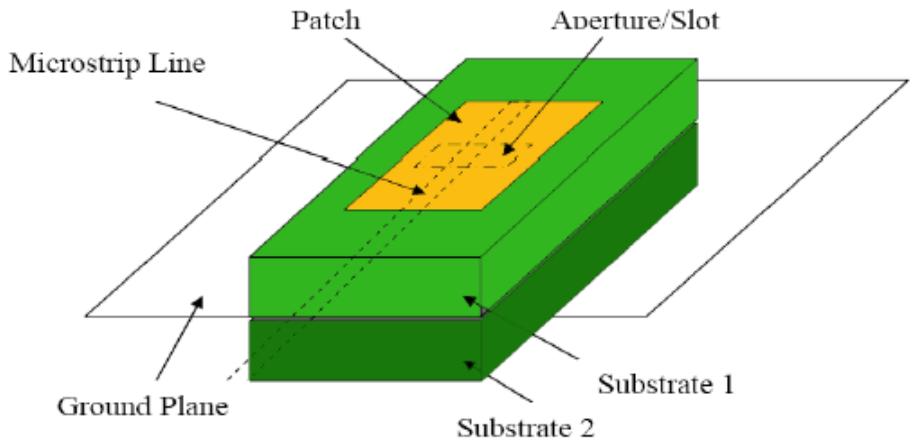


Figure 5.7: Aperture-Coupled Feed

An open-ended microstrip line can be placed on one side of the ground plane to excite a patch antenna situated on the other side through an opening slot in the ground plane, as shown in Fig.5.7 By using this slot-coupling or aperture-coupling approach, it is possible to prevent both soldering connections and patch radiation interference caused by line leakage radiation. Additionally, compared to the coaxial probe feed, this feed approach enables the patch to attain a broader bandwidth (>10) thanks to the use of a thick substrate. Figure illustrates the architecture of an aperture coupled feed microstrip patch antenna. When two resonators (slot and patch) having different but closely spaced resonance, wider

bandwidth is achieved. The main disadvantage of this feeding method is the back radiation from the slot. Advantages and disadvantages of all four feeding methods are shown in Table 5.1

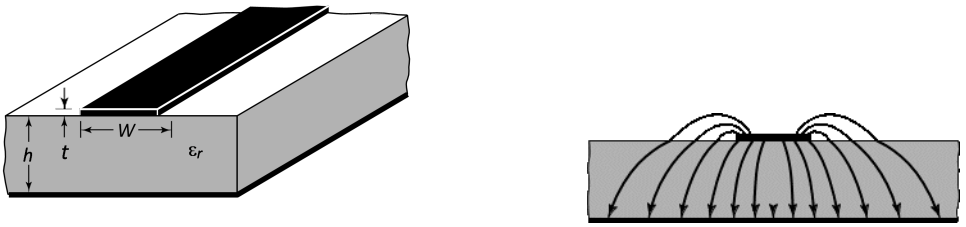
Table 5.1: Advantages and disadvantages of feeding methods

Feed	**Advantages**	**Disadvantages**
Coaxial feed	Easy to match impedance. Low spurious radiation.	Large Inductance. Soldering required.
Microstrip line	Monolithic. Easy to fabricate. Easy to match impedance.	Spurious radiation from Feed line for thick substrate.
Proximity Coupled	No direct contact between feed and patch. Thin feed substrate Thick patch substrate.	Requirement of Multilayer fabrication.
Aperture coupled	No direct contact between feed and patch avoids probe impedance. Two substrates avoids high dielectrc constant. No radiation from feed.	Requirement of multilayer fabrication. Higher backlobe. radiation

5.6 Method of Analysis

There are few methods of analysis for microstrip antennas. The most popular method are the transmission-line and full wave (which include primarily integral equations/Moment Method)[57] [68].The transmission-line model is the easiest of all, it gives good physical insight, but is less accurate and it is more difficult to model coupling . Compared to the transmission-line model, the cavity model

is more complex but good and accurate method. However, it also gives good physical insight and is rather difficult to model coupling, although it has been used successfully .The full-wave models can handle single elements, finite and infinite arrays, stacked elements, arbitrary shaped elements, and coupling and are generally quite accurate and adaptable when used appropriately. They are the most complicated models, nevertheless, and typically provide the least physical knowledge. Only the transmission-line will be discussed in this section. The only two patch configurations that will be discussed are the rectangular and circular ones because they are the most common and useful. The rectangular patch is by far the most widely used configuration. It is very easy to analyze using both the transmission-line and cavity models, which are most accurate for thin substrates . We begin with the transmission-line model because it is easier to illustrate. Transmission-Line Model It was indicated earlier that the transmission-line model



(a) Microstrip line (b) Electric field

Figure 5.8: Microstrip line field

is the easiest of all but it yields the least accurate results and it lacks the versatility. However, it does shed some physical insight. As it will be demonstrated using the cavity model, a rectangular microstrip antenna can be represented as an array of two radiating narrow apertures (slots), each of width W and height h, separated by a distance L. Basically the transmission-line model represents the microstrip antenna by two slots, separated by a low-impedance transmission line of length L. Fringing Effects that is ΔL, other dimensions of patch antenna ,actual and effective length of patch, effective permittivity resonance frequency width of patch are explained in section 5.4

5.7 Antenna parameters

If the reflection coefficient of antenna is smaller, then the more power the antenna is accepting. A significant reflection coefficient corresponds to poor impedance matching at the input terminal as seen from eq In most cases, coaxial and microstrip transmission lines feeding the antenna have an impedance of 50 Ω. To obtain maximum power transfer between the antenna and transmission line, the characteristic impedance Z_G of both should match. Both the antenna input impedance Z_A and return loss can be valuable and relate how efficiently the antenna accepts the supplied power. It is important to note that since the impedance is a function of frequency, the return loss also varies with frequency; thus, these values are usually plotted over a range of frequency

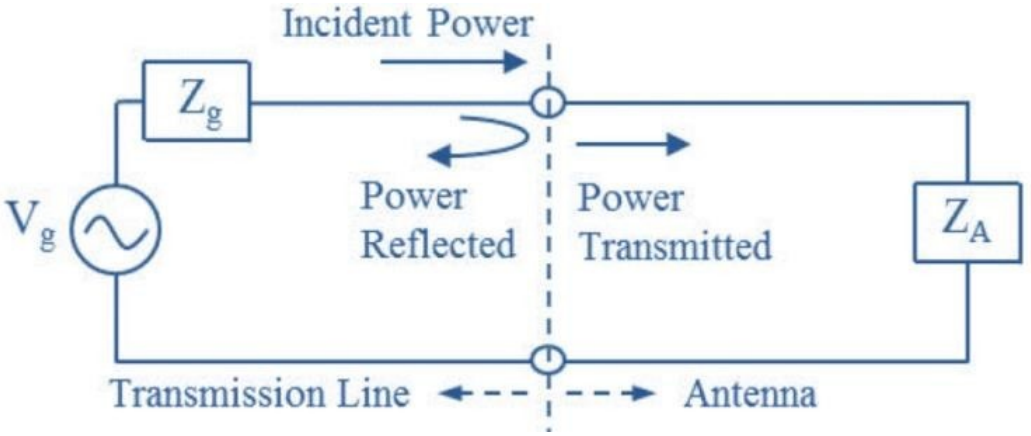


Figure 5.9: Different shapes of microstrip patch antenna

Reflection Coefficient =Return loss

$$S_{11}(dB) = 10\log_{10}\frac{P_{ref}}{P_{inc}} = 20\log\frac{|Z_A - Z_G|}{|Z_A + Z_G|} \tag{5.6}$$

$$S_L(dB) = 10\log_{10}\frac{P_{inc}}{P_{ref}} = -20\log\frac{|Z_A - Z_G|}{|Z_A + Z_G|} \tag{5.7}$$

Another measure for describing an antenna's behaviour is its radiation pattern. In the far field of an antenna, a radiation pattern is a three-dimensional depiction of the normalised power measured across a hypothetical spherical surface. The area surrounding an antenna in which the angular field distribution is unaffected

by the distance from the antenna is known as the far-field. You can think of the far-field as,

$R > 2D^2/\lambda$

where R is the distance away from the antenna, D is the largest dimension across the antenna structure, and λ is the operating wavelength. The next parameter is antenna gain, which is a representation of how much energy is concentrated in a specific direction with respect to the average energy radiated in all directions.

$$G(\theta, \phi) = \frac{U(\theta\phi)}{P_{in}/4\pi} \tag{5.8}$$

Where $U(\theta_\phi)$ represents the radiation intensity, and Pin is the net power accepted by the antenna. The gain is inherently a function ofθ and ϕ as shown in the formula, however often it is beneficial to know the maximum value, which is known as peak gain. The peak gain is useful because it can give a quick indication of an antenna efficiency and directivity when plotted versus frequency. Another quantitative description of an antenna is the radiation efficiency. The radiation efficiency is a ratio of the radiated power to input power.

$$e_r = \frac{P_{rad}}{P_{in}} = \frac{R_r}{R_r + R_L} \tag{5.9}$$

Where RL is the load resistance, also known as the antenna resistance, and Rr is the radiation resistance. An important factor to take into account is radiation efficiency since, even though an antenna exhibits good return loss and is absorbing power, this does not always correspond to the quantity of power emitted. The antenna's bandwidth is another important factor. The bandwidth of an antenna can be thought of as the precise frequency range on each side of its centre or resonant frequency where an antenna performance parameter falls within a reasonable range of values for those at the centre or resonant frequency. Either the absolute bandwidth or the fractional bandwidth can be used to describe an antenna's bandwidth. The absolute bandwidth, ABW, is expressed as a difference between the upper limit and the lower limit of the bandwidth. It is given

as where f_h and f_l are the upper limit and the lower limit respectively of the frequency range at a return loss of 10 dB loss.

Chapter 6

Design and development of metamaterial based microstrip patch antenna

6.1 Design and development of Metamaterial based patch antenna for 5G application

Microstrip patch antennas are being widely used for small wireless communication aerospace applications WiMAX, WLAN, and 5G applications. This antenna is compact lightweight and easy to design and fabricate. It can be designed in different shapes like rectangular, circular, and triangular. A patch antenna is designed on a dielectric substrate such as RT duroid with dielectric constant 2.2. The thickness of this dielectric substrate is 0.5 mm. If we use a substrate of higher thickness efficiency can be increased, however, as the height increases, surface waves are introduced which usually are not desirable because they extract power from the total available for direct radiation (space waves). The surface waves travel within the substrate and they are scattered at bends and surface discontinuities, such as the truncation of the dielectric and ground plane, and degrade the antenna pattern and polarization characteristics.Surface waves can be eliminated, while maintaining large bandwidths, by using metamaterials. If the impedance of the antenna does not match with the impedance of a transmission line then there will be a reflection of the signals and it causes high return loss and which will

lead to bad communication. [69], [70]. To avoid the problem of return loss, the antenna impedance should be matched with the transmission line impedance. To increase the bandwidth of patch antenna arrays can be used. Bandwidth also can be increased by loading metamaterial on a microstrip patch antenna. The authors have designed and simulated an Edge port-fed rectangular patch antenna for a 5G application using FEKO software. RT duroid 5880 a high-frequency laminate is used for designing a Patch antenna. The metamaterial-based Rectangular microstrip patch antenna (RMPA) is simulated and bandwidth, return loss, and gain are measured. Optimization is done by using FEKO software. A mu (single) negative metamaterial cells are loaded on the ground plane of the patch antenna. A significant improvement in patch antenna parameters has been observed.

6.1.1 Metamaterials, Double negative or Left-Handed metamaterials

They are artificial materials that show negative permittivity permeability and refractive index. These parameters are not found in natural materials. Due to the negative refractive index, phase velocities, as well as group velocity of electromagnetic waves are opposite to each other and opposite energy flow is observed. Metamaterials having either permittivity or permeability negative are called single negative metamaterials. Equations 6.1 and 6.2 are two of Maxwell's equations given to understand metamaterial[71]. [72]

$$\nabla \times E = -\mu_0 \mu_r \frac{\partial H}{\partial t} \tag{6.1}$$

$$\nabla \times H = -\epsilon_0 \epsilon_r \frac{\partial E}{\partial t} \tag{6.2}$$

$$\nabla^2 E = -\epsilon_0 \mu_0 \epsilon_r \mu_r \frac{\partial^2 E}{\partial t^2} \tag{6.3}$$

Where ϵ_r and μ_r are relative permittivity and permeability respectively and Equation 6.3 is a wave equation derived from the above equations. If ϵ_r and μ_r are

considered as real numbers, then one can observe that the wave equation does not change when signs of ϵ_r and μ_r are simultaneously changed. The Drude–Lorentz model describes the material properties in classical electromagnetic. The effective permittivity and permeability are given in equations

$$\epsilon_{eff} = 1 - \frac{f_p^2}{f^2 - j\gamma f} \tag{6.4}$$

$$\mu_e ff = 1 - \frac{f_{mp}^2 f_0^2}{f^2 - f_0^2 - j\gamma f} \tag{6.5}$$

The plasma frequency is denoted by f_p and f_{mp} in equations 6.4 and 6.5 f_0 is the resonance frequency, f is the frequency of the signal and damping factor γ , which is in connection to material losses. These equations can show microwave range to optical range properties of materials .

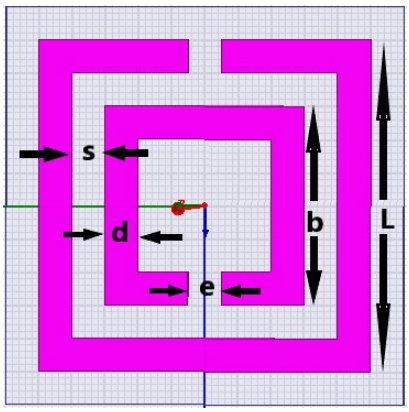


Figure 6.1: Square split-ring resonators (SSRR)

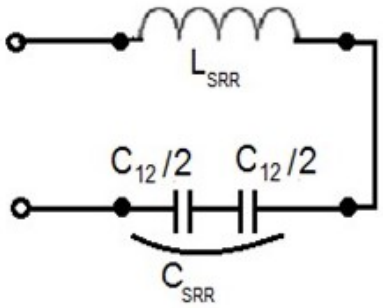


Figure 6.2: Equivalent circuit for SSRR

The SSRR Structure is designed using MATLAB code. In this way, a metal surface is obtained, as shown in (Fig,6.1) [70]. The equivalent circuit for SSRR is presented in (Fig,6.2). The inductance of the tank circuit model, Ls is calculated by assuming the uniform current throughout the loop. The capacitance of the tank circuit is assumed to be the parallel equivalent of the capacitances in each pair of adjacent loops. The SSRR creates a negative μ near resonance frequency. The magnetic field vector of the incident plane wave is perpendicular to the SSRR, which gives rise to the induced currents resulting in an effective magnetic moment

that eventually will yield the negative permeability. The metamaterial supported backward-wave propagation only for the magnetic field directed perpendicular to the SSRR. We have presented the retrieval of parameters of a metamaterial cell using MATLAB to verify the mu negativity of a cell. The inherent feature of CST is used to invoke its platform through MATLAB script file [40]

6.1.2 Design of square split ring resonator cell

The SSRR is designed on RT Duroid 5880 substrate with a permittivity value equal to 2.2 and thickness equal to 0.5 mm. The dimensions of 1x1 mm SSRR cell are, L= 0.9 mm, b=0.54 mm, s=0.05mm, d=0.06mm, and e=0.13mm. The resonance frequency is inversely proportional to the dimensions of the metamaterial cell and directly proportional to strip width and slit width.

6.1.3 Parameters of SSRR Metamaterial Cell

S_{11} and S_{21} of SSRR cell depicted in (Fig.6.3). The lowest magnitude of S_{11} indicates that the cell resonates at 26 GHz frequency. The Magnitude of S_{11} and S_{21} at 26 GHz frequency is 0.2 and 0.78 respectively. which shows that return loss is low at the resonance frequency. Both S parameters are important to calculate the epsilon and mu of the cell. Frequency v/s real and imaginary values of μ are plotted using MATLAB software. [73]

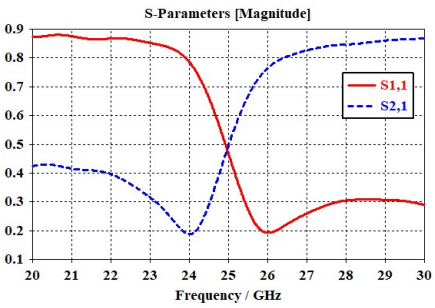


Figure 6.3: S_{11} and S_{21} of SSRR cell.

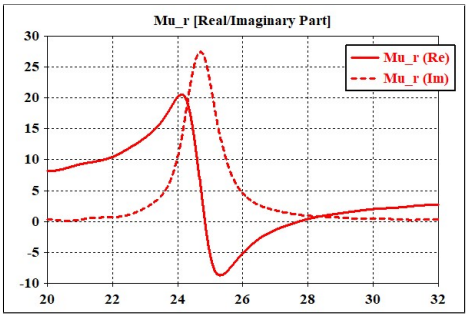


Figure 6.4: Real and imaginary values of μ of SSRR cell

Real and imaginary values of μ of SSRR are shown in(fig.6.4) . The nega-

tive mu appears in the frequencies between 24.8 GHz to 28 GHz. Therefore the antenna on metamaterial must be designed to operate within the range of frequencies. Hence, in this project, we considered a resonance frequency of 26 GHz. which is one of the frequency bands used for 5G applications.

6.1.4 Method to find parameters of metamaterial cell of complex Structure

It is sometimes difficult to calculate the effective parameters of certain metamaterials, due to the complex structure. In such cases, parameters can be found out from numerical simulations. First, we have to find out the transmission and reflection coefficient of the cell-based on numerical algorithms, such as (FDTD) and Finite Element Method (FEM). This method also can be used to extract parameters.

$$Z_{eff} = \pm\sqrt{\frac{(1+S_{11})^2 - S_{21}^2}{(1-S_{11})^2 - S_{21}^2}} \tag{6.6}$$

$$\eta_{eff} = \pm\frac{1}{kod}[[In(e^{i\eta_{eff}kod})] + 2m\pi - i[In(e^{i\eta_{eff}kod})]] \tag{6.7}$$

$$e^{i\eta_{eff}kod} = \frac{S_{21}}{(1 - S_{11}[(Z_{eff}-1)/(Z_{eff}+1)])} \tag{6.8}$$

equations6.6 and 6.7 refrective indexand and impedance tranmission coefficient (S_{21}) and reflection coefficient (S_{11}). wherek_0 is the wave vector in a vacuum, defined as $k_0 = \frac{2\pi}{\omega_0}$, d is the thickness of the substrate, and m is an integer. We can find Z_eff and η_{eff} from the above equation. Considering that metamaterial are passive media, That is a real part of the impedance is the positive and the imaginary part of the refractive index is negative. Further $\epsilon_{r,eff}$ and$\mu_{r,eff}$ can be obtained according to ,$\epsilon_{r,eff} = \eta_{eff}/Z_{eff}$ and $\mu_{r,eff} = \eta_{eff}Z_{eff}$

6.1.5 Edge Port fed Rectangular Microstrip patch Antenna (RMPA) Design on Substrate without Metamaterial

The design of Edge fed RMPA without metamaterial on RT duroid 5880 substrates is shown in (Fig.6.5) [70]

RMPA Design

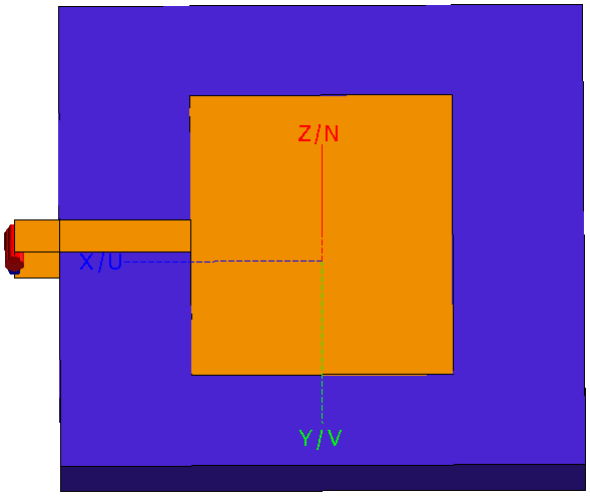


Figure 6.5: Design of edge-fed RMPA without metamaterial

Rectangular microstrip patch antenna. (RMPA) design on RT Duroid substrate with edge port feed at resonance frequency 26 GHz as employed in 5G communication and tested on software FEKO. The width of RMPA Effective permittivity and fringing length ΔL are shown in the equations shown below.[27] h=height of the substrate, w=width of rectangular patch L=Length of RMPA C_O =Speed of electromagnetic wave [20]

$$W = \frac{C_0}{2f_r}\sqrt{\frac{2}{\epsilon_r + 1}} \tag{6.9}$$

$$\epsilon_{reff} = \frac{\epsilon_r + 1}{2} + \frac{\epsilon_r - 1}{2}(1 + \frac{12h}{W})^{-1/2} \tag{6.10}$$

$$\Delta L = h\,(0.412)\,\frac{(\epsilon_{reff} + 0.3)\left(\frac{w}{h} + 0.264\right)}{(\epsilon_{reff} - 0.258)\left(\frac{w}{h} + 0.8\right)} \tag{6.11}$$

$$L_{eff} = \frac{C_0}{2f_r\sqrt{\omega_{reff}}} \tag{6.12}$$

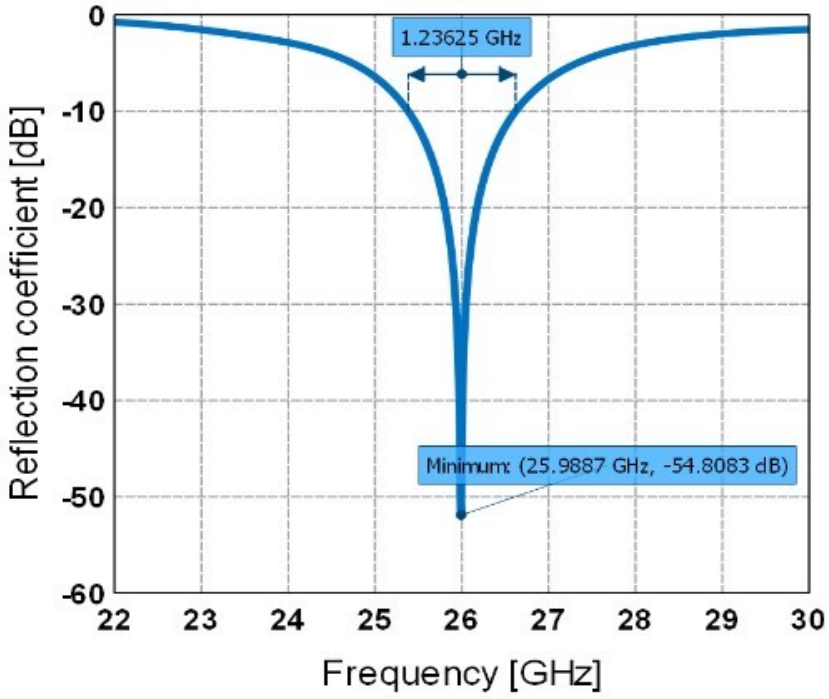


Figure 6.6: Reflection coefficient v/s frequency of RMPA without metamaterials

The reflection coefficient v/s frequency graph of RMPA is shown in (Fig.6.6). The antenna resonates at the resonance frequency 26 GHz. Design of edge fed RMPA without metamaterials is shown in Table 6.1. Resonance freq. = 26 GHz, Substrate: RT Duroid 5880, ϵ_r = 2.2, Loss tangent : 0.0009, height of substrate(h) = 0.5 mm. At resonance frequency, the return loss is very low (-54dB), which means the maximum power is radiated by the antenna.Fig.6.7 is a smith chart showing impedance matching of RMPA at 26 GHz. The impedance of the patch is zero at the center and increases to words edges. If at the edges impedance is very high then a quarter-wave transformer should be used for impedance matching. Otherwise, a microstrip line will match the 50 ohms port impedance.

Table 6.1: Design of RMPA without metamaterial

Patch dimensions	Calculated dimensions of patch antenna (mm)	Optimized dimensions of Patch antenna without metamaterial(mm)
Width of patch(W)	4.56	4.26
Length of patch (L)	3.57	3.25
Sub. width (Ws)	7.56	7.0
Sub. length (Ls)	6.57	6.5
Feed length	1.63	1.63
Feed width		0.49

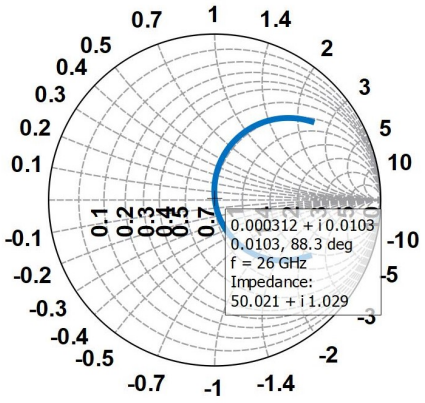


Figure 6.7: Smith chart showing impedance matching at 26GHz.

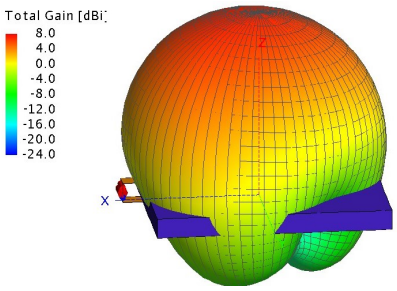


Figure 6.8: 3D view of far-field of an RMPA without metamaterials at 26 GHZ

The gain of an antenna is a very important parameter, gain should be very close to directivity so that the efficiency of the patch antenna increases.Fig.6.8 presents a 3D view of the far-field of an edge-fed patch antenna without metamaterial at 26GHz.The far field figure also depicts total gain of the antenna.[43]

6.1.6 Application of Metamaterial in designing edge port fed rectangular microstrip patch antenna.

Edge port fed rectangular microstrip patch antenna (RMPA) design with metamaterial at 26 GHz resonating frequency

Antennas can be fabricated using DNG or SNG Metamaterial cells. Which is used to increase the performance of the system. These cells could substantially

Table 6.2: Design of Edge port fed RMPA with metamaterial

Patch dimensions	**Optimized dimensions of Patch antenna with metamaterial(mm)**
Width of patch(W)	4.26
Length of patch (L)	2.9
Sub. width (Ws)	6.5
Sub. length (Ls)	6
Feed length	1.55

increase the gain and radiated power of an antenna. Furthermore, these antennas can improve efficiency-bandwidth performance. Various metamaterial-based antennas can be used for wireless communication, Cell phones, etc. Fig.6.9 depicts the design of edge-fed RMPA with metamaterial cells on the ground plane of the antenna.Fig.6.10 Shows reflection coefficient v/s frequency graph of RMPA with metamaterial [74] [75]

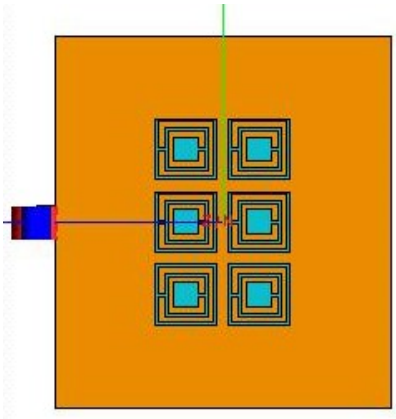


Figure 6.9: Design of metamaterial-loaded RMPA.

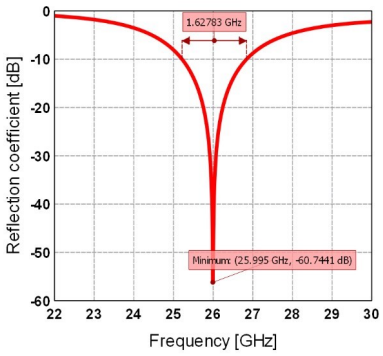


Figure 6.10: Reflection coefficient v/s frequency of metamaterial loaded RMPA

The optimized design of edge-fed microstrip patch antenna with metamaterial is shown in Table6.2. The patch antenna is designed on RT Duroid substrate. Resonance frequency = 26 GHz, Substrate: RT Duroid 5880 . $\epsilon_r = 2.2$, $Losstangent = 0.0009$, $heightofsubstrate(h) = 0.5mm$ (Fig.6.10) shows the reflection coefficient v/s frequency graph of RMPA with metamaterial. At the res-

onance frequency, the return loss is very low (-55dB), which means the maximum power is radiated by the antenna. (Fig.6.11) is a Smith chart showing impedance matching of RMPA with metamaterial at 26 GHz. At 26GHz the impedance is almost 50 ohms and reactive impedance is almost zero, which matches with source impedance. (Fig.6.12) presents the 3D view of the far-field of RMPA with metamaterials at 26 GHz resonance frequency. Total gain has been depicted in the figure. At 26GHz the impedance is almost 50 ohms and reactive impedance is almost zero, which matches with source impedance.

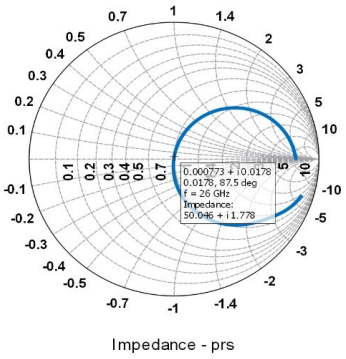


Figure 6.11: Smith chart.

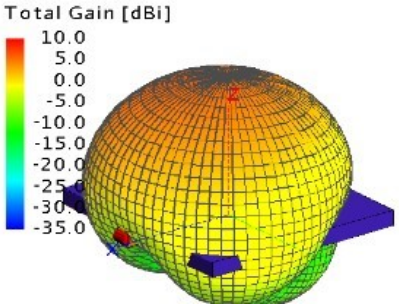


Figure 6.12: 3D view of the far-field of RMPA with metamaterials at 26 GHz resonance frequency

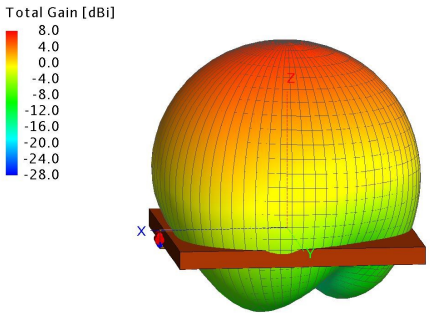


Figure 6.13: 3D view of far field of RMPA with metamaterials at 25 GHz

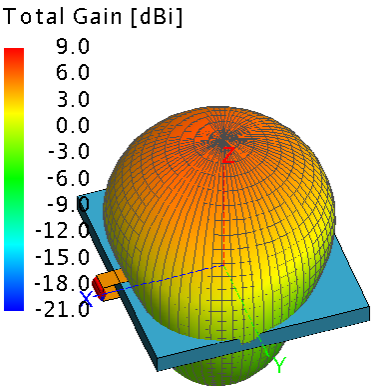


Figure 6.14: 3D view of far field of RMPA with metamaterials at 27 GHz

(Fig.6.12)(Fig.6.13) (Fig.6.14) presents the 3D view of far field of RMPA with metamaterials at 26 GHz,25 GHz and 27 GHz resonnce frequency respectively . The radiation performance in the antenna indicates the efficiency of the radiation

measured in terms of percentage and is obtained by calculating the value of the ratio of the amount of power feed to the antenna to that of the power emitted (radiated) from an antenna . This radiation efficiency boost the performance of the antenna useful for 5G wireless technology and its applications . The author's proposed antenna has higher radiation efficiency of 90.5% at 26 GHz.

6.1.7 Application of metamaterial in designing edge port fed Circular Microstrip Patch Antenna (CMPA).

Circular microstrip patch Antennas are designed using DNG or SNG Metamaterial cells. Which is used to increase the performance of the system. These cells could substantially increase the gain and radiated power of an antenna. Furthermore, these antennas can improve efficiency-bandwidth performance. Various metamaterial-based antennas can be used for wireless communication.

CMPA Design on Substrate without Metamaterial.

(6.13)

$$r = \frac{F}{\left(1 + \frac{2h}{\pi\epsilon_r F}\left[\ln\left(\frac{\pi F}{2h}\right) + 1.7726\right]\right)^{1/2}} \tag{6.14}$$

$$F = \frac{8.791 \times 10^9}{f_r\sqrt{\epsilon_r}} \tag{6.15}$$

(Fig.6.15) shows design of coaxial feed circular patch antenn Circular microstrip patch antenna (CMPA) design on RT Duroid substrate with edge port feed at resonance frequency 26 GHz as employed in 5G communication and tested on software FEKO. The radius of the the circular patch of CMPA is given by equation 6.16, [65]. Where r is the actual radius and F is the effective radius of the circular patch, h is the height of the substrate.The top view of antenna is shown in (Fig.6.15)

Design of edge fed CMPA without metamaterials is shown in Table6.3 Resonance freq. = 26 GHz, Substrate: RT Duroid 5880, ϵ_r = 2.2 Loss tangent =

Table 6.3: Design of Edge port fed CMPA without metamaterial

Patch dimensions	**Calculated dimensions of patch antenna (mm)**	**Optimized dimensions of Patch antenna without metamaterial(mm)**
Radius of patch	2.2	2.1
Sub. width (Ws)	7.4	7.2
Sub. length (Ls)	7.4	7
Feed length	1.4	1.4

0.0009,height of substrate(h) = 0.5 mm. (Fig.6.16) shows the reflection coefficient v/s frequency graph of CMPA. The return loss at resonance frequency is very low (-56 dB), which means the maximum power is radiated by the antenna.(Fig.6.17) Is a smith chart showing impedance matching of RMPA at 26 GHz. The impedance of the patch is zero at the center and increases towards edges. If at the edges impedance is very high then a quarter-wave transformer should be used for impedance matching. The graph of VSWR v/s frequency is presented in (Fig.6.18) VSWR of CMPA is 1.0 at 26 GHz. VSWR (voltage standing wave ratio) is the measure of RF power that is transmitted into a load. We would like to cite one example, power amplifier is connected to an antenna through a transmission line, ideally there will be no reflections and full signal from the power amplifier will be transmitted to the antenna. However in this world, no system is ideal, there will be some mismatches which will cause some of the signal to get reflected back in to the transmission line. If VSWR is one that means the system is perfectly matched.

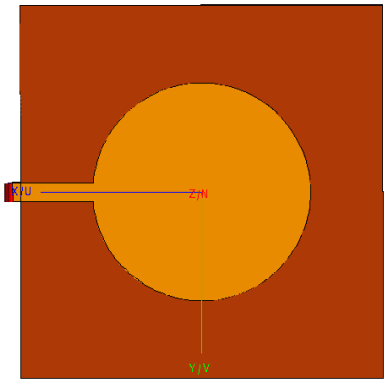


Figure 6.15: Design of CMPA.

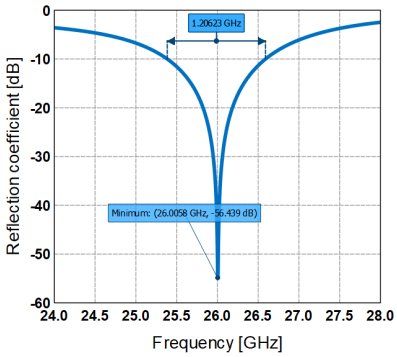


Figure 6.16: Reflection coefficient v/s frequency graph of CMPA without metamaterial

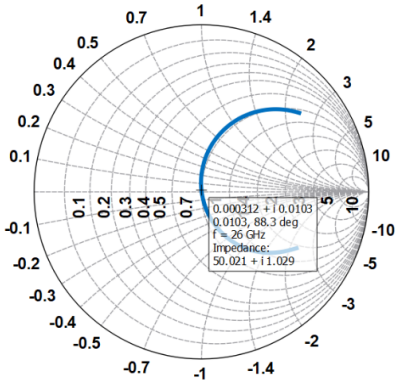


Figure 6.17: Smith chart showing impedance matching of CMPA.

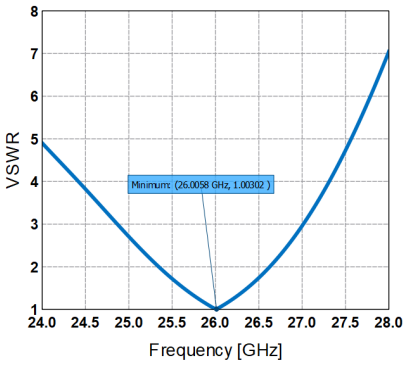


Figure 6.18: VSWR v/s Frequency of CMPA

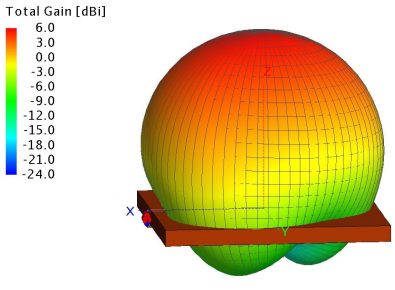


Figure 6.19: 3D view of the far-field of a CMPA without metamaterials at 25 GHz resonance frequency

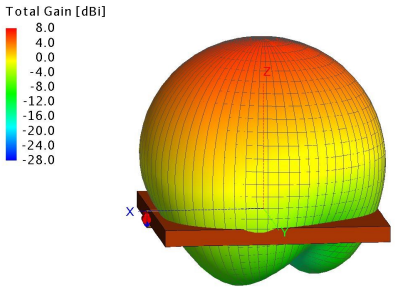


Figure 6.20: 3D view of the far-field of a CMPA at 26 GHz resonance frequency

The gain of an antenna is a very important parameter, gain should be very close to directivity so that the efficiency of the patch antenna increases. (Fig.6.19) and (Fig.6.20)presents a 3D view of the far-field of an edge-fed patch antenna without metamaterial at 25GHz and 26 GHz respectively.The total gain of an antenna

Table 6.4: Design of Edge port fed CMPA with metamaterial

Patch dimensions	Optimized dimensions of Patch antenna (mm)
Radius of patch(W)	1.92
Sub. width (Ws)	7.4
Sub. length (Ls)	6.75
Feed length	1.45
Feed width	0.34

also has been depicted in the figure. The gain is 8 dBi and 6 dBi at 26 GHz and 25 GHz respectively. The optimized design of edge-fed microstrip patch antenna with metamaterial is shown in Table6.4. The patch antenna is designed on RT Duroid substrate. Resonance freq. = 26 GHz, Substrate: RT Duroid 5880, ϵ_r = 2.2, Loss tangent =0.0009, height of substrate(h) = 0.5 mm.

The antenna with metamaterial loaded is depicted in (Fig.6.21) and (Fig.6.22) shows the reflection coefficient v/s frequency graph of CMPA with metamaterial. At the resonance frequency, the return loss is very low (-43dB), which means the maximum power is radiated by the antenna. (Fig.6.23)is a Smith chart showing impedance matching of CMPA with metamaterial at 26 GHz. At 26GHz the impedance is almost 50 ohms.(Fig.6.24) depicts the graph of VSWR v/s Frequency. The value of VSWR is 1.0.

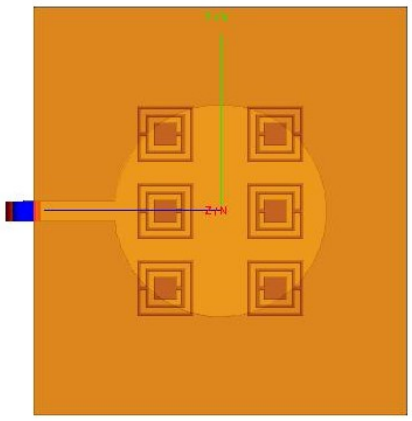


Figure 6.21: CMPA with metamaterial

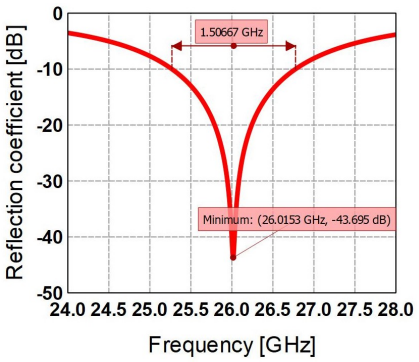


Figure 6.22: Reflection coefficient v/s Frequency of CMPA with metamaterial

(Fig.6.25) depicts the 3D view of the far-field of a CMPA at 26GHz resonance frequency. (Fig.6.26) is a 3D view of the far-field of a CMPA at 25 GHz frequency. (Fig.6.27)shows the Directivity of an antenna at 26 GHz. (Fig.6.28)3D view of a Theta gain of a CMPA at 26 GHz frequency. It is a gain at theta equal to zero and phi equal to 90 degrees.

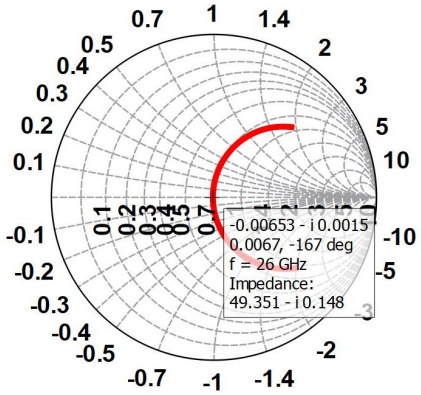


Figure 6.23: Smith chart showing impedance matching of CMPA with metamaterial

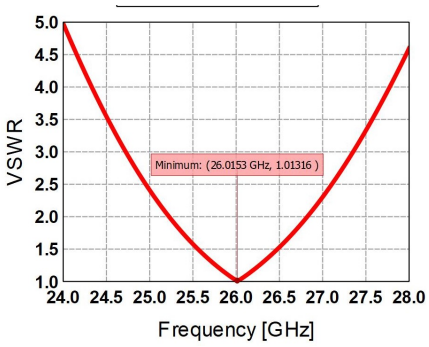


Figure 6.24: VSWR v/s Frequency of CMPA with metamaterial

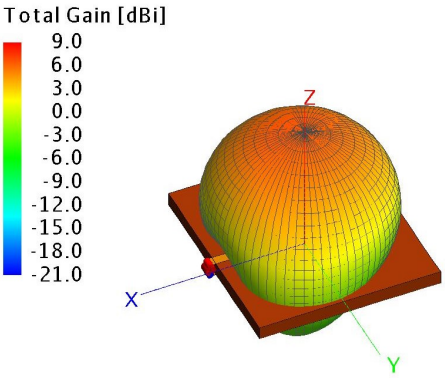


Figure 6.25: 3D view of the far-field of a CMPA at 26GHz resonance frequency

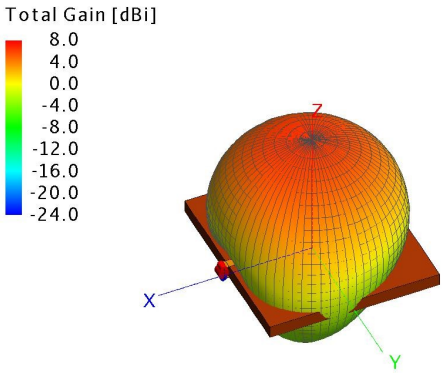


Figure 6.26: 3D view of the far-field of a CMPA at 25 GHz resonance frequency

Table 6.5: Different parameters of RMPA.

Parameters	RMPA without metamaterial	RMPA with metamaterial
Reflection coefficient	-54dB	-60.7 dB
Bandwidth (10dB)	1.23 GHz	1.62 GHz
Gain	8 dBi	10 dBi
VSWR	1.1	1.04

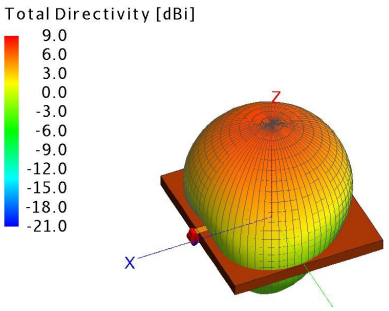


Figure 6.27: Directivity of antenna.

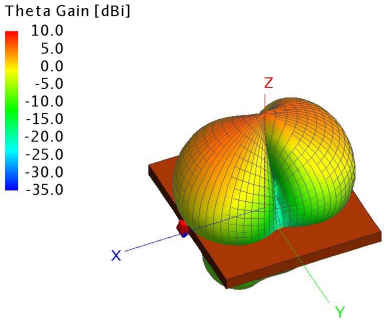


Figure 6.28: 3D view of theta gain of of a CMPA at 26 GHz frequency

6.1.8 Simulation results

The metamaterial cell comprising of SSRR is designed and simulated using MATLAB software, it has been found that the cell with SSRR is a single or mu negative cell that shows negative permeability. The comparison of the parameters of RMPA with and without metamaterial are listed in Table 6.5 And the comparison of the parameter of Conventional edge fed CMPA and CMPA loaded with metamaterial is listed in Table 6.6 on the ground plane is designed and simulated using FEKO, It has been observed that the gain and bandwidth of patch antenna increases in comparison to RMPA without metamaterial. RMPA loaded with and without metamaterial are simulated using FEKO, It has been found that the bandwidth of antenna loaded with metamaterial cells increases considerably in comparison to RMPA without cells. RMPA without cells returns loss and bandwidth are –54 dB and 1.23 GHz respectively. Whereas RMPA with metamaterial

Table 6.6: Different parameters of CMPA.

Parameters	**CMPA without metamaterial**	**CMPA with metamaterial**
Reflection coefficient	-56dB	-43.6 dB
Bandwidth (10dB)	1.20 GHz	1.50 GHz
Gain	8 dBi	9 dBi
VSWR	1.0	1.01

the values of return loss and bandwidth are -60.7 dB and 1.62 GHz respectively. Gain of conventional RMPA is 8 dBi and gain of antenna with metamaterial cells is found to be equal 10 dBi. So the bandwidth is increased by 400 MHz and gain is increased by 2 dBi. Based on simulated results it has been found that the bandwidth and gain of RMPA have improved. VSWR of the conventional antenna is 1.1 and that of the antenna with metamaterial is 1.02. Smaller the value better is impedance matching. The lowest value of VSWR for ideal antenna is equal to one. Conventional CMPA metamaterial loaded CMPA are simulated using FEKO, It has been found that the bandwidth of antenna loaded with metamaterial cells increases considerably in comparison to CMPA without cells. CMPA without cells returns loss and bandwidth are –56 dB and 1.20 GHz respectively. Whereas CMPA with metamaterial the values of return loss and bandwidth are -43.6 dB and 1.50 GHz respectively. Gain of CMPA without and with cells are found to be equal to 8 dBi and 9 dBi respectively. The bandwidth is increased by 300 MHz and the gain is increased by 1 dBi. Based on simulated results it has been found that the bandwidth and gain of CMPA have improved. VSWR of the conventional antenna is 1.0 and that of the antenna with metamaterial is 1.01.

6.2 Patch antenna design using complementary split ring resonator

This section discusses a band width improvement of circular patch antenna (CPA) realized by using electromagnetic metamaterial and operating at 12GHz resonance frequency. Electromagnetic Metamaterial is a artificial material which is made up of different structures on dielectric substrates. This structure is called unit cell of metamaterial. Periodic arrangement of this unit cell forms Metamaterial. Material consist of an atoms in the same way metamaterials are having small metallic resonators of different shapes depending on resonance frequency. This is having effect on external Electromagnetic waves. Circular patch antenna substrate is loaded with CSRR. Conventional patch antenna and proposed patch antenna are simulated using FEKO software. The bandwidth of both antennas are compared.[71]

6.2.1 Metamaterials

Material which shows both permeability and permittivity negative are referred to as double negativ metamaterials (here after written as metamaterial). Refractive index of metamaterial is -ve. The metamaterials which are having electric permittivity and magnetic permeability close to zero, But less than zero are called Zero Index metamaterials. Metamaterials is made up of periodic array of metallic resonant elements. The wavelength is very much higher than lattice constant of metamaterials. Electromagnetic waves bend in the gradient refractive index medium. A novel antenna design on metamaterials (CSRR) substrate for higher band width is discussed here, and presented the simulated characteristics of the proposed antenna. Many researchers has studied split ring resonators (SRRs). The electric and magnetic boundary conditions are exchanged in CSRR, This dual structure behaves like a dipole, whose propagation properties are just like negative-epsilon medium CPA on a metamaterials substrate with complimentary

split rings resonator (CSRRs) based ground plane have been simulated and observed the bandwidth, and other radiation parameters. The comparison of the BW between the CPA with and without metamaterials substrate is presented.

6.2.2 Double negative metamaterial

They are also called as Left-Handed metamaterials or Negative refractive index metamaterials. Metamaterials are artificial materials which shows negative permittivity ,permeability and refractive index, These parameters are not found in natural materials. Due to negative refractive index, phase velocities as well as group velocity of electromagnetic waves are opposite to each other and opposite energy flow is observed. Negative refraction can be achieved when both μ_r and ϵ_r are negative, Ifϵ_r and μ_r are considered as real numbers, then one can observe that the wave equation do not change when signs of ϵ_r and μ_r are simultaneously changed.[1] Due to the afore mentioned facts, these materials are known as left handed material. The Drude–Lorentz model describes the material properties in classical electromagnetic.Complimentary split ring resonator that is complement of split ring resonator is used.

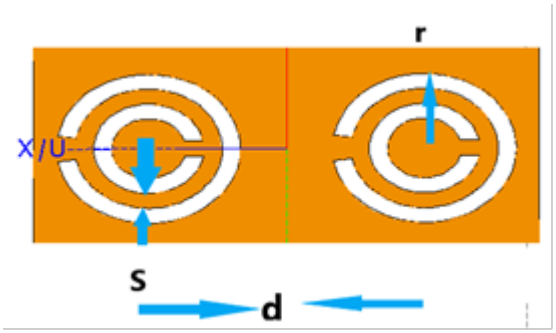


Figure 6.29: Complementary split ring resonators (CSRR)

Complementary split ring resonators (CSRR) is depicted in (Fig.6.29) , with outer radius r and width of ring s between the two gaps. Complementary split ring resonator (CSRR) structures is complementary to double split rings were designed by applying the babinet principle to the split rings . Which gives metal surface as shown in (Figure6.29).These CSRRs create negative ϵ instead of μ in

a narrow range near the resonance frequency.It is sometimes difficult to calculate the effective parameters of certain metams, due to the complex structure. In such cases parameters can be found out from numerical simulations. The first step is to find the transmission and reflection coefficient of the metamaterial.Then the refractive index and impedance is calculated, from transmission coefficient (t) and reflection coefficient (r) Further epsilon and mu is calculated from these parameters (Refer section 6.1.4)

6.2.3 Application of metamaterials in designing circular patch antenna

Antennas are fabricated using DNG or SNG metamaterials. Which is used to increase the performance of the system. The metamaterial could substantially increase the radiated power of an antenna. Increase gain of antenna. Furthermore, These antennas can improve efficiency-bandwidth performance. Improvement in antenna performance is boosted by using metamaterials which shows negative permittivity, (ENG), a negative magnetic permeability (MNG), or both are negative,which are called as left handed metamaterials.

6.2.4 Circular patch antenna design on circular substrate without Metamaterial

Circular patch antenna design on circular substrate without Metamateri and with coaxial feed at resonance frequency 12 GHz (used in Wireless communication and tested on software FEKO. Radius of patch antenna is given by equation 6.16

$$r = \frac{F}{\left(1 + \frac{2h}{\pi\epsilon_r F}\left[\ln\left(\frac{\pi F}{2h}\right) + 1.7726\right]\right)^{1/2}} \tag{6.16}$$

$$F = \frac{8.791 \times 10^9}{f_r\sqrt{\epsilon_r}} \tag{6.17}$$

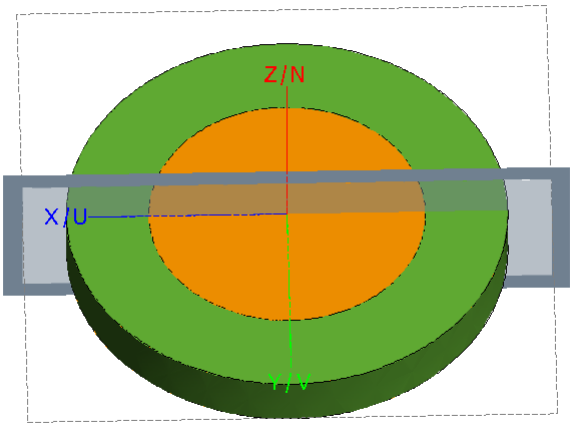


Figure 6.30: coaxial feed circular patch antenna on circular substrate

(Fig. 6.30) shows design of conventional coaxial feed circular patch antenna on circular substrate obtained from FEKO. h=height of substrate, r=radius of circular patch Resonance freq. = 12 GHz Substrate :RT/duroid , r= 2.2 , h=1.58 mm, Radius = 4.38 mm F=4.94 Coaxial feed=2.22mm Substrate Radius =6.2 mm

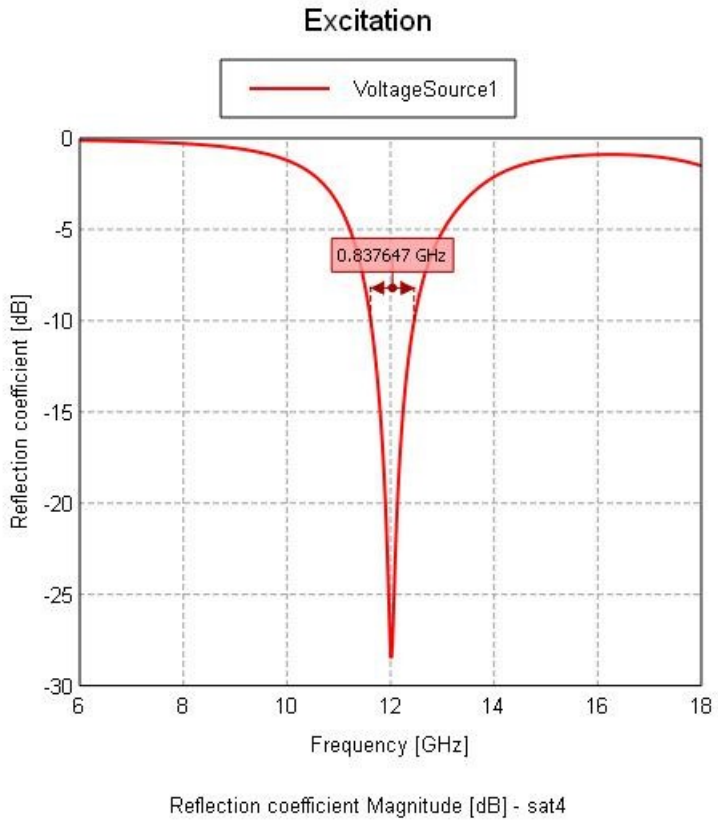


Figure 6.31: Reflection coefficient v/s frequency of CPA without metamaterial

(Fig.6.31)Shows graph of reflection coefficient v/s frequency of CPA without

metamaterial. The BW of CPA is 837 MHz and Return loss = -29 dB

6.2.5 Circular patch antenna design with Metamaterials

Circular patch antenna design with metamaterials and with coaxial feed at resonance frequency 12 GHz . Substrate :RT/duroid. Resonance frequency = 12 GHz , ϵ_r = 2.2

h = 1.58 mm

Loss tangent =0.002

Calculated parameters

Radius = 4.01 mm

F = 4.94

Substrate radius =6.4mm

Coaxial feed=2.37 mm

CSRR design.

Permittivity of dielectric substrate =2.2

Outer radius of first ring (outer ring)= 2.2 mm

Inner radius of first ring = 1.8 mm.

S is the gap between the internal and external ring =0.2mm.

Outer Radius of Second ring (inner ring)= 1.6mm.

Inner radius of second ring =1.2 mm

Split or Gap = 0.2mm.

Wavelength= 25 mm.

Lattice constant =6 mm.

(Fig.**??**) shows the ground plane and design of coaxial feed CPA on circular substrate obtained from FEKO.(with metamaterial)

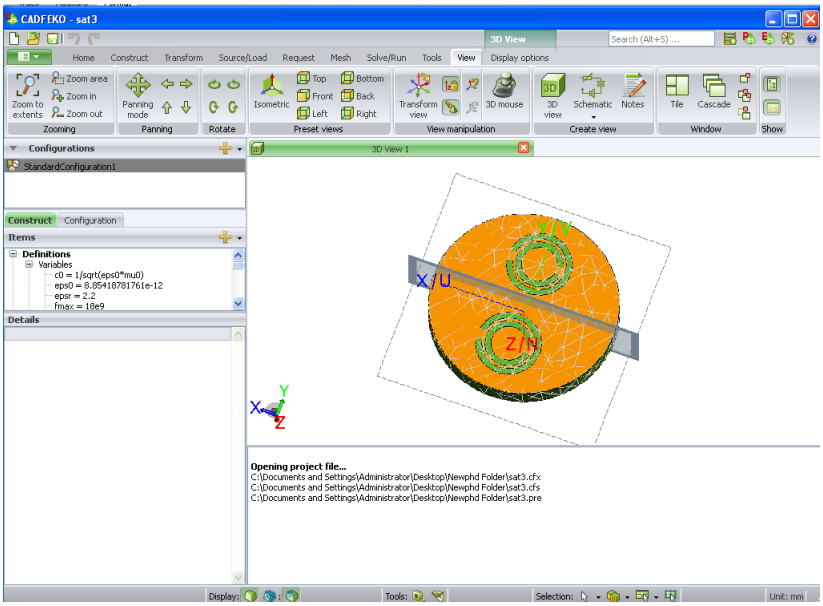


Figure 6.32: CPA on circular substrate with Metamaterial

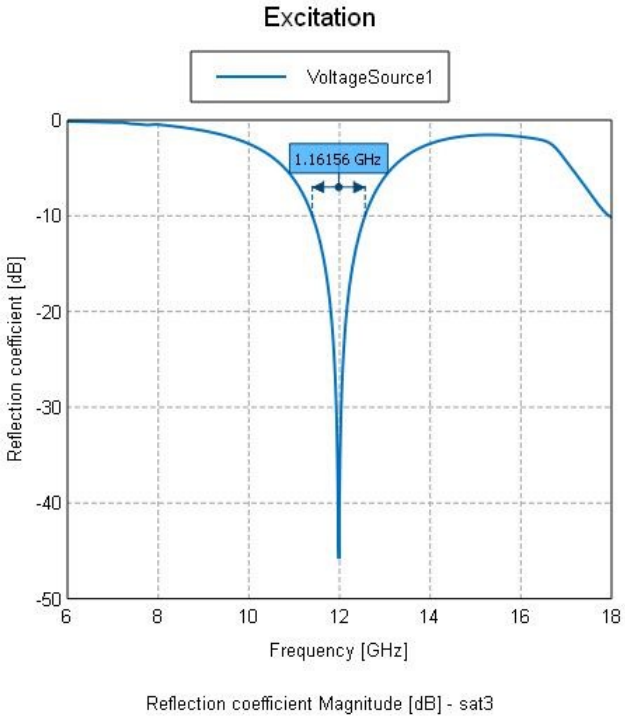


Figure 6.33: Reflection coefficient v/s frequency of CPA with metamaterials

6.2.6 Simulation Results

When the CPA with the proposed metam Structure on circular shape substrate is simulated using FEKO ,It has been found that the bandwidth of antenna increases in comparison to CPA without metam. CPA without metam Return loss and bandwidth are - 29dB and 837 MHz respectively. This antenna with

metam loaded the values of Return loss and bandwidth are -45dB 1.161 GHz respectively. So the bandwidth is increased by 324 MHz. On the basis of the simulated results it is found that the CPA bandwidth has improved.

6.3 Design and development of coaxial feed circular patch antenna on a metamaterial substrate

Metamaterial is made up of periodic array of metallic resonant elements. Size of an element and unit cells are small relative to wavelength. Lattice constants of metamaterials are much smaller than the wavelength. Electromagnetic waves bend in the gradient refractive index medium. The split ring resonator which gives negative permeability acts just like an artificial magnetic dipole. The distance between both the rings i.e Space between the two consecutive rings acts as a capacitor while the rings behaves like an inductor ,Which becomes LC resonant circuit. Just below resonance, the magnetic dipole due to the split rings will lag the H field nearly 180 degree to give negative permeability. Negative permittivity is obtained by the array of thin wire of aluminum, silver, and gold. We can verify the value of ϵ andμ theoretically with the help of mathematics.

6.3.1 μ (mu)negative metamaterial structures

Split ring resonators (SRRs) are one of the original designs for strong artificial magnetism. Each SRR consists of concentric split rings that may be two or three with the gap in the opposite directions. From the point of view of equivalent circuits, an SRR can be considered as an LC circuit with the natural resonant frequency given by$\omega_0 = 1/\sqrt{LC}$ with L and C denoting the geometric inductance and capacitance of the SRR structure, respectively. Within a certain frequency region centred at the vicinity of ω_0 the magnetic flux is produced at SRR or CSSR The strong circulating current are induced resulting in an effective magnetic moment. CSSR The formula to calculate dimensions of CSSR are given in chapter

3 Complementary split ring resonators (CSRR), with outer radius r and width of ring s between the two gaps

Complementary Split Rings (CSRR) Structures complementary to double split rings were designed by applying the Babinet principle to the split rings . In this way structures with apertures in metal surface are obtained, These complementary split rings (CSRR) create negative ϵ instead of μ in a narrow range near the resonance frequency. Alternatively we can obtain the effective parameters from numerical simulations.

6.3.2 Circular patch antenna design without Metamaterial and with coaxial feed at resonance frequency 10GHz (used in Wireless communication and tested on software FEKO

Circular patch antenna without metamaterials is shown in fig.6.34,freq v/s Reflection coeficient is shown in (Fig.6.35a). Circular patch antenna without metamaterial is shown in , h=height of substrate, r=radius of circular patch Resonance freq. = 10 GHz Substrate :RT/duroid , ϵ_r=2.2 h = 1.58 mm. Loss tangent =0.0002

Calculated parameters.

Radius =5.5 mm, F =5.92, Coaxial feed=3.2mm

Substrate dimensions

Lsub =20 mm, Wsub = 20 mm.

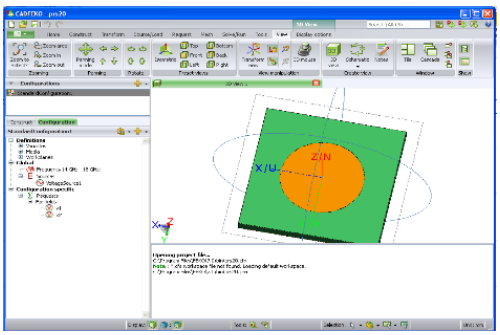
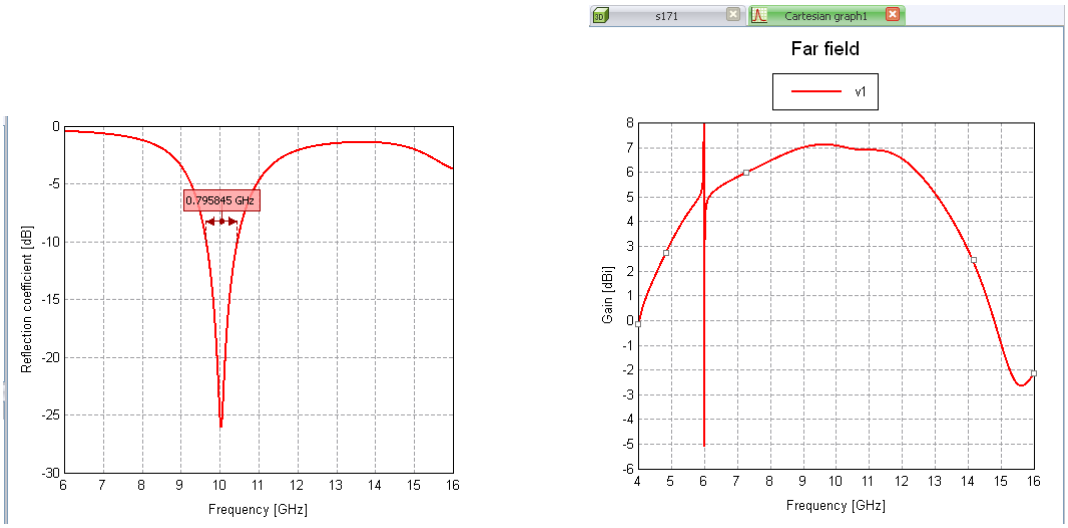


Figure 6.34: Circular patch antenna without Metamaterial

Graph of frequency v/s reflection coefficient of circular patch antenna without metamaterial is shown(Fig.6.35a), the bandwidth is equal to 795 MHz and reflection coefficient is equal to -26 dB.



(a) Frequency v/s Reflection coefficient(without Metamaterial

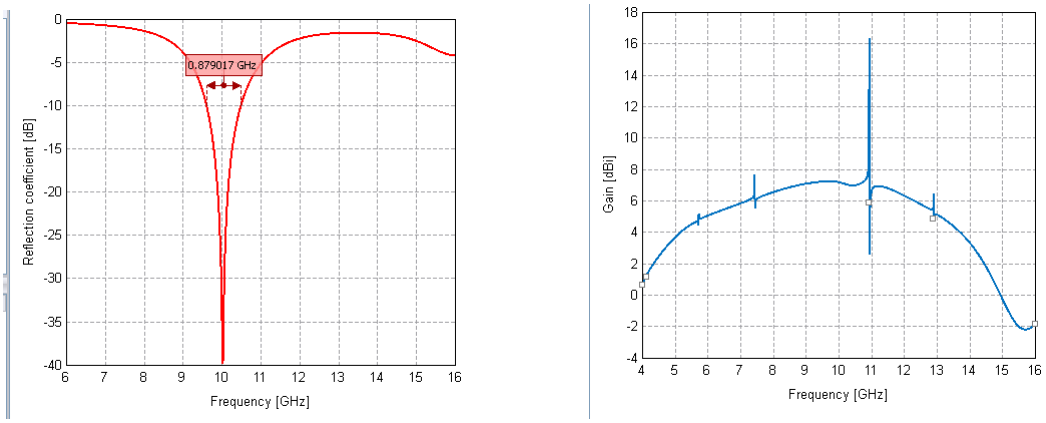
(b) Frequency v/s Gain (without metamaterial

Figure 6.35: Circular antenna parameters)

Frequency v/s gain graph of antenna without metamaterial is shown in (Fig.6.35b) . Gain remain constant through out band of frequencys. And it is equal to 7 dBi

6.3.3 Patch antenna design with Metamaterial and with coaxial feed at resonance frequency 10GHz (Tested on software FEKO)

Antennas are fabricated using double negative (DNG) or single negative (SNG) metamaterials. Which is used to increase the performance of the system. The metamaterials could substantially increase the bandwidth of antenna radiated power of an antenna. Increase gain of antenna. (Fig.6.36a)frequency v/s reflection coefficient (with metamaterial). frequency v/s gain graph of antenna with metamaterial is shown in (Fig.6.36b). Gain remain constant through out band of frequency. Increase in bandwidth is observed keeping the gain same as that of the patch antenna without metamaterial. The gain is found to be equal to 7 dBi.



(a) Freq v/s Reflection coefficient(with Metamaterial

(b) Frequency v/s gain graph of antenna with metamaterial

Figure 6.36: Parameters of metamaterial loaded circular antenna

Table 6.7: Different parameters of circular patch antenna

Parameters	**Patch antenna without metamaterials)**	**patch antenna with metamaterial)**
Reflection coefficient	-26 dB	-40 dB
Bandwidth(-10 dB)	795 MHz	880 MHz
Gain	7 dBi	7 dBi
3 db beam width	79 degree	73 degree

6.3.4 Simulation Results

The simulated results are presented in this section. When the circular patch antenna with the proposed metamaterial Structure is simulated at 10 GHz using FEKO software, it has been found that the bandwidth of antenna increases significantly in comparison to circular patch antenna without metamaterial. Circular patch antenna without metamaterial Reflection coefficient and bandwidth are 26 dB and 795MHz respectively. This antenna with metamaterial loaded the values of Reflection coefficient and bandwidth are -40dB and 880 MHz respectively. So the bandwidth is increased by 85 MHz. Gain remain constant through out bandwidth. .Increase in bandwidth is observed keeping the gain same as that of the patch antenna without metamaterial.And it is equal to 7 dBi .Comparison of 3db

beam width and other parameters is shown in Table 6.7

6.4 Design and Extraction of Parameters of Metamaterial cell and its Application to enhance the performance of Patch Antenna

Extraction of parameters of a square split ring resonator with a metal strip on a ground to verify double negativity of a cell and only square split-ring resonator to verify mu negativity of cell. A rectangular microstrip patch antenna is loaded with mu negative metamaterial cells. This helps in the improvement of patch antenna parameters. The coaxial feed rectangular patch antenna is operating at 2.8 GHz resonance frequency. A novel antenna design on square split ring resonator (SSRR) substrate for higher bandwidth is discussed here and presented the simulated characteristics of the proposed antenna. Also, a cell comprising of SSRR is designed and simulated to find mu negativity of a cell at the same resonance frequency. The proposed double negative and mu negative metamaterial cells are designed and tested using MATLAB. A conventional antenna and a proposed novel coaxial feed rectangular microstrip patch antenna (RMPA) with resonance frequency 2.8 GHz and a ground plane of the substrate is loaded with square split-ring resonators is simulated using FEKO software, analyzed and comparison of parameters such as bandwidth, return loss, gain and VSWR is presented. This patch antenna is designed on FR-4 substrate with permittivity value equal to 4.4 and thickness equal to 1.6 mm.FR-4 material is cheaper and easily available. Surface wave propagation is reduced by metamaterial-loaded substrate, thereby increasing the performance of an antenna.

6.4.1 Double negative metamaterial

They are also called Left Handed or Negative refractive index metamaterials. They show negative permittivity, permeability, and refractive index. The phase

velocities and group velocities of electromagnetic waves are opposite to each other due to the negative refractive index, and contrary energy flow is detected

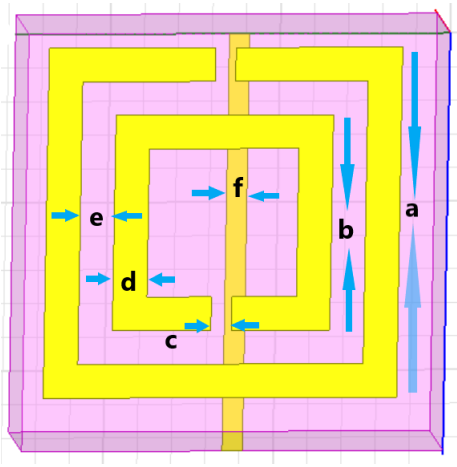


Figure 6.37: Square split-ring resonators (SSRR) with a metal strip

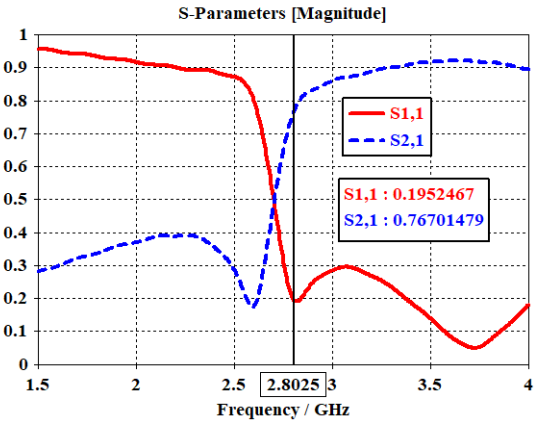
A Square Split Rings Resonator (SSRR) Structures with metal strip in ground plane and also only SSRR is designed using MATLAB code. Fig.6.37 shows the SSRR with a metal strip on the ground plane. This SSRR creates negativeμnear the resonance frequency. Also when the ground plane of SSRR is loaded with a conductor it shows a negative permittivity andμ. We have presented the retrieval of parameters of a metamaterial cell using MATLAB to verify the double negativity of a cell and only mu negativity of a second (without strip) cell. The parameters like μ, ϵ ,S_{11} S_{21} and refractive index are obtained.μ is the permeability of the metamaterial cell,ϵ is the permittivity of a cell, S_{11} is a reflection coefficient. S_{21} is a transmission coefficient.

6.4.2 Design of SSRR (Double negative metamaterial cell

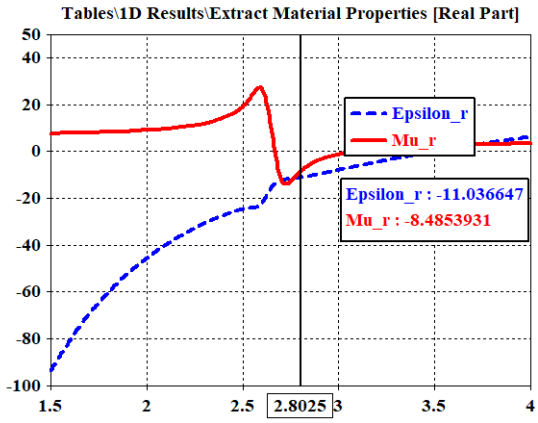
The SSRR is designed on FR-4 substrate with a permittivity value equal to 4.4 and thickness equal to 1.6 mm. The dimensions of 8x8 mm SSRR are, a =7.2 mm, b=5 mm, c=0.6 mm, d=0.7 mm, e=0.4 mm and f=0.6.

6.4.3 Parameters of SSRR

. Fig.6.38b shows the real part of permittivity and permeability of SSRR which are negative and the maximum value at 2.8 GHz is equal to -11.03 and - 8.4 respectively. The negative permittivity and permeability exist between 2.6 GHz to 3.2 GHz frequency. Therefore in this work, we have considered 2.8 GHz resonance frequency.



(a) S_{11} and S_{21} of SSRR with the strip



(b) permittivity and permeability of SSRR with the strip on the ground plane

Figure 6.38: Parameters of metamaterial cell.

(Fig.6.38a shows the S_{11} and S_{21} of SSRR, (Fig.6.38b) permittivity and permeability of SSRR with the strip on the ground plane. The metamaterial cell resonates at 2.8 GHz frequency, The refractive index of SSRR is equal to -10,It is depicted in (Fig.6.39)

Table 6.8: Different parameters of SSRR.

	Frequency	Permittivity	Permeability	Refrective index
parameters of the proposed cell	2.8 GHz	-11.03	-8.4	-10.15
Parameters of other researcher	10GHz	-8.2	-6.4	-5.4

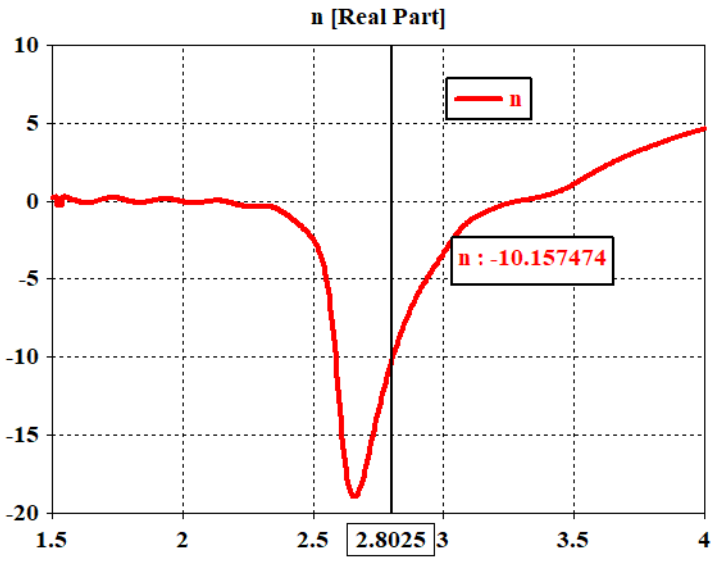


Figure 6.39: refractive index of SSRR

Our proposed cell is 8x8 mm, If the cell is designed with smaller dimensions then it will show the negative value of permittivity and permeability at higher frequency. Other researcher have designed such metamaterial cells. 2.2x2.2 mm which shows negative values of the permeability at around 10 GHz . Different parameters of SSRR metamaterial cells are given in Table 6.8.

6.4.4 Single negative Metamaterial cell

Design of single negative Metamaterial cell.

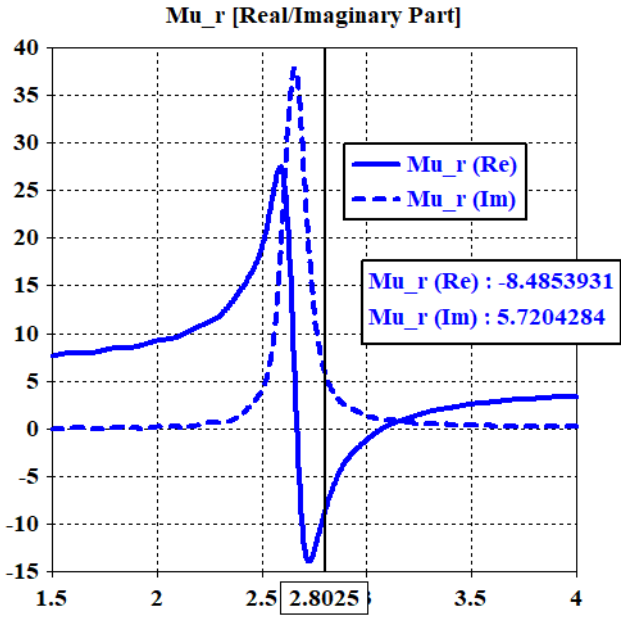


Figure 6.40: Real and imaginary values of Mu of SSRR

Cells that show either permeability negative or permittivity negative are referred to as single negative metamaterial cells. If permeability is negative then it is called a mu negative metamaterial cell. The SSRR was designed on FR-4 substrate with a permittivity value equal to 4.4 and thickness equal to 1.6 mm. The dimensions of 8x8 mm SSRR are, a = 7 mm, b=5.6 mm, c=0.5mm, d=0.7mm, and e=0.5mm. Real and imaginary values of mu of SSRR are shown in Fig,6.40. The Real and imaginary values of Mu of SSRR are shown in figure. The negative mu appears in the frequencies between 2.6 GHz to 3.1 GHz. Therefore the antenna on metamaterial must be designed to operate within the range of frequencies. Hence, in this project, we considered a resonance frequency of 2.8 GHz.

6.4.5 Rectangular microstrip patch antenna (RMPA) design on the substrate without Metamaterial

Design of RMPA.

The coaxial feed RMPA (Fig:6.41)is designed at resonance frequency 2.8 GHz (used in wireless communication and tested on software FEKO .) Refer section 6.1.5 for design equations of rectangular microstrip patch antenna.

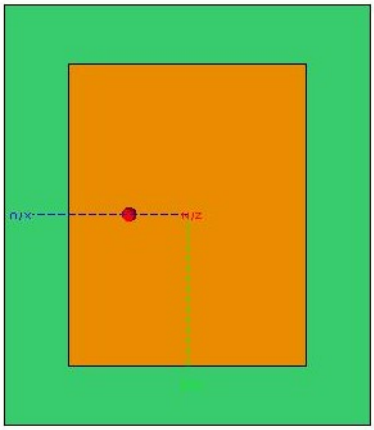


Figure 6.41: Microstrip patch antenna

Table 6.9: Design of RMPA without metamaterial

Patch dimensions	**Calculated dimensions of patch antenna (mm)**	**Optimized dimensions of Patch antenna without metamaterial(mm)**
Width of patch(W)	32.6	28.8
Length of patch (L)	25.18	23.5
Sub. width (Ws)	42.2	42
Sub. length (Ls)	34.8	34
Feed length		1.63
Feed width		5.8

6.4.6 Parameters of RMPA

Fig.6.42 Shows graph of Reflection coefficient v/s frequency of RMPA without metamaterials. The BW of RMPA is 85 MHz and Return loss = -33.09 dB,For impedance matching refer Smith chart Fig:6.43

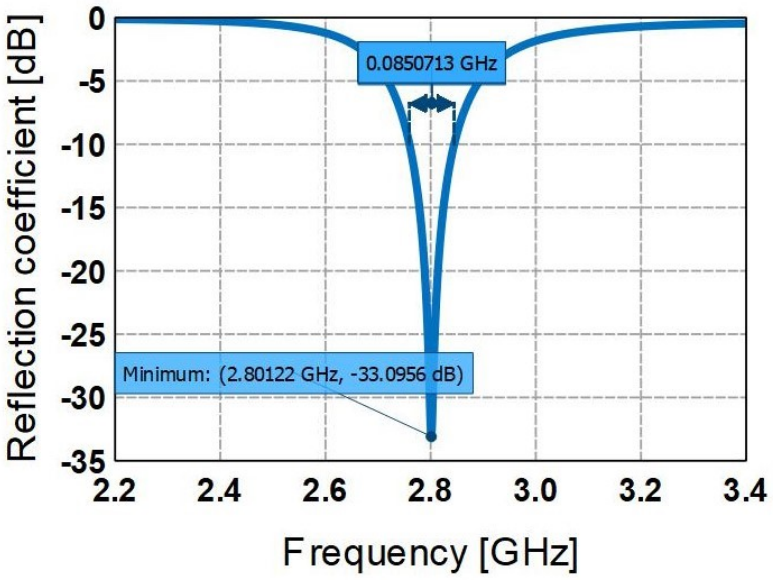


Figure 6.42: Reflection coefficint V/S Frequency graph

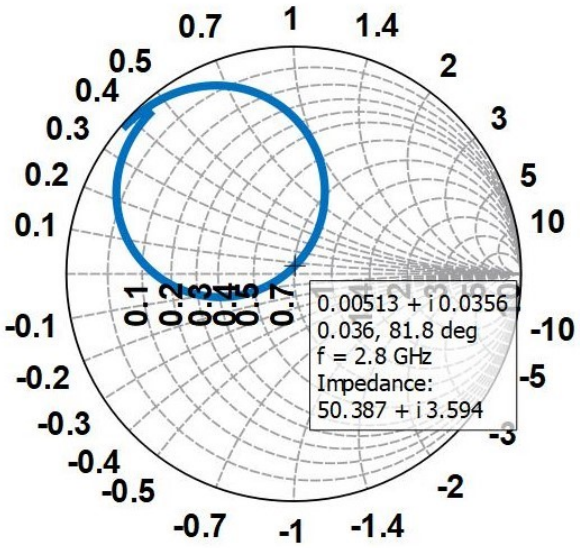


Figure 6.43: smith chart showing impedance matching at 2.8GHz

Fig.6.44 depicts the 3D view of the far-field of patch antenna without meta-material at 2.8GHz. The gain is equal to 3 dBi.

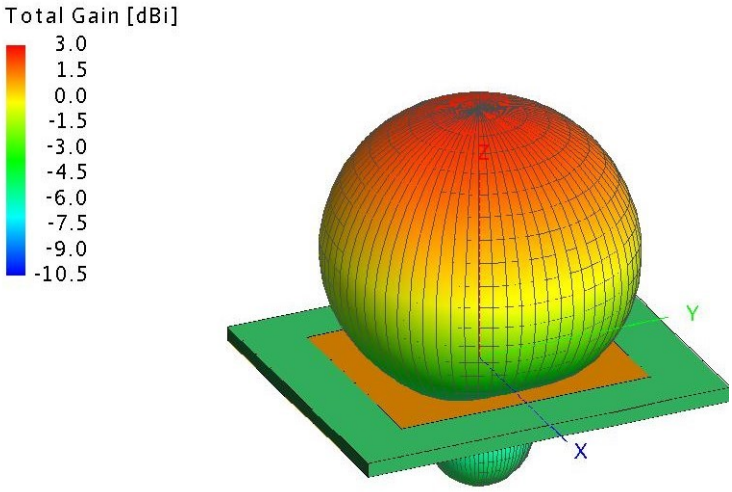


Figure 6.44: 3D view of far-field of patch antenna without metamaterial at 2.8GHz

6.4.7 Rectangular microstrip patch antenna (RMPA) design on a substrate with metamaterial

Design RMPA with metamaterial substrate. RMPA with metamaterial substrate and coaxial feed is designed at resonance frequency 2.8 GHz (used in Wireless communication and tested on software FEKO) Resonance freq. = 2.8 GHz, Substrate :FR-4 , $\epsilon_r = 4$ Loss tangent =0.01 (Fig.6.45)Shows RMPA with six cells of SSRR on its ground plane.

Table 6.10: Design of RMPA with metamaterial

Patch dimensions	**Optimized dimensions of Patch antenna with metamaterial(mm)**
Width of patch(W)	28
Length of patch (L)	22
Sub. width (Ws)	39
Sub. length (Ls)	34
Feed length	5.44

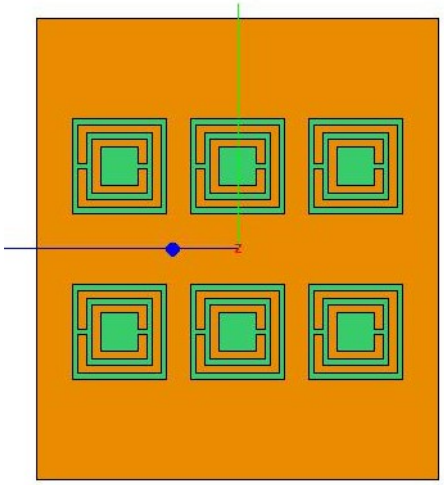


Figure 6.45: RMPA with six cells of SSRR on its ground plane

6.4.8 Parameters of RMPA with metamaterial substrate

(Fig.6.46) Presents the graph of Reflection coefficient v/s frequency of RMPA with metamaterial. The BW of RMPA is 113 MHz and Return loss = -35.24 dB. Surface waves are more easily excited when materials with higher dielectric constants and thicker material are used. Metamaterial cells reduce surface wave propagation and increase the bandwidth of RMPA.

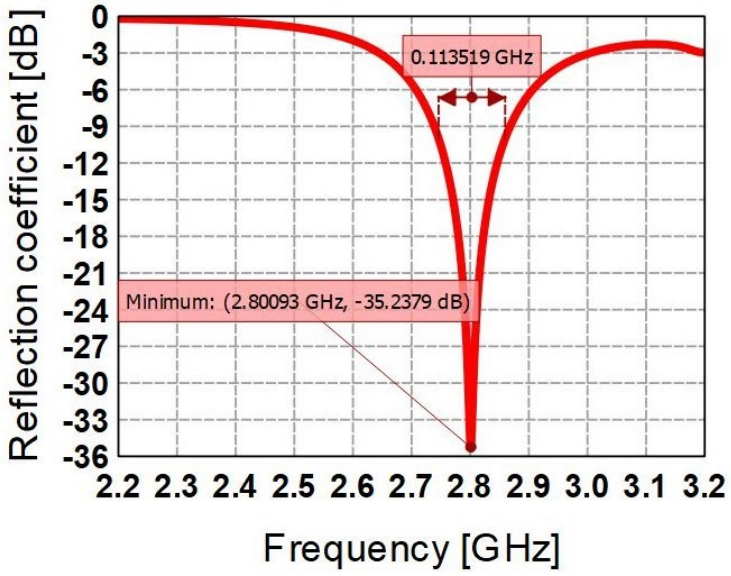


Figure 6.46: Reflection coefficient v/s frequency of RMPA with metamaterial

(Fig.6.47)shows the 3D view of the far-field patch antenna with metamaterial loaded and at 2.8GHz. The gain of antenna is 3.5 dBi.

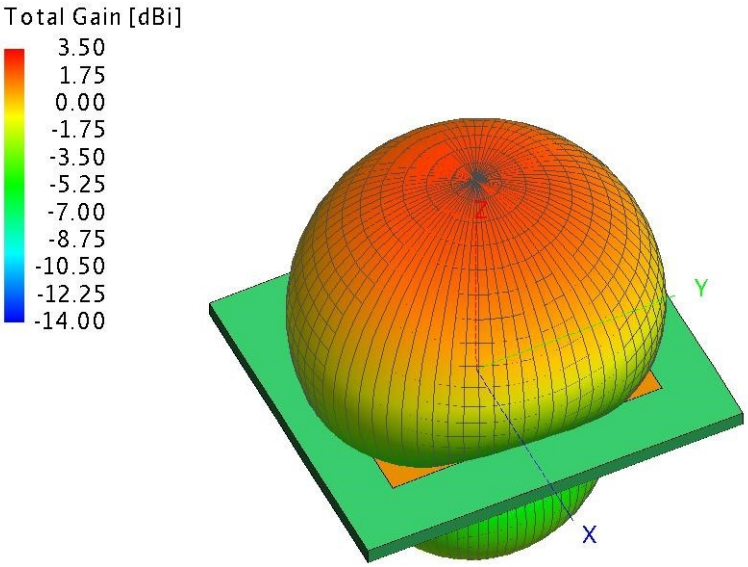


Figure 6.47: 3D view of the far-field patch antenna with metamaterial loaded and at 2.8GHz

(Fig.6.48) depicts a graph of VSWR v/s frequency. VSWR is the ratio between the maximum voltage and minimum voltage in the transmission line. It shows the system matching. If the reflection coefficient is zero then the value of VSWR is 1 and it is the lowest value possible. It is the best value for any antenna. The smaller the value better the impedance matching and more power are delivered.

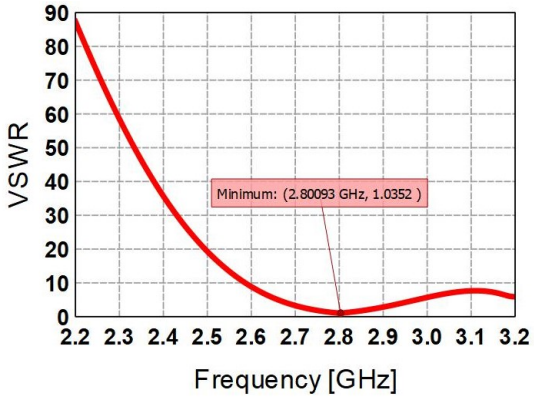


Figure 6.48: Graph of VSWR v/s frequency of metamaterial loaded RMPA.

Different parameters of RMPA with and without metamaterial are given in table 6.11. Fig: 7.80. 3D view of far-field of Metamaterial loaded patch antenna at 2.8GHz

Table 6.11: Different parameters of RMPA.

Parameters	RMPA without metamaterial	RMPA with metamaterial
Reflection coefficient	-33dB	-35.23 dB
Bandwidth (10dB)	85 MHz GHz	113MHz
Gain	3 dBi	3.6 dBi
VSWR	1.04	1.03
Half power Beam width	101 degree	89 degree

6.4.9 Simulation Results

When the SSRR with a metal strip on the ground plane is designed and simulated, it has been found that the permittivity, permeability, and refractive index are being negative, which implies that it is a left-handed metamaterial cell. The values of parameters are listed in Table 6.11. RMPA loaded with and without metamaterial are designed and simulated using FEKO, It has been found that the bandwidth of antenna increases in comparison to RMPA without metamaterial. Its return loss and bandwidth are – 33.09dB and 85 MHz respectively. This antenna with metamaterial loaded the values of Return loss and bandwidth are -35.23 dB and 113 MHz respectively. So the bandwidth is increased by 28 MHz, based on the simulated results it is found that the RMPA bandwidth has improved.

6.5 Capacitive Coupled Circular Patch Antenna for band suppression and Gain improvement by loading Circular Slot on Coupling

Wireless communication is increasing at very fast rate.With rapid growth in technology there has been a demand for high performance durable antennas for various applications. This proposed antenna capacitive coupled coaxial feed circular patch antenna (CCCCPA) also behave as good receiving elements at the har-

monics of the design frequency.When this proposed antenna is used as receiving antenna it blocks the resonance frequency near the designed frequency that is 6 GHz, there by avoiding need of band pass/low pass filter. So the received signals can be fed to diode detector. Harmonic rejection antennas has been presented by researchers using different techniques, like the proximity-coupling for harmonic suppression [76], slot coupled slot loop antenna , use of defected ground ,right angle slits , ground pin , compact microstrip resonant cell (CMRC) , photonic bandgap (PBG) structures spurious free antenna etc. In this paper, a CCCCPA is designed at resonance frequency 6GHz and band at resonance frequency 11.5 GHz is suppressed by loading semi-circular slot on coupling, The gain of antenna has been improved after loading semi-circular slot on coupling. CCCCPA without slot and with slot on coupling has been simulated using FEKO software. This antenna can be used for wireless power transfer and reception. [77] [78]

6.5.1 CCCCPA design on a rectangular substrate without slot on coupling at resonance frequency 6 GHz (used in Wireless communication and tested on software FEKO

Radius of patch antenna can be calculated using equation given in the section 6.2.(Fig.6.49) shows design and geometry CCCCPA on a rectangular substrate obtained from FEKO.(without semicircular slot) [72] [79] The antenna is printed on the RT Duroid laminate of thickness (h) 1.58 mm, relative permittivity ϵ_r = 2.2 loss tangent 0.0009. The actual radius "r" of the circular patch for resonance frequency (f_r) 6 GHz can be calculated using the cavity model approach.

Resonance frequency = 6 GHz

Calculated radius of circle =9.36mm

Optimised Radius of circle =8.9 mm

centre =- 4mm , F =9.878

Coaxial feed=10.2mm

Elliptic arc 1 radius (ru)=9.8mm, rv=9.8mm

centre (C-1)= -3.7mm,start angle=-980 degrees, Stop angle=980 degrees Elliptic arc2 radius(ru)=14.5mm, rv=10.5mm, C-2 =-3.3 , start angle =-1000 degrees Stop angle = 1000 degrees Substrate dimensions

Lsub =38 mm, Wsub = 32mm.

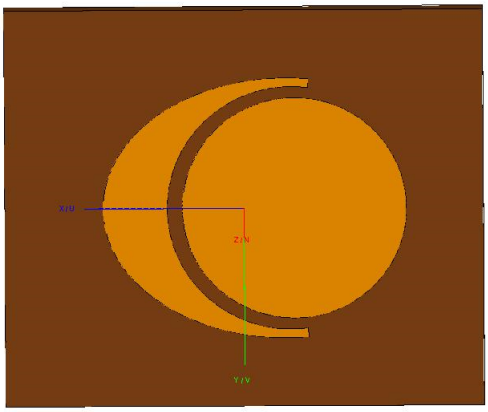


Figure 6.49: CCCCPA on rectangular substrate without slot

6.5.2 Parameters of CCCCPA

(Fig.6.50) Shows graph of reflection coefficient and gain v/s frequency of CCC-CPA without slot. The BW of CPA is 445 MHz and Return loss = -31 dB. Gain equal to 5.5 dBi, also we have one more band at resonance frequency 11.5 GHz

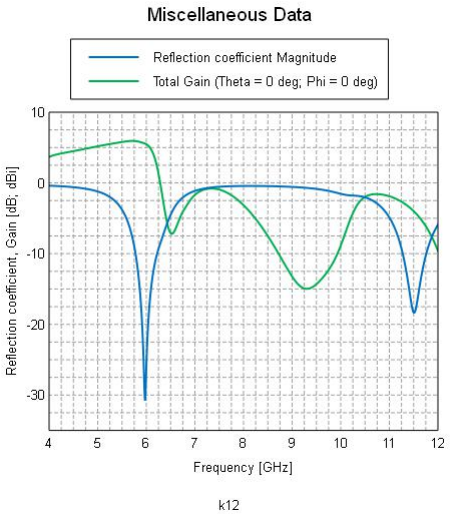


Figure 6.50: Freq v/s Reflection coefficient and gain (without slot)

6.5.3 CCCPA design on a Rectangular substrate with slot on Coupling at Resonance frequency 6 GHz

(Fig.6.51) shows the CCCCPA design on a rectangular substrate with a slot on coupling at resonance frequency 6 GHz (used in Wireless communication) [76][80] The optimised radius of circular patch is equal to 8.8 mm, Coaxial feed=10.2mm Substrate dimensions

Lsub =35 mm, Wsub = 30 mm.Centre of semi-circular slot is 10.2 mm,inner radius equal to 2.5 mm and outer radius equal to 3 mm,Slot width equal to 0.5 mm

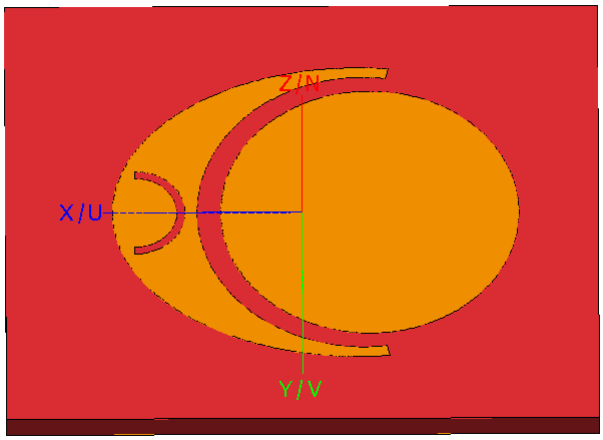


Figure 6.51: CCCCPA design on a rectangular substrate with a slot on coupling

(Fig.6.52) Shows graph of frequency v/s reflection coefficient and Gain of CCCCPA with semi-circular slot on coupling. The BW of CCCCPA is 430 GHz and Return loss = - 26 dB. Gain equal to 6.5 dBi .It has been observed that the band at 11.5 GHz resonance frequency is being supressed[77].

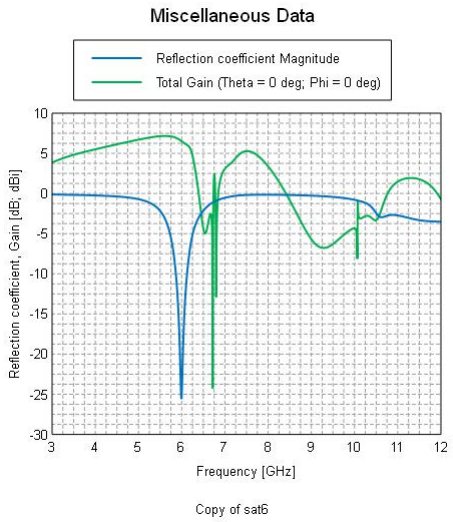


Figure 6.52: Freq v/s Reflection coefficient and Gain of CCCCPA(with semi-circular slot)

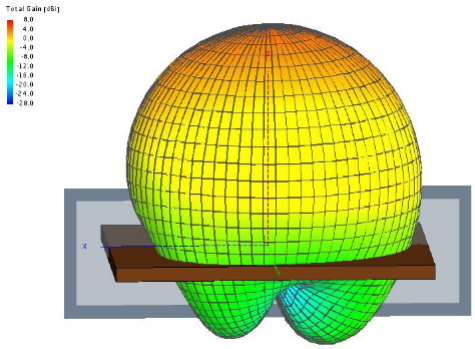


Figure 6.53: 3D view of far field of CCCCPA 6 GHz

(Fig.6.53) shows the far field 3D view of CCCCPA at 6 GHz

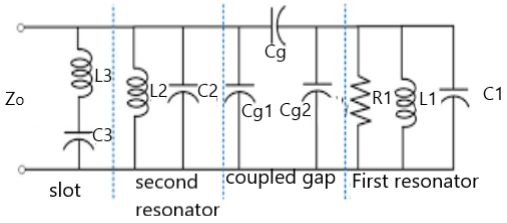


Figure 6.54: Equivalent circuit model of the proposed CCCCPA with slot

The circular patch is represented by the first resonator (consisting of R1, L1, C1), the capacitive gap is represented by the pi-network (consisting of Cg, Cg1 and Cg2), and the semi-circular coupling is represented by the second resonator (consisting of L2, C2). The series resonator consisting of L3–C3 represents the slot.

6.5.4 Simulation Results

CCCCPA with resonance frequency 6 GHz for suppressing band for wireless power reception and transmission application is designed. Initially, a capacitive coupled circular patch antenna has been designed based on the cavity model approach and FEKO software for optimization. The initial antenna shows unnecessary band at 11.5 GHz with 20dB return loss and gain at 6 GHz is 5.5 dBi. In order to suppress this band modifications are done in design. Semicircular slot is loaded on coupling which serves as filter to supress band at 11.5 GHz. From Frequency v/s Reflection coefficient and Freq v/s Gain graph of capacitive coupled antenna. It is observed that reflection coefficient at11.5GHz is almost -4db (suppressed band), And the Gain is almost 6.6 dBi at 6 GHz.So the gain of antenna has improved .

6.6 Characterization of patch Antenna with Rectangular slot for 5G Application

A Microstrip Patch Antenna is fed by edge port.It is designed on RT duroid substrate for 5G application. The impedance of 50 ohms has been achieved. A rectangular slot is loaded on a patch antenna. The variations and improvement in patch antenna parameters are reported.[81] [82] Microstrip patch antenna are being widely used for small wireless communication aerospace application WiMAX, WLAN and 5G application. Patch antenna is designed on dielectric substrate such as RT duroid with dielectric constant 2.2. Thickness of this dielectric substrate is 0.5 mm. If we use substrate of higher thickness efficiency can be increased, However, as the height increases, surface waves are introduced which usually are not desirable because they extract power from the total available for direct radiation (space waves). [83]. The authors have designed and simulated Edge port fed rectangular patch antenna for 5G application. The Rectangular

microstrip patch antenna (RMPA) is simulated and band width, return loss gain are measured. Also a rectangular slot is loaded on patch antenna. A significant improvement in patch antenna parameters has been observed.[84] [85]

6.6.1 Design of antenna

Rectangular microstrip patch antenna.(RMPA) design on RT Duroid substrate with edge port feed at resonance frequency 26 GHz as employed in 5G communication. (Fig.6.55)shows design of Edge fed RMPA obtained from FEKO .

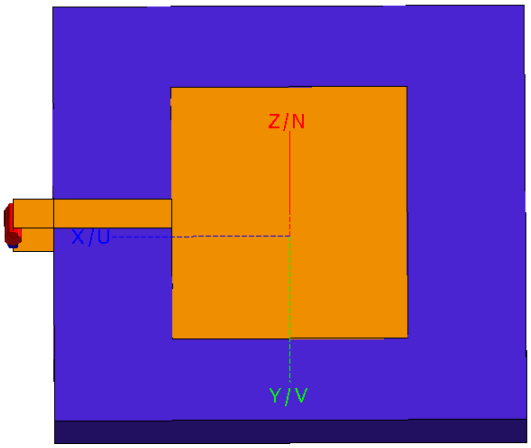


Figure 6.55: Edge fed RMPA on RT duroid substrate

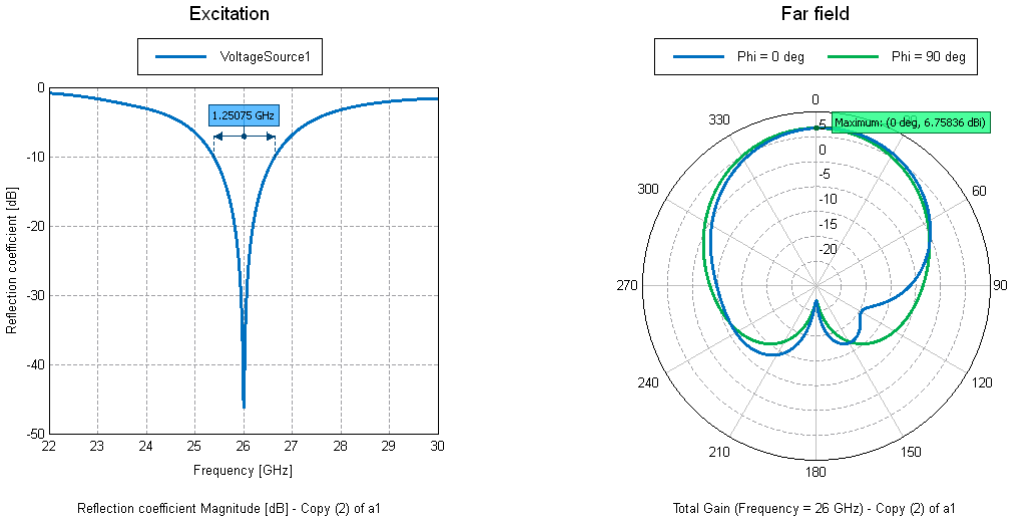
Design of edge fed RMPA on RT duroid substrate. Resonance freq. = 26 GHz Substrate: RT Duroid 5880 ϵ_r= 2.2 Loss tangent : 0.0009, height of substrate(h) = 0.5 mm

Table 6.12: Dimensions of RMPA

Patch dimensions	**Calculated dimensions of patch antenna (mm)**	**Optimized dimensions of Patch antenna without metamaterial(mm)**
Width of patch(W)	4.56	4.26
Length of patch (L)	3.57	3.24
Sub. width (Ws)	7.56	7
Sub. length (Ls)	6.57	6.5
Feed length		1.63

6.6.2 Parameters of RMPA without slot

(Fig.6.56a)Shows graph of Reflection coefficient v/s frequency of RMPA. The bandwidth of RMPA is 1.25 GHz and Return loss = 45 dB



(a) Freq v/s Reflection coefficient

(b) Total gain of RMPA

Figure 6.56: Parameters of antenna

Gain of antenna is a very important parameter, Gain should be very close to directivity so that efficiency of patch antenna increases. (Fig.6.56b)Shows total gain of RMPA, which is equal to 6.75 dB.

6.6.3 Rectangular microstrip patch antenna.(RMPA) design with rectangular slot at 26 GHz resonating frequency

(Fig.6.57) Shows design of edge fed RMPA with rectangular slot on patch. The optimised design of edge fed microstrip patch antenna with slot on patch The patch antenna is being designed on RT Duroid substrate. Resonance freq. = 26 GHz Substrate : RT Duroid 5880 ϵ_r = 2.2, Loss tangent =0.0009 hight of substrate(h) = 0.5 mm

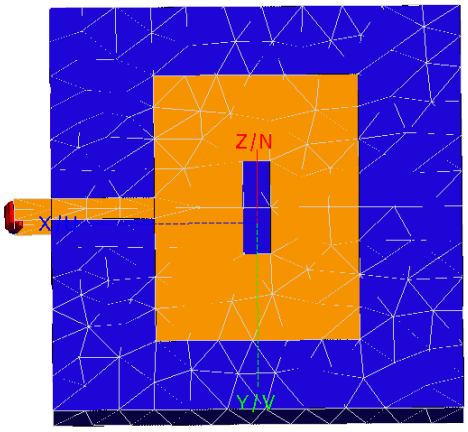
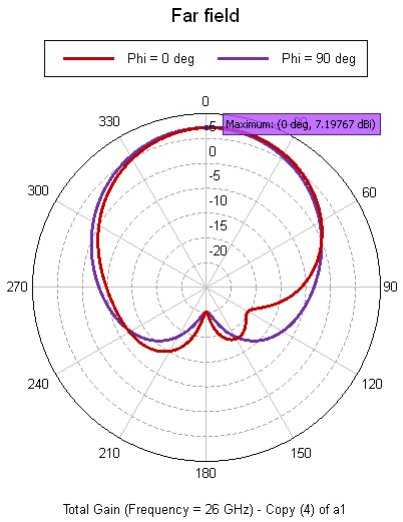


Figure 6.57: RMPA with rectangular slot on patch.

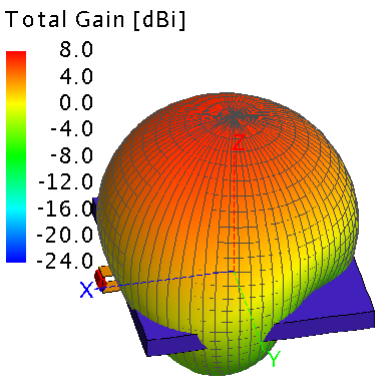
Table 6.13: Dimensions of RMPA with slot

Patch dimensions	Optimized dimensions of patch antenna (mm)
Width of patch(W)	4.28
Length of patch (L)	3.01
Sub. width (Ws)	6.5
Sub. length (Ls)	6.05
Feed length	1.52

6.6.4 Parameters of RMPA with slot



(a) Total gain of RMPA with slot



(b) 3D view of far field of patch antenna at 26 GHz

Figure 6.58: Parameters of antenna

2D far field radiation pattern of antenna is presented in (Fig.6.58a). The total gain of RMPA is equal to 7.19 dB. (Fig.6.58b) shows the 3D view of far field of patch antenna at 26 GHz resonance frequency.

6.6.5 Simulation Results

Conventional edge fed RMPA and edge fed RMPA loaded with slot is designed and simulated using FEKO, It has been observed that the gain of antenna increases in comparison to RMPA without slot. RMPA without slot the bandwidth and return loss are 1.25 GHz and -45 dB respectively and the gain is 6.7dB. This antenna after loading slot the gain is increased to 7.19 dB.

Chapter 7

Design of Microstrip Patch Antenna using Mathematical Modeled Metamaterial Cell

7.1 Characterization of microstrip patch antenna using mathematically modelled metamaterial cell

A square split ring resonator cell is mathematically modeled and used to design the microstrip patch antenna.Broad study of this material is being carried out by mathematically modeling and simulating a single negative metamaterial cell which consists of a square split ring resonator with two rings. The Rogers RT/Duroid substrate with dielectric constant 2.2 has been used in this design. For a specific range of frequencies, this metamaterial cell depicts negative values of permeability. These metamaterial cells have a lot of contributions to the design of microstrip patch antennae by improving their characteristics such as reflection loss, bandwidth, and gain. The resonance frequency obtained by simulating the metamaterial cell is compared with the calculated value from the circuit model. The theoretical value of resonant frequency calculated using a mathematical equation is found to be extremely close to the frequency obtained by simulating metamaterial structure. The S parameters curves and complex permeability curves are obtained. These modeled cells are used for designing rectangular microstrip patch antennae. Square split ring resonating cells are placed on the ground plane

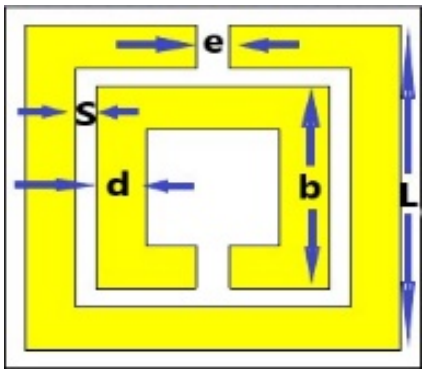
of the edge-fed microstrip patch antenna. The parameters such as bandwidth, Gain, return loss, VSWR of conventional antenna, and metamaterial-based antenna are compared and recorded.[72],[17], [86] The authors noted that dielectric characteristics affect distributed capacitance associated with the rings of SRR, but inductance is unaffected. We've covered some of the key characteristics of mu negative metamaterials [87]. Mathematical modeling of mu negative metamaterial cells with two rings and structured on Rogers RT/Duroid 5880, Inductance and distributed capacitance of SSRR and hence the resonance frequency are calculated and compared with simulated value. MATLAB is used to obtain the curve of the S parameter and complex permeability. Using this modeled cell rectangular microstrip patch antenna (RMPA) has been designed. Its parameters are recorded and judged the advantages of loading SSRR cells on the ground plane of the patch antenna [88].

7.1.1 Double negative or left-handed metamaterials

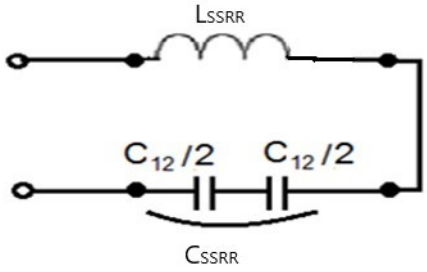
They are materials of artificial form and their permittivity permeability and refractive index are negative. Due to the negative refractive index, phase velocities, as well as the group velocity of electromagnetic waves, are opposite to each other and opposite energy flow is observed.

7.1.2 Design of mu negative metamaterial cell on RT/Duroid 5880 substrate

The SSRR with two rings as shown in (Fig.7.1a) is designed on Rogers RT/ Duroid 5880 substrate with a permittivity value equal to 2.2 and thickness equal to 0.5 mm. The dimensions of the 1x1 mm SSRR cell are, L= 0.9 mm, b= 0.54 mm, e=0.08mm, Strip width d = 0.13 mm, and spacing between n and (n+1) turn is s = 0.05 mm, The resonance frequency is inversely proportional to the size of the cell, and it also depends on strip width, slit, spacing between n th and (n+1) ring. (Fig.7.1a) shows the geometry of the SSRR consisting of two



(a) Square split-ring resonators (SSRR) meta-material cell with two square split rings on top of a substrate



(b) Equavalent circuit 0f SSRR

Figure 7.1: square split ring resonator

rings with their slit displaced by 180 degrees. The equivalent circuit for SSRR is presented in(Fig.7.1b) . The inductance of the tank circuit, Ls is calculated by assuming the uniform current throughout the loop. The capacitance of the tank circuit is a parallel equivalent of the capacitances in each pair of adjacent loops. The total strip length Ln of an nth ring of the SSRR and the total spacing length Lg between the nth and (n+1) turn of SSRR are determined.[87] Then the total inductance and the total distributed capacitance between two consecutive rings of SSRR, of strip width d are shown in the following equations

$$L_n = 4[L - 2d(n-1) - 2S(n-1) \tag{7.1}$$

$$L_g = 4[L - (n + 1/2)(d + s)] \tag{7.2}$$

$$C_{SSRR} = \frac{N-1}{2}[2L - (2N-1)(d+s)C_{pul} \tag{7.3}$$

$$C_{pul} = \epsilon_0 \epsilon_{reff} \frac{K(k^{'})}{K(k)} \tag{7.4}$$

$$\frac{K(k^{'})}{K(k)} = [\frac{1}{\pi} ln(2\frac{1+\sqrt{k^{'}}}{1-\sqrt{k^{'}}})] \tag{7.5}$$

$$L_{SSRR} = \frac{\mu_0}{2}\frac{L_{avg}}{4} 4.86[ln(0.98/\rho) + 1.84\rho] \tag{7.6}$$

$$L_(avg = 4[L - (N-1)(s+d)] \tag{7.7}$$

$$L_{SSRR} = \frac{\mu_0}{2}\frac{L_{avg}}{4}4.86[ln(0.98/p) + 1.84p] \tag{7.8}$$

$$f_r = \frac{1}{2\pi\sqrt{L_{SSRR}C_{SSRR}}} \tag{7.9}$$

C_{pul} is the capacitance per unit length of two parallel strips of width d apart by distance s. The dielectric substrate affects the distributed capacitance only and is given by equation 7.3. Values of K(k) and $K(k')$ also can be taken from(Fig.7.2). K(k) is known as the complete elliptical integral of the first kind, and $K(k')$ is its complex value. It is defined for $0 < k < 1$ Eq.7.7 presents the average length of the strip. Resonance frequency is given by Eq.7.9 The dielectric substrate used in SSRR does not affect the inductance [17]. The inductance of SSRR is given by Eq.7.8 Where ρ is the fill ratio of SSRR and is stated as ρ=((N-1)(s+d))/(L-(N-1)(s+d))

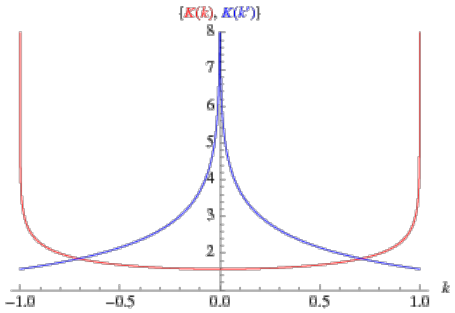


Figure 7.2: Graph of k v/s K(k) and K(k')

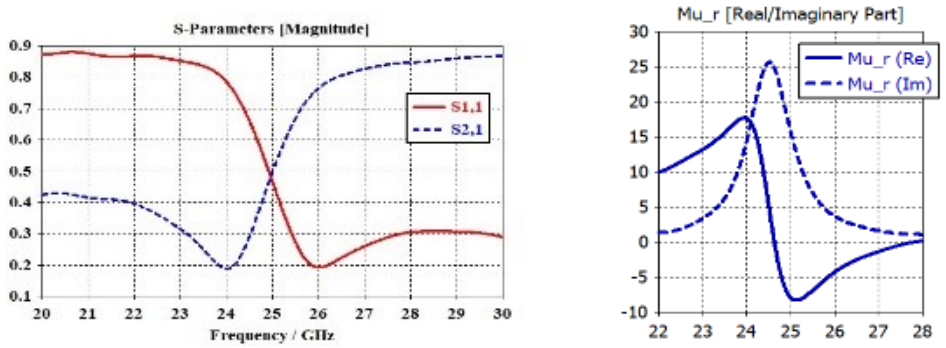
7.1.3 Method to find Parameters of SSRR Metamaterial

A Square Split Rings Resonator (SSRR) Structure is designed using MATLAB code. (Fig.7.1a) shows the SSRR with a two-metal split ring on the surface of the substrate. This SSRR creates negative *mu* near the resonance frequency. We have presented the retrieval of parameters of a metamaterial cell using MATLAB to verify the mu negativity of the cell. The SSRR with two rings and substrate Rogers Duroid/RT 5880 has been simulated and different parameters like μ ,ϵ,

Table 7.1: Comparison of calculated and simulated resonance frequency of SSRR with Rogers RT/Duroid dielectric materials

substrate	Dielectric constant	No.of turns	Lengthof side(L)mm	Ls(nH)	C(pf)	calculated res. freq.(GHz)	Measured freq.(GHz)	res.eff.permeability
Roger RT/Duroid	2.2	02	0.86	4.0	0.01	25.5	26	-0.5

S_{11}, S_{21}, and refractive index are obtained [44].μ is the permeability of the metamaterial cell,ϵ is the permittivity of a cell, Both S parameters of metamaterial cells are depicted in(Fig.7.3a). Equations used to calculate impedance and refractive index are shown in section 6.1.4.



(a) The graph of S_{11}, S_{21} v/s frequency of SSRR with Roger RT Duroid 5880 substrate

(b) The graph of Permeability V/s frequency of SSRR with Roger RT Duroid 5880 substrate

Figure 7.3: SSRR parameters

It is also observed in (Fig.7.3b) that permeability of the cell is negative at 26 GHz frequency and the value of mu is -5 at 26 GHz.Comparison of calculated and simulated resonance frequencies of SSRR with Rogers RT/Duroid dielectric materials is presented in Table7.1

7.1.4 RMPA design on the substrate without metamaterial at 26 GHz resonance frequency

Rectangular microstrip patch antenna. (RMPA) design on RT Duroid substrate with edge port feed at resonance frequency 28 GHz as employed in 5G communi-

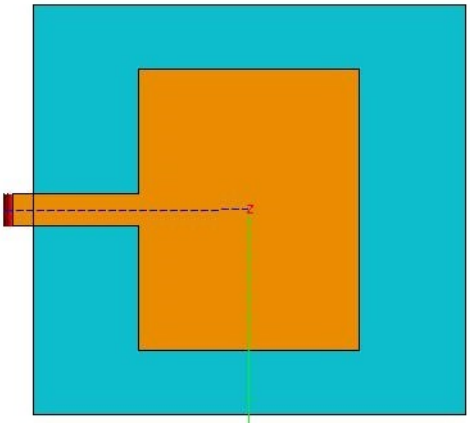


Figure 7.4: Design of edge-fed RMPA without metamaterial.

Table 7.2: Design of RMPA without metamaterial

Patch dimensions	**Calculated dimensions of patch antenna (mm)**	**Optimized dimensions of Patch antenna without metamaterial(mm)**
Width of patch(W)	4.56	4.26
Length of patch (L)	3.57	3.35
Sub. width (Ws)	7.56	6.8
Sub. length (Ls)	6.57	6.25
Feed length	1.57	1.57

cation. The width of RMPA Effective permittivity and fringing length Δ L are shown in equations.(Refer 6.1.5) The design of edge-fed RMPA without metamaterial on RT duroid 5880 substrates is shown in (Fig.7.4) .

The design of RMPA without metamaterials is shown in Table7.2. Resonance freq. = 26 GHz, Substrate: RT Duroid 5880, $\epsilon_r = 2.2$, Loss tangent : 0.0009, height of substrate(h) = 0.5 mm The BW, gain, return loss, and VSWR are shown in Table 7.4. Return loss Of the antenna depends on its impedance matching. Return loss is very low for the perfectly matched antenna. (Fig.7.5) depicts the reflection coefficient v/s frequency graph of RMPA. These parameters determine the ratios of the amplitudes in the transmitted and reflected wave when a plane wave incident on the dielectric DNG medium.The performance of the microstrip patch antenna is getting a boost once a split-ring resonator is loaded on the patch.

At the resonance frequency, the return loss is equal to (-45 dB).

(Fig.7.6) presents a 3D far-field radiating pattern at 26 GHz resonance frequency.

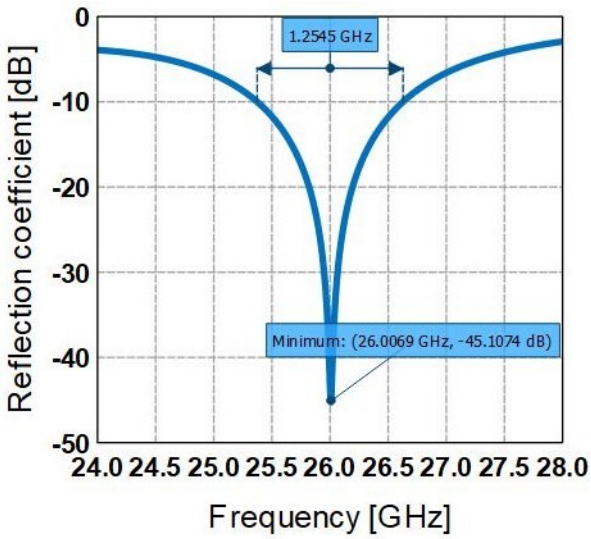


Figure 7.5: Reflection coefficient v/s freq of RMPA without metamaterials

The gain of an antenna is 8.0 dBi at 0 degrees at 26 GHz. The gain of the antenna at total bandwidth remains almost the same. It slightly decreases at the lower end of the band of frequency.

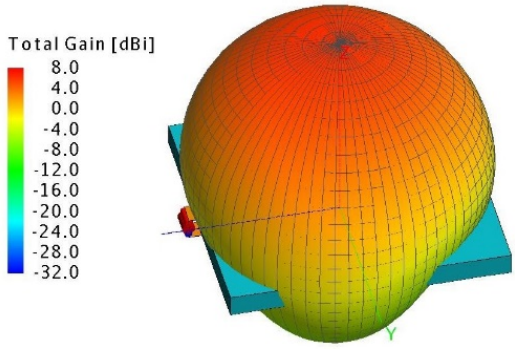


Figure 7.6: 3D far-field radiating pattern at 26 GHz

7.1.5 Rectangular microstrip patch antenna (RMPA) design with a modeled metamaterial at 26 GHz resonating frequency

Antennas are designed using DNG or SNG Metamaterial cells. Which are used to increase the performance of the system. These cells could substantially increase the gain and radiated power of an antenna. Furthermore, these antennas can

Table 7.3: Design of RMPA with metamaterial

Patch dimensions	**Optimized dimensions of Patch antenna with metamaterial(mm)**
Width of patch(W)	4.26
Length of patch (L)	2.99
Sub. width (Ws)	6.8
Sub. length (Ls)	6.2
Feed length	1.6
Feed width	0.48

improve efficiency-bandwidth performance. (Fig.7.7) Shows the design of RMPA with metamaterial cells on the surface of a rectangular patch.

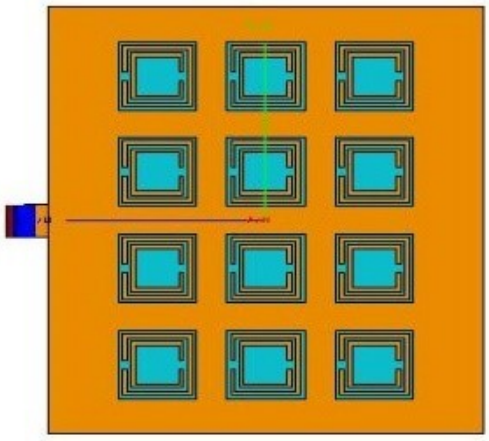


Figure 7.7: Design of edge-fed RMPA with metamaterial.

The optimized design of the edge-fed microstrip patch antenna with metamaterial is shown in Table7.3. The patch antenna is designed on an RT Duroid substrate. Resonance freq. = 26 GHz, Substrate : RT Duroid 5880, ϵ_r= 2.2, Loss tangent =0.0009,height of substrate(h) = 0.5 mm. (Fig.7.8)shows the reflection coefficient v/s frequency graph of RMPA with metamaterial. At the resonance frequency, the return loss is (-50.8 dB).

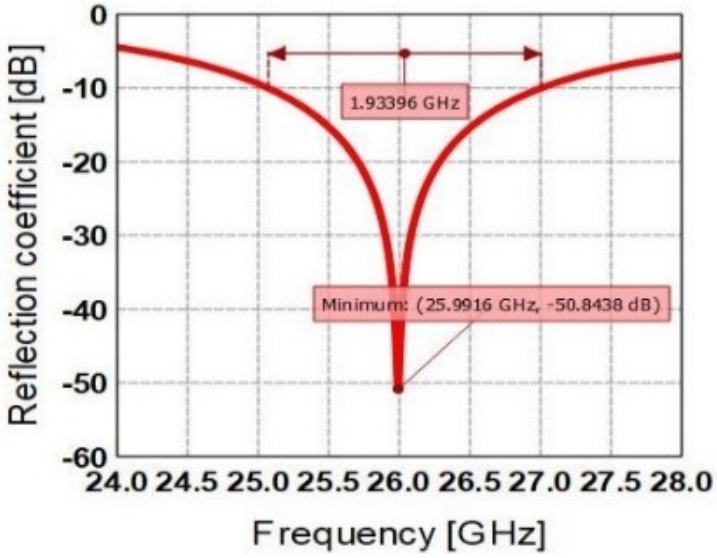


Figure 7.8: Reflection coefficient v/s freq of RMPA with metamaterials

(Fig.7.9)and (Fig.7.10) present a far-field radiating pattern of RMPA with metamaterial showing gain at resonance frequency 26 GHz and 25GHz respectively. The gain of an antenna is 9 dBi at 26 GHz and 8 dBi at 25 GHz.

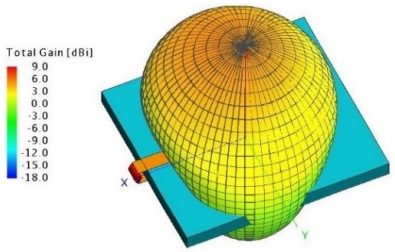


Figure 7.9: 3D view of the far-field of a RMPA at 26GHz resonance frequency

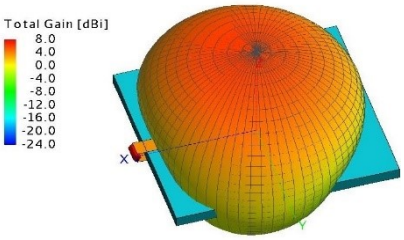


Figure 7.10: 3D view of the far-field of a RMPA at 25GHz

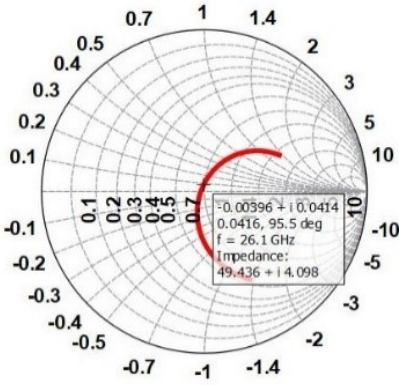


Figure 7.11: Impedance matching of RMPA at 26GHz

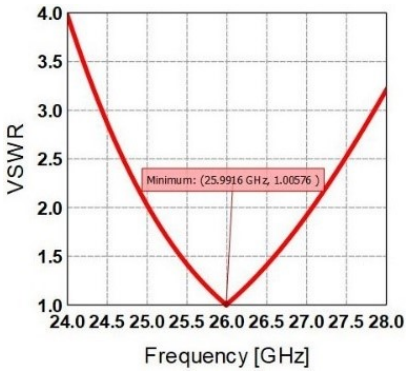


Figure 7.12: VSWR of RMPA with metamaterial

(Fig.7.11) Is a Smith chart that shows the impedance matching of RMPA with

metamaterial at 26 GHz. At 26 GHz the impedance is almost 50 ohms and the reactive impedance is almost zero, which matches with source impedance.(Fig.7.12) presents VSWR, Its is equal to 1.00 which signifies perfect matching of source impedance of 50 ohms with an antenna. The radiation performance in the antenna indicates the efficiency of the radiation measured in terms of percentage and is obtained by calculating the value of the ratio of the amount of power fed to the antenna to that of the power emitted (radiated) from an antenna. This radiation efficiency boosts the performance of the antenna useful for 5G wireless technology and its applications. The proposed antenna has higher radiation efficiency of 88.8 % at 26 GHz.

7.1.6 Simulation Results

A Square split ring resonator a metamaterial cell is designed and simulated using the software. A metamaterial cell consisting of only SSRR shows a negative permeability to state it as a single or mu-negative metamaterial cell. The comparison of the parameters of RMPA and metamaterial-based RMPA with the same resonance frequency is listed in Table7.4 Rectangular microstrip patch antenna for 5G wireless Network technology is effectively designed, implemented, and compared the performance at a 26 GHz resonance frequency. Conventional RMPA and RMPA loaded with metamaterial on the patch of the antenna system are simulated at a frequency of 26 GHz. It has been observed that the gain of a antenna increases by 1dBi and the bandwidth of patch antenna increases considerably in comparison to RMPA without metamaterial. RMPA without cells returns loss and bandwidth is –45.1 dB and 1.25 GHz respectively. Whereas RMPA with metamaterial the values of return loss and bandwidth are – 50.8 dB and 1.93 GHz respectively. Gain of RMPA without and with cells are found to be equal to 9 dBi and 8 dBi respectively. So the bandwidth is increased by 0.68 GHz. Based on simulated results it has been found that the bandwidth of RMPA has improved. VSWR of the conventional antenna is 1.01 and that of the

Table 7.4: Different parameters of RMPA.

Parameters	RMPA without metamaterial	RMPA with metamaterial
Reflection coefficient	-45.2dB	-50.7 dB
Bandwidth (10dB)	1.25 GHz	1.93 GHz
Gain	8 dBi	9 dBi
VSWR	1.01	1.0

antenna with metamaterial is 1.00 which indicates that the antenna impedance is perfectly matched.

7.2 Mathematical Modelling of Metamaterial Cell and its Application in Design of Microstrip Patch Antenna

7.2.1 Mathematical modelling of mu negative metamaterial cells with two rings and structured on Rogers RT/Duroid 5880

The Inductance and the distributed capacitance of SSRR and hence the resonance frequency are calculated and compared with simulated value. Parameters of mu negative metamaterial cell are extracted using full-wave simulator HFSS. Data files (.csv) of S_{11} and S_{21} are then exported and applied MATLAB script to obtain the curve of complex permeability. Using this modelled cell Rectangular microstrip patch antenna (RMPA) has been designed[75]. Its parameters are recorded and judged the advantages of loading SSRR cells on the surface of the patch[89] [90]. The SSRR showed in (Fig.7.13) with a number of rings equal to two is designed on Rogers RT/ Duroid 5880 substrate with permittivity value equal to 2.2 and thickness equal to 0.5 mm.

The dimensions of 1 mm x 1 mm SSRR cell are, L= 0.9 mm, b= 0.6 mm, e=0.08mm, Strip width d = 0.1mm, and spacing between n and (n+1) th turn is d = 0.05 mm, Fig.7.13 shows the geometry of the SSRR consisting of two rings with their slit displaced by 180 degrees. The inductance of the tank circuit , The

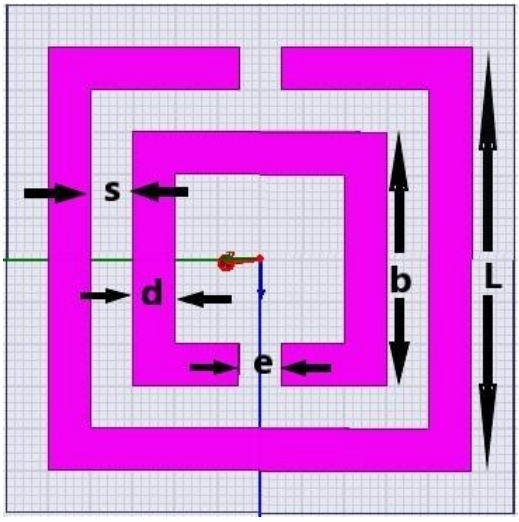


Figure 7.13: Square split-ring resonators (SSRR) metamaterial cell

capacitance of the tank circuit and the inductance Ls is calculated by assuming the uniform current throughout the loop. The equations to find total strip length Ln of an nth ring of the SSRR and the total spacing length Lg between nth and (n+1) th turn of SSRR are determined. Then the total inductance and of the total distributed capacitance between two consecutive rings of SSRR, of strip width d and resonating frequency are obtained using equation shown in section 7.1.2.

7.2.2 Method to find Parameters of SSRR Metamaterial

(Fig.7.14) presents metamaterial cell simulation in the waveguide.

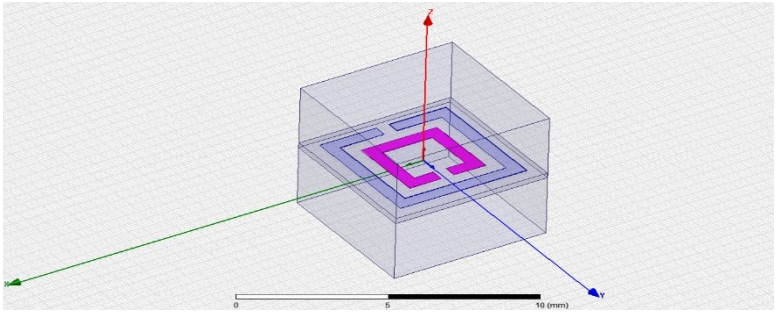


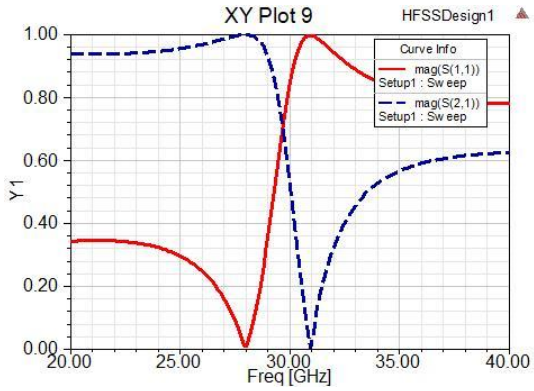
Figure 7.14: Metamaterial cell simulation in the waveguide

The effective parameters of SSRR can be found out in numerical simulations. First We have to find out the transmission and reflection coefficient of the cell-based on numerical algorithms, such as (FDTD) and Finite Element Method

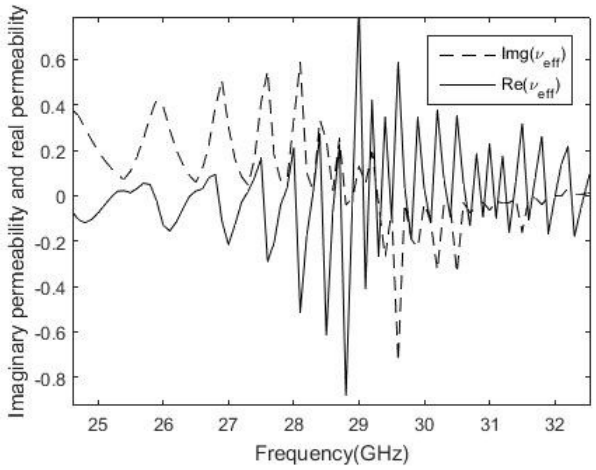
Table 7.5: Comparison of calculated and simulated resonance frequencies of SSRR with Rogers RT/Duroid dielectric materials

subst material	Dielectric const	No.of turns	side(L)mm	Ls(nH)	C(pf)	cal.res.freq.(GHz)	Meas res. freq.	Mu eff
Roger RT/Duroid	2.2	02	0.9	3.36	0.01	26.5	28	-0.5

(FEM). This method also can be used to extract parameters.Calculate impedance and refractive index , from the transmission coefficient S_{21} and reflection coefficient S_{11}. And further to calculate complex permeability and permittivity. Both the coefficients S_{11} and S_{21} are exported to MATLAB to extract real and an imaginary curves of permeability using equations.[43] After simulation, It is observed that the resonance frequency of the metamaterial cell is 28 GHz. The graph of S_{11} and S_{21} v/s frequency is presented in (Fig.7.15a). It is also observed



(a) S_{11} and S_{21} v/s frequency of SSRR with Roger RT Duroid 5880 substrate



(b) Permeability V/s frequency of SSRR with Roger RT Duroid 5880 substrate

Figure 7.15: SSRR parameters

from (Fig.7.15b) that permeability of the cell is negative at 28 GHz frequency. Also, the values of inductance, capacitance, and resonance frequency of SSRR are presented in Table7.5.

7.2.3 Application of modelled metamaterial in designing Rectangular microstrip patch antenna. (RMPA)

MPA Design on Substrate without Metamaterial

Rectangular microstrip patch antenna (RMPA) design on RT Duroid substrate with edge port feed at resonance frequency 28 GHz as employed in 5G communication. Rectangular microstrip patch antenna (RMPA) design without metamaterial at 28 GHz resonating frequency. (Fig.7.16). shows the design of RMPA without metamaterial on RT duroid 5880 substrate.

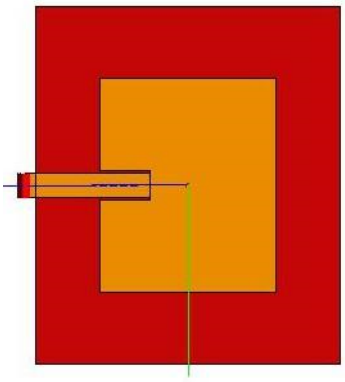


Figure 7.16: Design of edge fed RMPA without metamaterial

The design of RMPA without metamaterials is shown in Table7.6. Resonance freq. = 28 GHz, Substrate: RT Duroid 5880 $\epsilon_r = 2.2$, Loss tangent : 0.0009, height of substrate(h) = 0.25 mm

(Fig.7.17) dipicts the reflection coefficient v/s frequency graph of RMPA. At the

Table 7.6: Design of RMPA without metamaterial

Patch dimensions	Calculated dimensions of patch antenna (mm)	Optimized dimensions of Patch antenna (mm)
Width of patch(W)	4.24	4.11
Length of patch (L)	3.48	3.36
Sub. width (Ws)	7.85	6.84
Sub. length (Ls)	6.0	5.8
Feed length	2.17	1.97

resonance frequency the return loss is -54 dB.

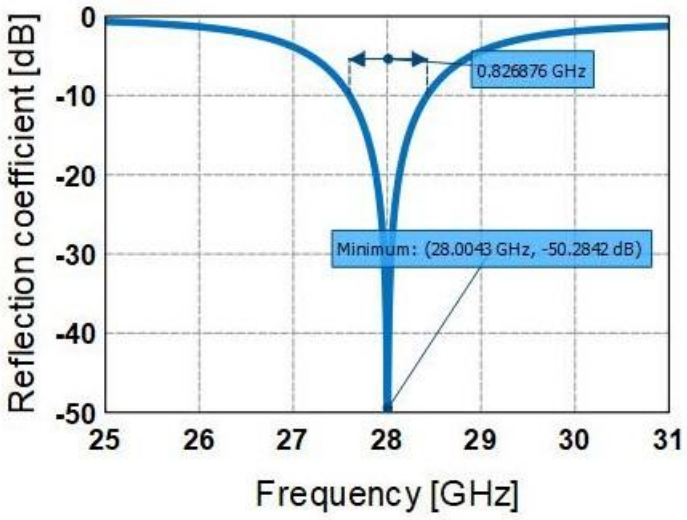


Figure 7.17: Reflection coefficient v/s freq of RMPA without metamaterials

At resonance frequency the return loss is very low, which means the maximum power is radiated by antenna. The BW, gain, return loss and VSWR are shown in Table7.8. Return loss Of antenna depends on its impedance matching.Return loss is very low for perfectly matched antenna.

(Fig.7.18) presents far field radiating pattern in UN and VN plane at 28 GHz resonance frequency. The gain of antenna is 6.39 dBi at 0°. And directivity equal to 7.64 dBi at 28 GHz.

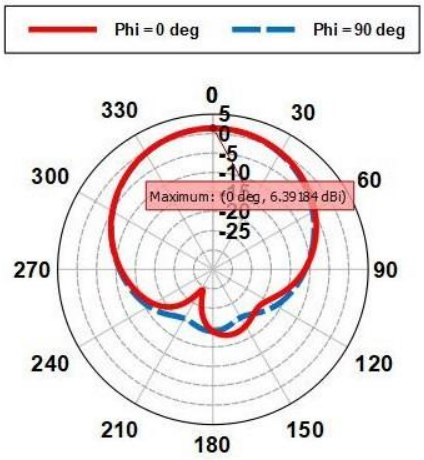


Figure 7.18: Far field radiating pattern and total gain at 28 GHz

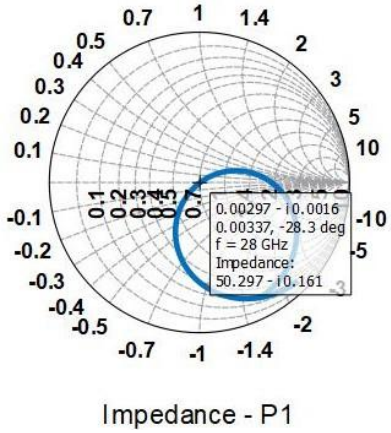


Figure 7.19: smith chart with impedance matching

The smith chart showing impedance matching at 28 GHz of RMPA is presented

in (Fig.7.19). At 28 GHz the impedance is almost 50 ohms.Total surface current and far field view are depicted in (Fig.7.20)

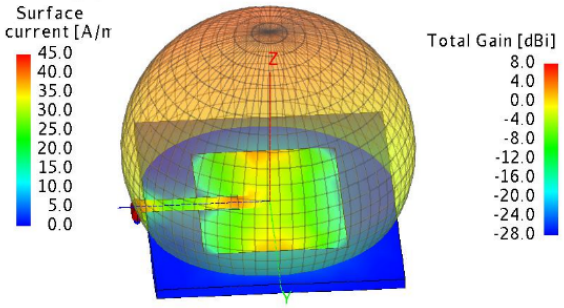


Figure 7.20: 3D view of far field and surface current

7.2.4 Rectangular Microstrip Patch Antenna (RMPA) design with Metamaterial at 28 GHz Resonating Frequency

(Fig.7.21) Shows the design of RMPA with metamaterial cells on the surface of rectangular patch.

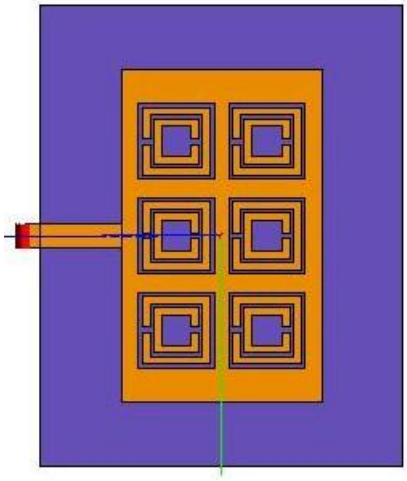


Figure 7.21: Design of edge fed RMPA with metamaterial

The optimized design of edge fed microstrip patch antenna with metamaterial is shown in Table 7.7. The patch antenna is designed on RT Duroid substrate. Resonance freq. = 28 GHz, Substrate : RT Duroid 5880, $\epsilon_r = 2.2$, Loss tangent = 0.0009, height of substrate(h) = 0.2 mm. (Fig.7.22) show the reflection coefficient v/s frequency graph of RMPA with metamaterial. At resonance frequency, the return loss is very low (-39 dB).

Table 7.7: Design of RMPA with metamaterial

Patch dimensions	**Optimized dimensions of patch antenna with metamaterial(mm)**
Width of patch(W)	4.4
Length of patch (L)	2.65
Sub. width (Ws)	6.1
Sub. length (Ls)	4.81
Feed length	1.08
Feed width	0.35

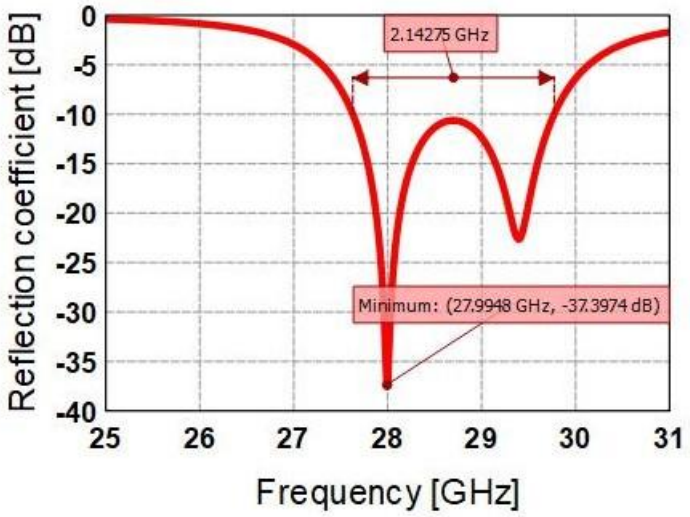


Figure 7.22: Reflection coefficient v/s freq.ofRMPA with metamaterial

(Fig.7.23) and (Fig.7.24) presents 2D and 3D far field radiating pattern of RMPA with metamaterial showing gain in UN and VN plane at 28 GHz resonance frequency. The gain of antenna is $6.31dBi$ at 0°.Directivity equal to $7.66dBi$ at 28 GHz. (Fig.7.26) is a Smith chart showing impedance matching of RMPA with metamaterial at 28 GHz. At 28 GHz the impedance is almost 50 ohms and reactive impedance is almost zero, which matches with source impedance. (Fig.7.25) presents VSWR, Its is equal to 1.00 which signifies perfect matching of source impedance of 50 ohms with antenna.

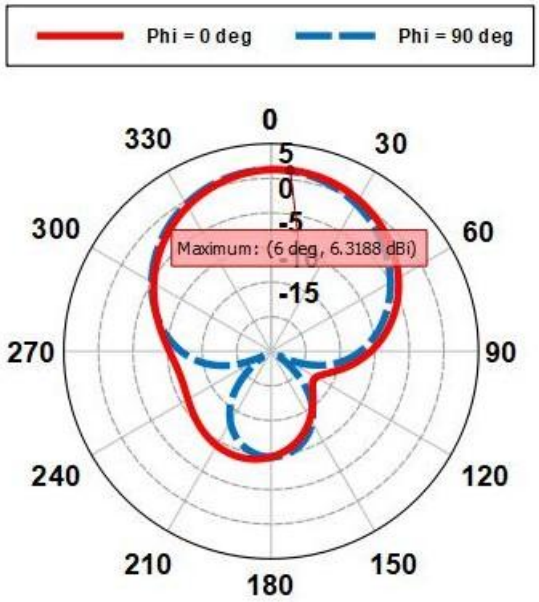


Figure 7.23: Far field radiation pattern of antenna with metamaterial

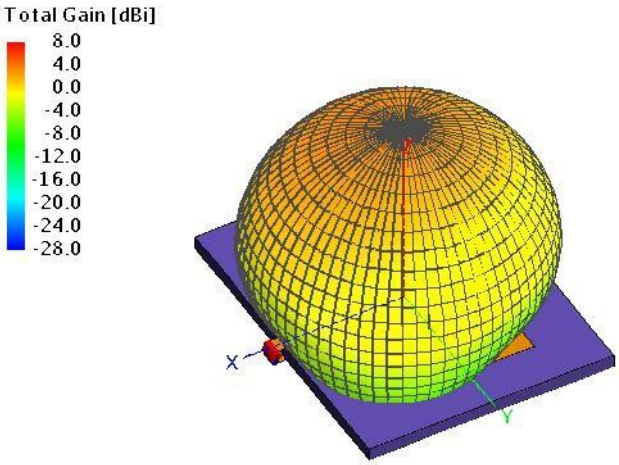


Figure 7.24: 3D far field radiation pattern

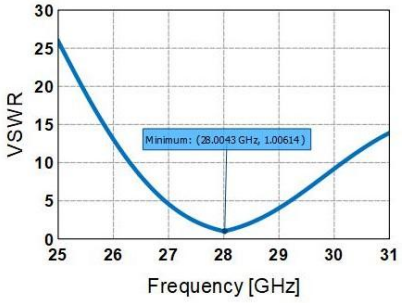


Figure 7.25: VSWR

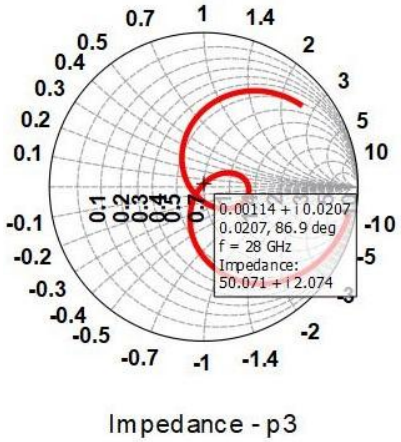


Figure 7.26: impedance matchingat 28 GHz

Table 7.8: Different parameters of RMPA.

Parameters	RMPA without metamaterial	RMPA with metamaterial
Reflection coefficient	-50dB	-39 dB
Bandwidth (10dB)	0.826 GHz	2.14 GHz

The 3D view of far-field of RMPA with metamaterials at 28 GHz resonance frequency is presented, Total gain has been depicted in the figure.

7.2.5 Simulation results

The metamaterial cell comprising of SSRR is designed and simulated using the software. A metamaterial cell with only SSRR shows negative permeability to state it as a single or mu negative metamaterial cell. The comparison of the parameters of RMPA and metamaterial-based RMPA with the same resonance frequency is listed in Table 7.8. Rectangular microstrip patch antenna for 5G wireless Network technology is effectively and efficiently designed, implemented, and compared for better performance at a 28 GHz resonance frequency. Conventional RMPA and RMPA loaded with metamaterial on the patch are simulated at frequency 28 GHz. It has been observed that the gain of antennas remains almost constant and the bandwidth of patch antenna increases considerably in comparison to RMPA without metamaterial.

RMPA without cells returns loss and bandwidth are –50 dB and 0.826 GHz respectively. Whereas RMPA with metamaterial the values of return loss and bandwidth are -39 dB and 2.14 GHz respectively. So the bandwidth is increased by 1.32 GHz[91]. Based on simulated results it has been found that the bandwidth of RMPA has improved. VSWR of the conventional antenna is 1.01 and that of the antenna with metamaterial is 1.00 which indicates that antenna impedance is perfectly matched with the source impedance of 50 ohms.

7.3 Mathematical Modelling of Metamaterial Cell on Various Dielectric Substrates and comparison with Numerical simulations

7.3.1 Introduction

Mathematically modeling and simulating a single negative metamaterial cell comprising of a square split ring resonator with two rings.Various dielectric substrates like FR4, Rogers RT/Duroid5880 and Roger RT/Duroid 6006 are used for modeling metamaterial cell This metamaterial cell depicts negative values of permeability for a specific range of frequencies. The resonant frequency predicted analytically is found to be extremely close to the frequency obtained by modeling metamaterial structure. The curves for the metamaterial's complex permeability based on its unit element are calculated using a parameter-retrieval method employing the S parameters. The S parameters are extracted using simulating software. The method used to extract the S parameters is one using perfect electric and perfect magnetic (PE-PM) boundary conditions.Parameter extraction procedure is described in section 7.2.2. [79]

7.3.2 Design of mu negative metamaterial Cell on RT/Duroid 5880 substrate

. The SSRR shown in fig.7.27 with two rings is designed on Rogers RT/ Duroid 5880 substrate with permittivity value equal to 2.2 and thickness equal to 0.5 mm. The dimensions of 5x5 mm SSRR cell are, L = 5 mm, b = 3 mm, c= 0.5 mm, Strip width e = 0.5 mm, and spacing between n and (n+1) th turn is d = 0.5 mm, The resonance frequency is inversely proportional to the size of the cell, and it also depends on strip width, slit, spacing between (n+1) and n th ring.(Fig.7.27) shows the geometry of the SSRR consisting of two rings with their slit displaced by 180°.

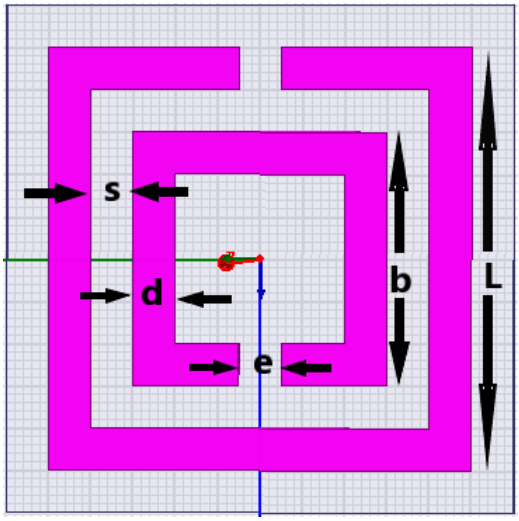


Figure 7.27: Square split-ring resonators (SSRR) metamaterial

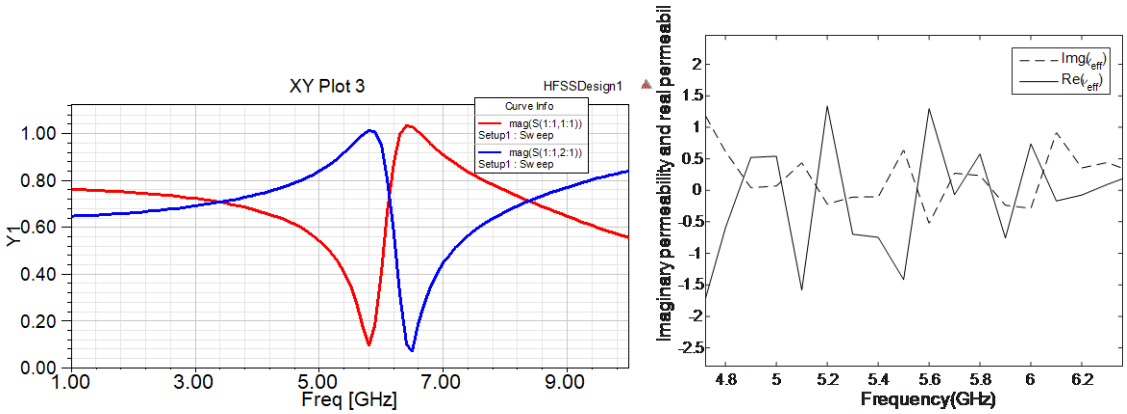
Calculation of total strip length Ln of nth ring of the SSRR and the total spacing length Lg between nth and (n+1) th turn of SSRR, total inductance and of the total distributed capacitance between two consecutive rings of SSRR, of strip width d is explained in previous section, shown in the equations 7.3 to 7.6.[92]

7.3.3 Method to find parameters of SSRR metamaterial cell

Metamaterial cell simulation in the waveguide is explained in section 7.2.2 .

7.3.4 Simulated results

The SSRR with two rings on a substrate Rogers RT/ Duroid 5880 has been simulated within waveguid, perfect electric and perfect magnetic (PE-PM) boundary conditions are set up on appropriate axis and excitation is applied to reveal electromagnetic propagation through the structure. After simulation, It has been observed that the metamaterial cell resonates at 5.8 GHz frequency. The graph of S_{11} and S_{21} v/s frequency is presented in (Fig.7.28a) . The resonating frequency thus observed is shown in the figure. It is also observed from(Fig.7.28b) that permeability of the cell is negative at 5.8 GHz frequency. Also, the values of inductance, capacitance, and resonance frequency of SSRR are presented in Table7.9 The SSRR with the substrate FR4 has been simulated within waveguide, It has been observed that the resonance frequency of metamaterial cell is

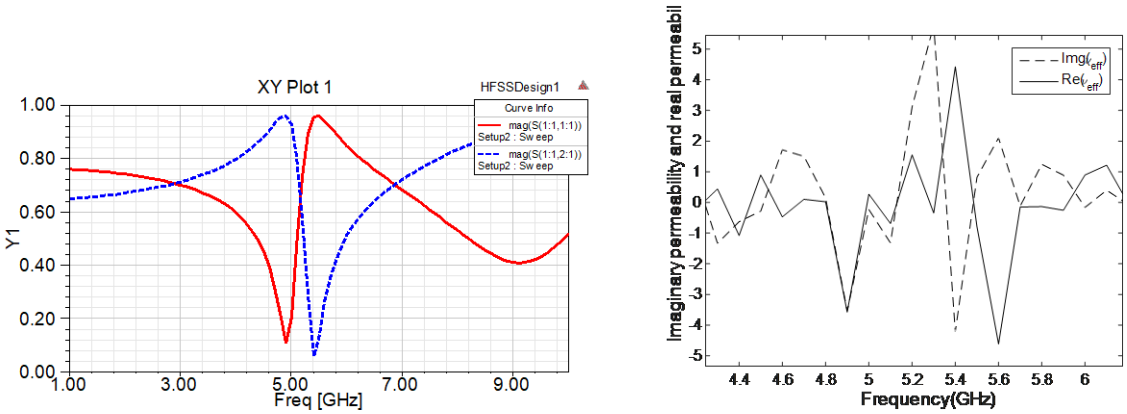


(a) The graph of S_{11} and S_{21} v/s frequency of SSRR with Roger RT Duroid 5880 substrate

(b) The graph of Permeability V/s frequency of SSRR with Roger RT Duroid 5880 substrate

Figure 7.28: SSRR parameters

4.9 GHz. The graph of S_{11} and S_{21} v/s frequency is presented in (Fig.7.29a). The resonating frequency thus observed is shown in the figure. It is also observed from figure and (Fig.7.29b). that permeability of cell is negative at 4.9 GHz frequency.[13] [93] (Fig.7.30a) depicts the graph of S_{11} and S_{21} v/s fre-

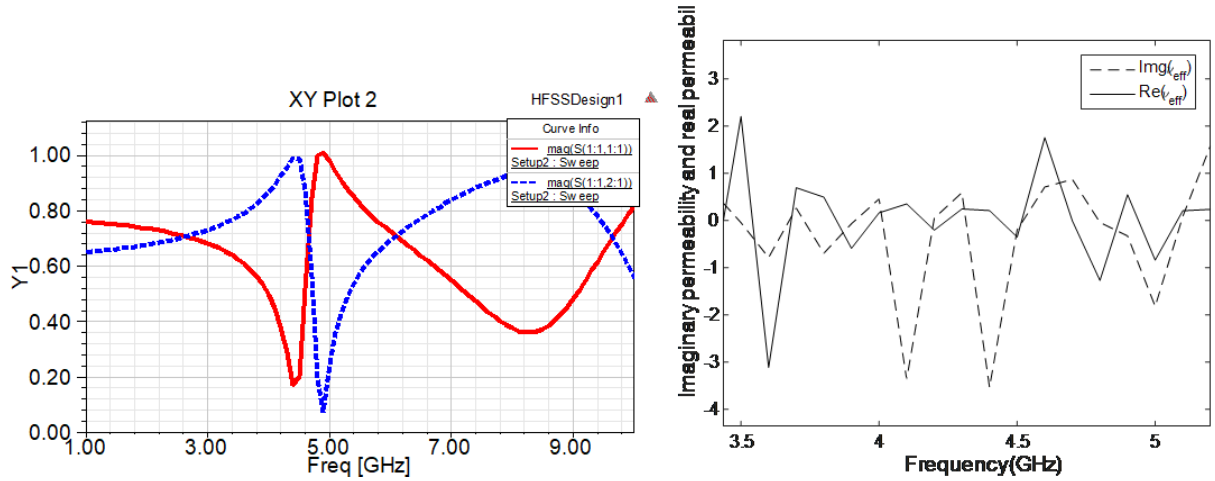


(a) The graph of S_{11} and S_{21} v/s frequency of SSRR with FR4 substrate

(b) The graph of Permeability V/s frequency of SSRR with FR4 substrate

Figure 7.29: SSRR parameters

quency of SSRR with substrate Rogers RT/Duroid 6006. It is observed that the resonance frequency of metamaterial cell is 4.4 GHz. The resonating frequency thus observed is shown in the fig.7.30a It is also observed from (Fig.7.30b) that permeability of the cell is negative at 4.4 GHz frequency.[94] [77]



(a) The graph of S11 and S21 v/s frequency of SSRR with Roger RT Duroid 6006 substrate

(b) The graph of Permeability V/s frequency of SSRR with Roger RT Duroid 6006 substrate

Figure 7.30: SSRR parameters

Table 7.9: Comparison of calculated and simulated resonance frequencies of SSRR with various dielectric materials

substrate material	Dielectric constant	No of turns	length of side Of SSRR (L) mm	Ls (nH)	C(pf)	Calculated resonance frequency(GHz)	Measured resonance frequency (GHz)	Effe. Permeability at resonance frequency
Rogers RT/Duroid 5880	2.2	02	05	7.9	0.104	5.56	5.8	-0.5
FR4	4.4	02	05	7.9	0.146	4.69	4.9	-0.4
Rogers RT/Duroid 6006	6.15	02	05	7.9	0.2	4	4.4	-3.5

Chapter 8

Design and development of metamaterial based bioinspired patch antenna

8.1 Introduction

This chapter attempts to discuss some novel architectures and techniques for designing conventional and metamaterial loaded bio-inspired planar microstrip patch antennas such as hibiscus leaf and Kaju leaf shape antennas. Both antennas are loaded with mu negative metamaterial cells, With the introduction of the internet, the demand for and popularity of mobile terminals (laptops, cell phones, etc.) has skyrocketed, propelling the telecommunications industry to new heights. The digital information system and wireless communication technology play an important role in the development of society. Various wireless services, such as Wi-Fi, Bluetooth, GPS, NFC, 4G, and 5G systems that operate in multiple frequency bands, necessitate the use of portable devices for broadband applications. The rapid expansion of wireless communication systems necessitates the use of a base station and a portable terminal outfitted with the best antenna. The portable terminals should satisfy some important characteristics, such as miniaturization, system integration, and multiband or broadband operation. Microstrip antennas are ideal for wireless communication applications due to several important characteristics. For further advances and suitability for the construction of antennas, the researchers concentrated on using bio-inspired geometrical

shapes. The most important one is bioinspired plant geometries, which employ plant part shapes such as leaves, fruits, and flowers to create antennas for various frequencies and technologies. The study of microstrip antennas based on models inspired by leaves (leaf-shaped antennas) has piqued researchers' curiosity due to promising outcomes. We propose hibiscus and Kaju shape geometries for patch antennas. The second category is bioinspired antennas in animals, which strive to mimic the operation of antennas used in communication systems by using the shape of exterior components or the shape of organs of the animals.[95] [93].These antennas are loaded with metamaterials for improvement in their performance. The development of planar antenna technology in recent years has fundamentally changed the microwave and millimeter-wave communication fields. Planar antennas can be printed on different types of dielectric substrates with minimum cost and processing. One fundamental factor that makes planar antennas so desirable and important is their easy way of integration with microwave or millimeter-wave circuit components. A metamaterial is an artificial material that is constructed using an array of metallic resonant cells. Metamaterials' lattice constants should be much smaller than their wavelengths. A conventional antenna and a proposed novel edge port fed bio-inspired microstrip patch antenna (BMPA) with a resonance frequency of 5.8 GHz and a ground plane of the substrate loaded with square split-ring resonators are simulated using software, analyzed and comparison of parameters such as bandwidth, return loss, gain and VSWR is presented. This patch antenna is built on an FR-4 substrate with a permittivity of 4.4 and a thickness of 1.6 mm. The FR-4 material is cheaper and more easily available. Surface wave propagation is decreased by a metamaterial-loaded substrate, which improves antenna performance.This patch antenna with improved parameters can be used for WiMAX applications. It is a wireless technology based on the IEEE 802.16 standard that provides fast data over a widespread area. The WiMAX stands for Worldwide Interoperability for Microwave Access, and it is a point to multipoint wireless networking technology . It works in three layers: the phys-

ical layer, MAC layer, and convergence layer. The bandwidth required for the band with a center frequency of 5.8 GHz is 300 MHz. And, with a bandwidth greater than required, the proposed patch antenna was found to be suitable for this application. The parameters of the conventional antenna are compared with the metamaterial-loaded antenna.

8.2 Circular Microstrip Patch Antenna

8.2.1 Circular microstrip patch antenna(CMPA)

The Microstrip patch antenna was patented in 1955. But around the 1970s, this started receiving considerable attention. Microstrip antennas, as shown in figure 2.1, consist of a dielectric substrate sandwiched between a very thin metallic strip (patch) and the ground plane. A Circular microstrip patch antenna (CMPA) shown in (Fig.8.1)is an initiator for the proposed bioinspired microstrip patch antennas (BMPA). That is a hibiscus and Kaju leaf shape patch antenna. Refer section 6.2.4 for the design equations of CMPA. For the resonant frequency (fr) at 5.8 GHz, the radius of the patch (r) is 6.48 mm. The radius of the substrate is 9.6 mm. The feed length is 2.4 mm. The diameter of CMPA is 12.96 mm. Then the resultant CMPA is perturbed to achieve the proposed BMPA structure.Where the length of the axis of the proposed BMPA for a resonance frequency of 5.8 GHz is in line with the diameter of the CMPA[25]. The proposed structure is built on FR4 substrate with a dielectric constant of 4.4, a loss tangent of 0.02, and the height of the substrate is 1.6 mm. The graph of reflection coefficient v/s frequency of CMPA is depicted in (Fig.8.2) . The bandwidth of the antenna is 250 MHz

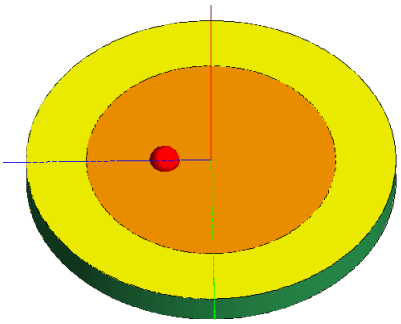


Figure 8.1: Circular MPA

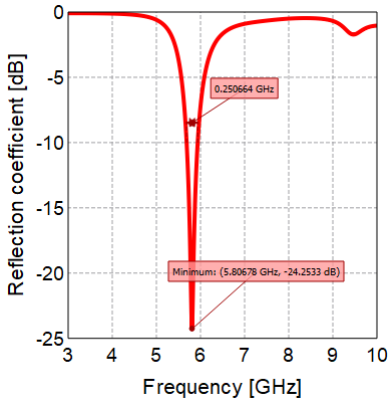


Figure 8.2: Reflection coefficient v/s frequency of CMPA

The shape of hibiscus and Kaju leaves is very close to the circle hence designed initiator is the circular microstrip patch antenna (CMPA). Hibiscus is a flowering plant and Kaju is an important dry fruit crop found in Goa. The real images of the proposed hibiscus and Kaju leaves are shown in (Fig.8.3)

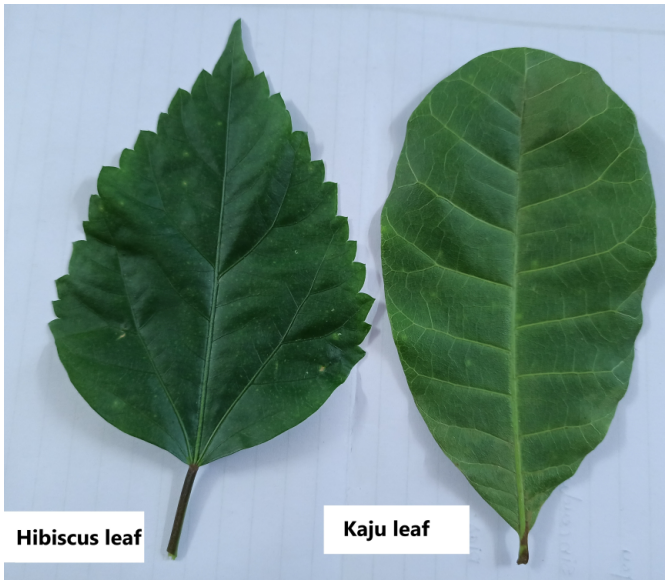


Figure 8.3: Hibiscus and Kaju leaves

8.3 Metamaterial Design

8.3.1 Double negative metamaterials

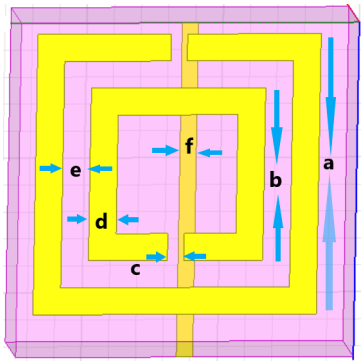


Figure 8.4: split-ring resonators (SSRR)

The SSRR Structure is designed using MATLAB code.The metal surface obtained is shown in the (Fig.8.4). The SSRR and conductor strip on the ground plane create negative μ and negative ϵ respectively near resonance frequency.[43].

8.3.2 Design of the SSRR Cell

The SSRR and strip are designed respectively on the top and bottom of the FR-4 substrate as shown in Fig.8.4. Its permittivity is 4.4, and thickness is equal to 1.6 mm. The dimensions of 4.8 mm x 4.8 mm SSRR are, a= 3.9 mm, b=3.2 mm, c=0.22 mm, d=0.35 mm, and e=0.45 mm. Strip width f = 0.6 mm and strip length= 4.8 mm.

8.3.3 Parameters of the SSRR Metamaterial Cell

S_{11} and S_{21} of the SSRR cell depicted in(Fig.8.5) The lowest magnitude of S_{11} indicates that the cell resonates at a 5.8 GHz frequency. The magnitude of S_{11} and S_{21} at the 5.8 GHz frequency is 0.2 and 0.79, respectively. This shows that the return loss is low at the resonance frequency. Both S parameters are important for calculating the epsilon and mu of the cell. Frequency v/s epsilon and mu are plotted using MATLAB software.

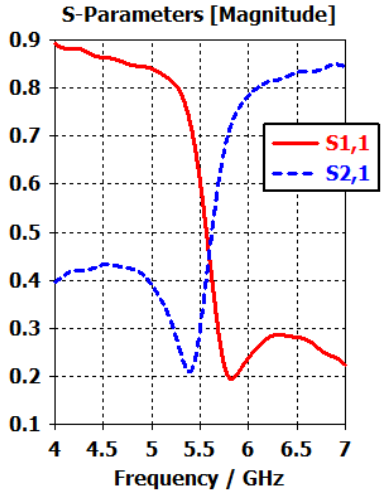


Figure 8.5: S_{11} and S_{21} of SSRR cell

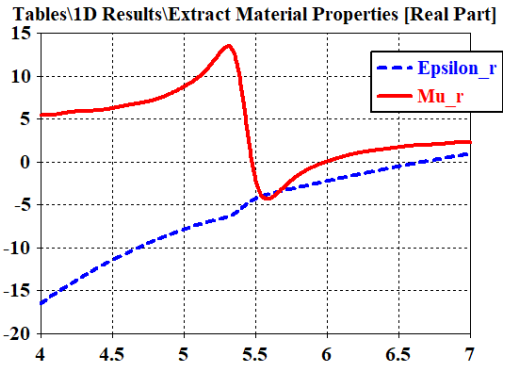


Figure 8.6: Permittivity and permeability of SSRR

(Fig.8.6) shows the real part of the permittivity (epsilon) and permeability (mu) of SSRR, which are negative. The negative epsilon and mu appear in the frequencies between 5.5 GHz to 6.2 GHz. Therefore, the antenna on the metamaterial must be designed to operate within a range of frequencies. At 5.8 GHz, the permeability is -4.5, and the permittivity is -3.6. (Fig.8.7) shows the real and imaginary refractive index and impedance of SSRR. It is observed that the real refractive index is negative near the resonance frequency. Imaginary impedance equal to almost zero and real impedance equal to 50 ohms at the resonance frequency.

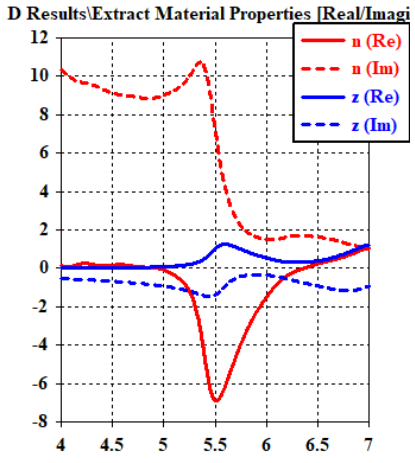


Figure 8.7: Refractive index and impedance of double negative SSRR

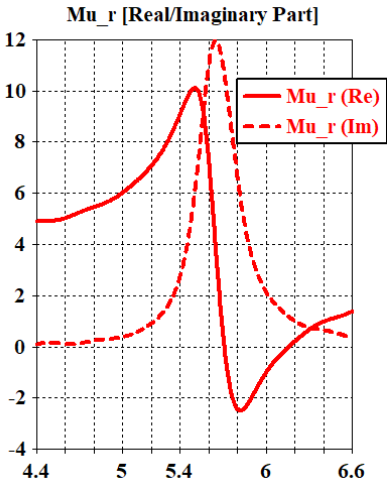


Figure 8.8: Mu of SSRR at frequency 5.8 GHz.

The proposed cell is 4.8 mm x 4.8 mm, Smaller dimensions cell will show

the negative value of permittivity and permeability at a higher frequency. Some authors have designed such a cell. 2.2mm x 2.2 mm cell shows negative values of a parameter at around 10 GHz.

8.3.4 Single negative metamaterial cell

Cells that show either permeability negative or permittivity negative are referred to as single negative metamaterial cells. If permeability is negative then it is called a mu negative metamaterial cell. The SSRR was designed on FR-4 substrate with a permittivity of 4.4 and thickness equal to 1.6 mm. The dimensions of 4.8mm x 4.8 mm SSRR are, a =4 mm, b=3 mm, c=0.22 mm, d=0.5 mm, and e=0.4 mm. Real and imaginary values of mu of SSRR are shown in Fig.8.8. The negative mu appears in the frequencies between 5.65 GHz to 6.2 GHz. Therefore, the antenna on the metamaterial must be designed to operate within the range of frequencies. Hence, in this project, we considered a resonance frequency of 5.8 GHz. Which is one of the frequency bands used for WiMAX applications in India.

8.4 Hibiscus leaf shape Microstrip Patch Antenna

8.4.1 Design of Hibiscus leaf shape Microstrip patch Antenna (HLMPA) for WIMAX and other Wireless Applications

The hibiscus leaf shape is somewhat similar to the circle hence, to begin with, a circular microstrip patch antenna (CMPA) with a resonating frequency of 5.8 GHz has been designed and its radius was found to be 6.47 mm. The proposed bioinspired structure of the hibiscus leaf is presented in (Fig.8.9) The circular patch was designed to determine the approximate length of the major axis of the hibiscus leaf microstrip patch antenna (HLMPA). Then the resultant CMPA is perturbed to acquire the proposed HLMPA structure[26]. The dimensions of an antenna are optimized using FEKO. This antenna resonates at frequencies 5.8 GHz, 10 GHz, and 13.4 GHz. The dimensions of HLMPA are shown in Table 8.1

Table 8.1: Design of HLMPA

Patch dimensions	Optimized dimensions of Patch antenna (mm)
Major axis of patch	14.1
Minor axis of patch	10
Sub. width (Ws)	18
Sub. length (Ls)	20
Feed length	3.3
Feed width	0.8

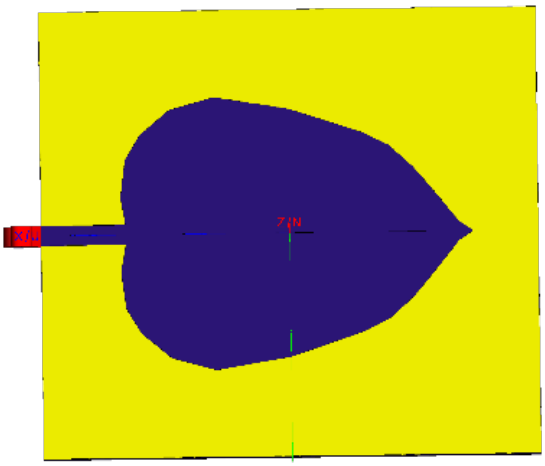
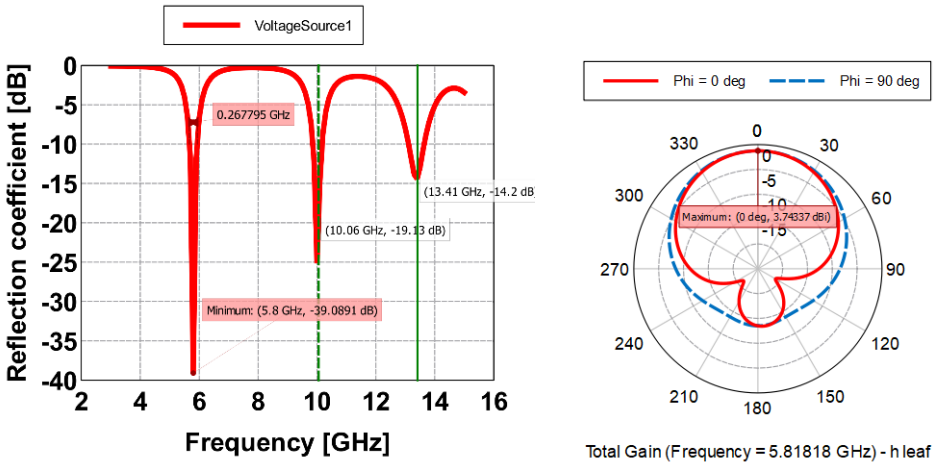


Figure 8.9: Hibiscus leaf microstrip patch antenna

8.4.2 Different parameters of HLMPA

The gain is an important parameter of an antenna that describes an it's performance. Although the antenna gain is closely related to directivity, it is a metric that considers the antenna's efficiency as well as its directional capabilities. The pattern controls the directional qualities of the antenna, which are a function of the antenna's directivity. The gain of an antenna in a particular direction is defined as the ratio of the intensity in that direction to the isotropically radiated antenna's radiation intensity. The second significant antenna parameter is bandwidth, which is defined as the frequency range in which the antenna's properties

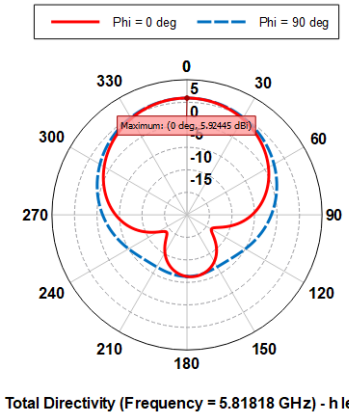
support set standard values. It is the frequency range on both sides of the center frequency. when the antenna input impedance, pattern, beamwidth, polarization, gain, and radiation efficiency are all satisfactory at the center frequency [9]. The graph of reflection coefficient v/s frequency of HLMPA is depicted in (Fig.8.10a). It resonates at 5.8 GHz, 10 GHz and 13.4 GHz. These parameters determine the ratios of the amplitudes of the transmitted and reflected wave when a plane wave is an incident on the dielectric medium. The BW, gain, return loss, and VSWR are shown in Table 8.2. The return loss of an antenna depends on its impedance matching. Fig.8.10b presents a far-field radiating pattern in the UN and VN plane at 5.8 GHz resonance frequency. The gain of an antenna is 3.74 dBi at 0° degrees. And directivity is equal to 5.9 dBi at 5.8 GHz shown in (Fig.8.11a). Far-field radiating patterns in the UN and VN planes at resonance frequencies of 10 GHz has been presented in (Fig.8.11b). At 10 GHz, the gain of an antenna is 3.51dBi at −48°. At 13.4 GHz resonance frequency, the gain of an antenna is 1.9 dBi at −64°.



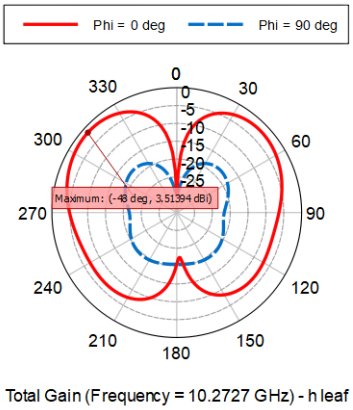
(a) Reflection coefficient v/s frequency of HLMPA.

(b) Far-field radiating pattern at 5.8 GHz of HLMPA.

Figure 8.10: Hibiscus leaf antenna parameters-1



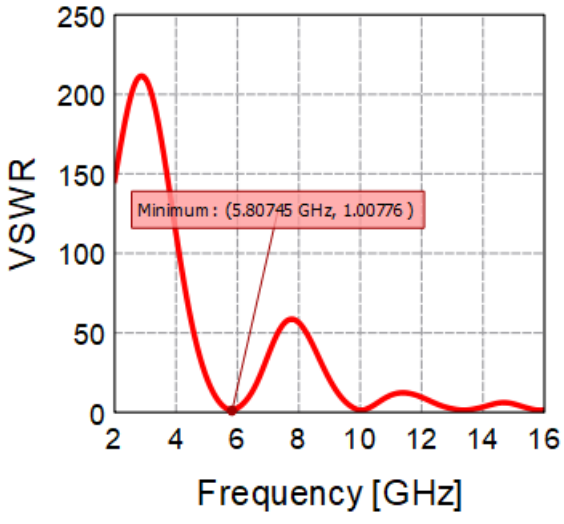
(a) Directivity of antenna



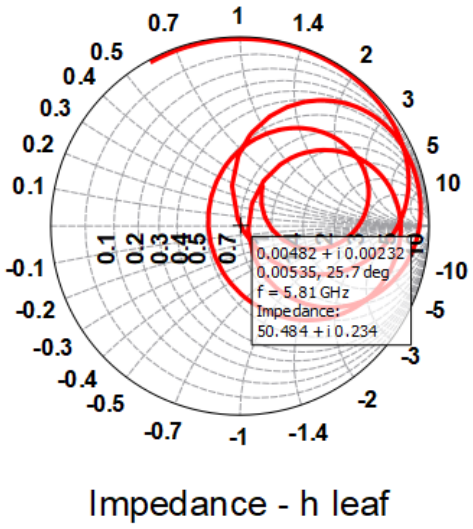
(b) Far-field radiating pattern at 10 GHz.

Figure 8.11: Hibiscus leaf antenna parameters-2

The smith chart showing impedance matching at 5.8 GHz of HLMPA is presented in (Fig.8.12b) At 5.8 GHz the impedance is almost 50 ohms. VSWR is depicted in fig.8.12a Its value at 5.8 GHz is 1.01. (Fig.8.13) presents a 3D view of the far-field of an edge-fed HLMPA without metamaterial at 5.8 GHz.The total gain of an antenna also has been depicted in the (Fig.8.13) .



(a) VSWR of HLMPA



(b) Impedance matching of HLMPA at 5.8GHz.

Figure 8.12: Hibiscus leaf antenna parameters-3

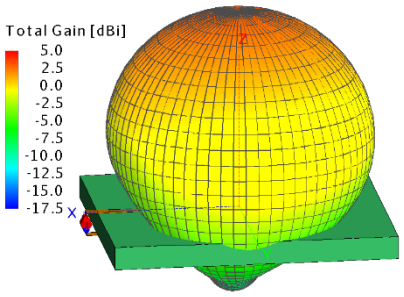


Figure 8.13: 3D view of the far-field of HLMPA.

Table 8.2: Different parameters of HLMPA.

Resonance Frequency	5.8 GHz	10 GHz	13.4 GHz
Reflection coefficient	-39.1dB	-24.1 dB	-14 dB
Bandwidth (10dB)	267.7MHz	280.5 MHz	450.8 MHz
Gain	3.74 dBi	3.51dBi	1.9 dBi
VSWR	1.01	1.04	1.12

8.4.3 Design of metamaterial-loaded HLMPA (MHLMPA) for WIMAX and other wireless applications

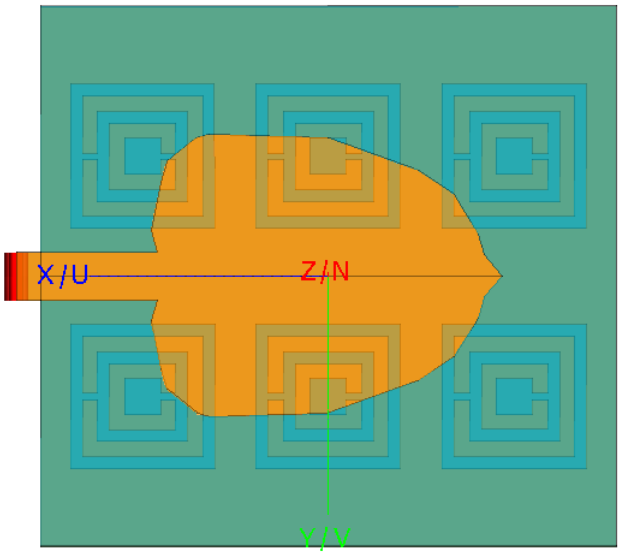


Figure 8.14: Metamaterial loaded HLMPA(MHLMP)

(Fig.8.14) shows the design of an edge-fed HLMPA with mu negative metamaterial cells on the ground plane of an antenna. Optimized dimensions of the patch antenna are presented in Table 8.3 Reflection coefficient v/s frequency graph of

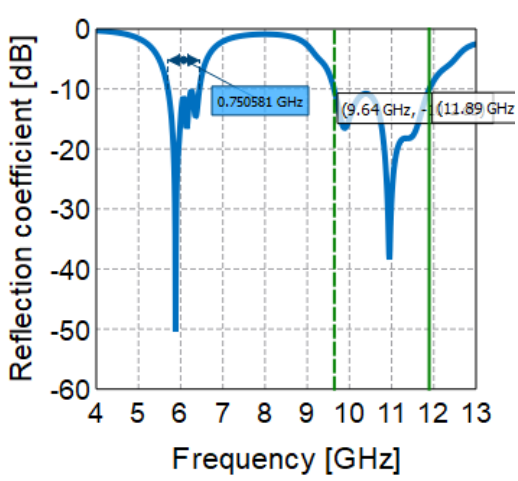
Table 8.3: Design of MHLMPA

Patch dimensions	**Optimized dimensions of Patch antenna (mm)**
Major axis of patch	11
Minor axis of patch	9.4
Sub. width (Ws)	18
Sub. length (Ls)	19
Feed length	3.8
Feed width	1.6

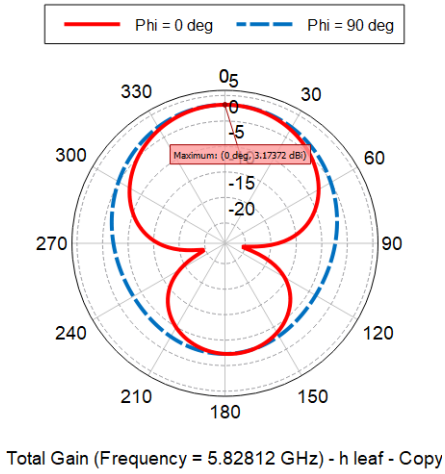
HLMPA with metamaterial (MHLMPA) is shown in (Fig.8.15a). At the resonance frequency, the return loss is very low (-50dB), Radiation of power mainly depends on the return loss. The lower the return loss, the higher the radiated power.

8.4.4 Different parameters of MHLMPA

Improvement in parameters of patch antenna has been observed after loading metamaterial cells on edge feed HLMPA. The graph of reflection coefficient v/s frequency of MHLMPA is depicted in (Fig.8.15a) It resonates at 5.8 GHz, and 11 GHz. At the resonance frequency, the return loss is very low, The BW, gain, return loss, and VSWR are presented inTable 8.4. (Fig.8.15b) presents a far-field radiating pattern in the UN and VN plane at 5.8 GHz resonance frequency. The gain of an antenna is 3.1 dBi at 0°. (Fig.8.16a) presents a far-field radiating pattern in the UN and VN plane at 11 GHz resonance frequency. At 11 GHz, the gain of an antenna is 1.8 dBi at $-44°$.



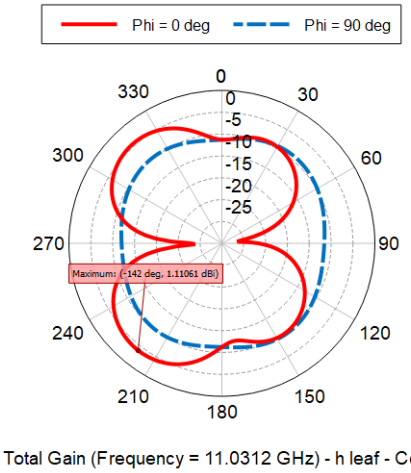
(a) Reflection coefficient v/s frequency of MHLMP



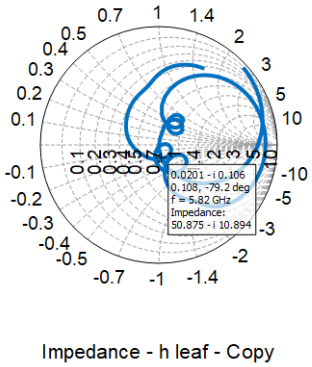
(b) Far-field radiating at 5.8 GHz of MHLMPA

Figure 8.15: MHLMPA antenna parameters

The smith chart showing impedance matching at 5.8 GHz of MHLMPA is presented in (Fig.8.16b) At 5.8 GHz, the impedance is almost 50 ohms. VSWR is depicted in (Fig.8.15b) Its value at 5.8 GHz is 1.02. The gain of an antenna is a very important parameter.



(a) MHLMPA Far-field radiating pattern at 11.3 GHz.



(b) Impedance matching of MHLMPA at 5.8GHz

Figure 8.16: MHLMPA antenna parameters

(Fig.8.15b) presents a 3D view of the far-field of an edge fed MHLMPA at 5.8 GHz. The total gain of an antenna has been shown in the figure.

Table 8.4: Different parameters of MHLMPA.

Resonance Frequency	5.8 GHz	11 GHz
Reflection coefficient	-50 dB	-38.6 dB
Bandwidth (10dB)	750MHz	2.25 GHz
Gain	3.1 dBi	1.19dBi
VSWR	1.02	1.04

8.5 Kaju leaf shape Microstrip Patch Antenna

8.5.1 Design of geometrical structure of Kaju leaf shape Microstrip Patch Antenna

The shape of the Kaju leaf also matches with the geometry of the circle to a great extent. Hence, the design has been initiated from a circular microstrip patch antenna (CMPA) with a radius of 6.47 mm. The proposed bioinspired structure of the Kaju leaf is presented in(Fig.8.17) It resonates at frequencies of 5.8 GHz and 9.67 GHz. Then the resultant CMPA is perturbed to achieve the proposed KLMPA structure . The proposed structure is built on an FR4 substrate. Its dielectric constant is 4.4, loss tangent 0.02, and the height of the substrate is 1.6 mm .The dimensions of KLMPA are presented Table 8.5.

Table 8.5: Design of KLMPA

Patch dimensions	**Optimized dimensions of Patch antenna (mm)**
Major axis of patch	14.2
Minor axis of patch	10.6
Sub. width (Ws)	20
Sub. length (Ls)	21
Feed length	2.5
Feed width	0.6

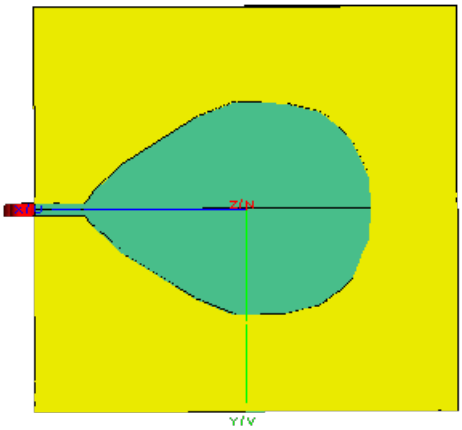
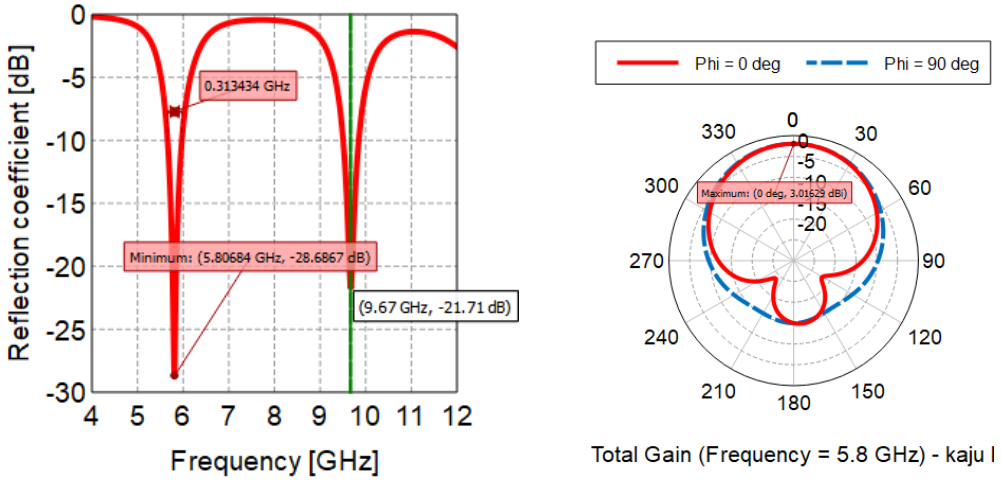


Figure 8.17: KLMPA

8.5.2 Different parameters of KLMPA

The graph of reflection coefficient (dB) v/s frequency (GHz) of HLMPA is presented in (Fig.8.18a). It resonates at 5.8 GHz and 9.67 GHz. The BW, Gain, return loss, and VSWR are shown in Table 8.6.(Fig.8.18b) presents a far-field radiating pattern in the UN and VN plane at 5.8 GHz resonance frequency. The gain of an antenna is 3.1 dBi.(Fig.8.19a) presents a far-field radiating pattern in the UN and VN plane at 9.7 GHz resonance frequency.(Fig.8.19b) is for impedance matching.



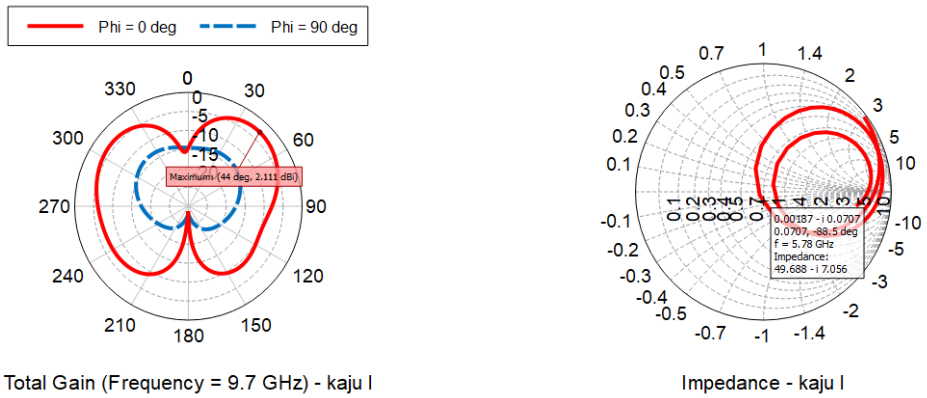
(a) Reflection coefficient v/s frequency of KLMPA.

(b) Far-field radiating at 5.8 GHz of KLMPA.

Figure 8.18: KLMPA antenna parameters-1

Table 8.6: Different parameters of KLMPA.

Resonance Frequency	5.8 GHz	9.67 GHz
Reflection coefficient	-28.6 dB	-21.7 dB
Bandwidth (10dB)	313.9 MHz	390.5 MHz
Gain	3.1 dBi	2.11dBi
VSWR	1.02	1.04



(a) Far-field radiating pattern at 9.7 GHz. (b) Impedance matching of KLMPA at 5.8GHz.

Figure 8.19: KLMPA antenna parameters-2

8.5.3 Design of metamaterial-loaded KLMPA (MKLMPA) for wireless application

The proposed bioinspired structure of the metamaterial-loaded Kaju leaf (MKLMPA) is presented in(Fig.8.20) The various dimensions of an antenna are shown in Table 8.6. It resonates at frequencies 5.8 GHz and 9.18 GHz.

Table 8.7: Design of MKLMPA

Patch dimensions	Optimized dimensions of Patch antenna (mm)
Major axis of patch	12.7
Minor axis of patch	9.8
Sub. width (Ws)	19
Sub. length (Ls)	22
Feed length	3.1
Feed width	0.6

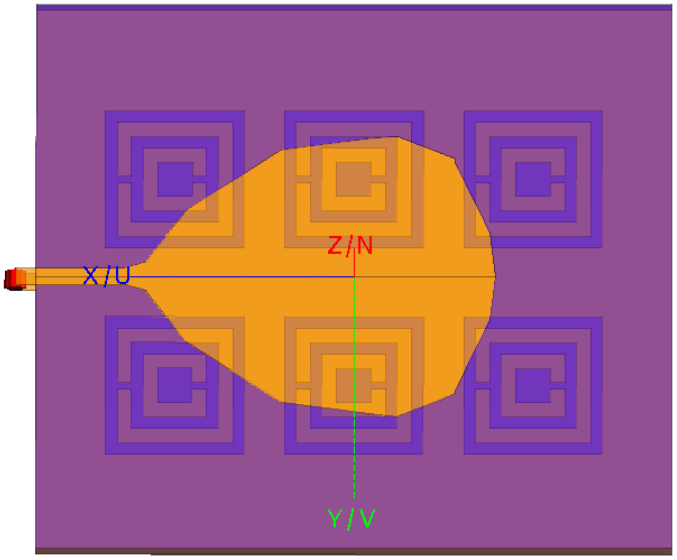


Figure 8.20: Metamaterial loaded Kaju leaf microstrip patch antenna

8.5.4 Different parameters of MKLMPA

The reflection coefficient v/s frequency graph of HLMPA is presented in(Fig.8.21) The frequencies at which it resonates are 5.8 GHz and 9.18 GHz. The BW, gain, return loss, and VSWR are depicted in Table 8.8 . The return loss is very low for a perfectly matched antenna. (Fig.8.22a) presents a far-field radiating pattern in the UN and VN plane at 5.8 GHz resonance frequency. The gain of an antenna is 3.79 dBi. (Fig. 8.22b) presents a far-field radiating pattern in the UN and VN plane at 9.18 GHz resonance frequency. The gain of an antenna and other

parameters are shown in Table 8.8. Fig. 8.23a presents impedance matching of antenna.Fig.8.23b presents 3D view of a far-field of MKLMPA and the total surface current distribution at 5.8 GHz frequency is shown in(Fig.8.24)

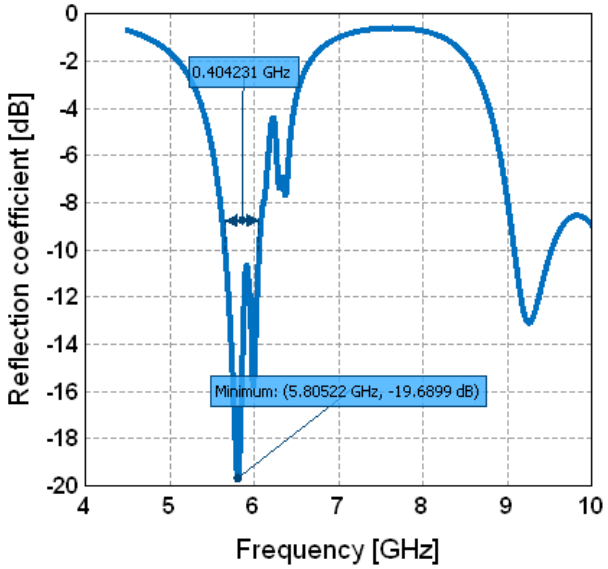
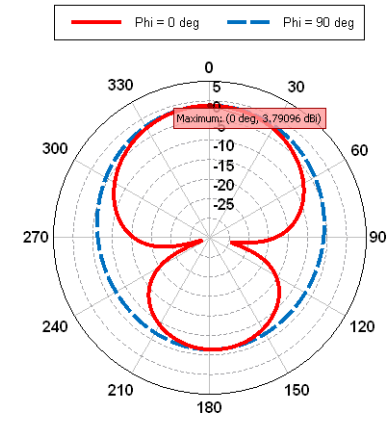
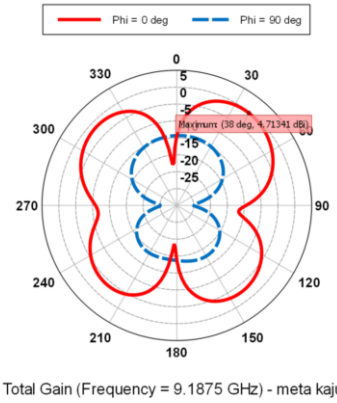


Figure 8.21: Reflection coefficient v/s frequency of KHLMPA



(a) Far-field radiating pattern at 5.8 GHz of MKLMPA

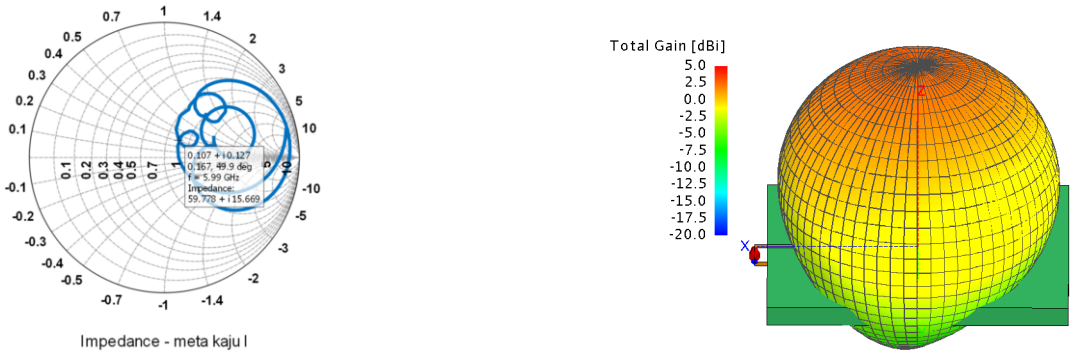


(b) Far-field radiating at 9.1 GHz of MKLMPA

Figure 8.22: MKHLMPA antenna parameters -1

Table 8.8: Different parameters of MKLMPA.

Resonance Frequency	5.8 GHz	9.18 GHz
Reflection coefficient	-19.68dB	-14 dB
Bandwidth (10dB)	404.4MHz	480.5 MHz
Gain	5 dBi	4.7 dBi
VSWR	1.04	1.14



(a) Impedance matching of MKLMPA at 5.8GHz (b) 3D view Far-field radiating MKLMPA

Figure 8.23: MKHLMPA antenna parameters -2

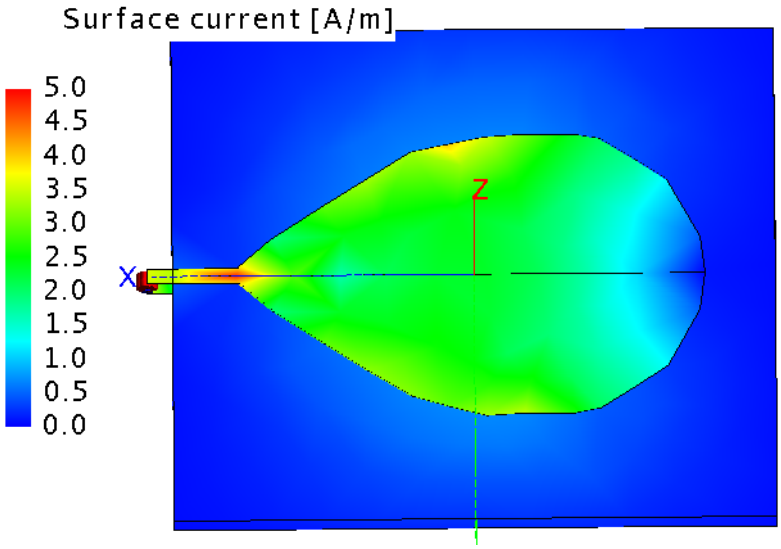


Figure 8.24: Total surface current distribution at 5.8 GHz.

8.6 Results and Discussion

The metamaterial cell comprising of SSRR and a copper strip on the ground plane of the substrate is designed and simulated using MATLAB software.

Table 8.9: The comparison of the parameters of HLMPA(HL), MHLMPAM(MH), KLMPA(KL), and MKLMPA(MK)

		HL	HL	HL	MH	MH	KL	KL	MK	MK
Resonance Frequency	GHz	5.8	10	13.4	5.8	11	5.8	9.67	5.8	9.18
Reflection coefficient	dB	-39.1	-24.1	-14	-50	-38	-28.6	-21.7	-19.7	-14
Bandwidth (10dB)	MHz	267.7	280.5	450.8	750	2250	314	391	404	480
Gain	dBi	3.74	3.51	1.9	3.1	1.2	3.2	2.1	5	4.7
VSWR	1.01	1.04	1.12	1.02	1.03	1.02	1.04	1.04	1.12	1.02

Metamaterial cell with SSRR is simulated using the software. It has been found that the cell with SSRR and strip depicts negative permittivity and permeability. A metamaterial cell with only SSRR shows negative permeability to state it as a single or mu negative metamaterial cell. The initiator circular microstrip patch antenna (CMPA) structure with a radius equal to 6.48 mm has been designed to resonate at 5.8 GHz. These bands are useful for applications such as WiMAX, WLAN, and other wireless communication. Hence, the perturbation of the initiator (CMPA) is used to realize the bio-inspired microstrip patch antenna. Conventional and metamaterial loaded edge-fed Hibiscus leaf shape and Kaju leaf shape patch antennas has been designed. All the proposed antennas resonate at 5.8 GHz and also some other frequencies as presented in Table 8.9. Improvement in parameters of metamaterial loaded antenna has been observed. The comparison of the parameters of HLMPA, KLMPA,metamaterial loaded (HLMPA) and metamaterial loaded (KLMPA) has been listed in Table 8.9.

Chapter 9

Design simulation and fabrication of metamaterial based rectangular microstrip patch antenna

9.1 Introduction

The metamaterial cells show exceptionally great applications in the design of microstrip patch antennas by improving its characteristics such as bandwidth, return loss, and gain.The proposed double negative and mu negative metamaterial cells are designed and tested using MATLAB software.[96] [97] [98]. A conventional antenna and a proposed novel coaxial feed rectangular microstrip patch antenna (RMPA) with resonance frequency 3.5GHz and a ground plane of substrate is loaded with square split ring resonators is simulated using FEKO software, analysed and comparison of parameters such as bandwidth, return loss, gain and VSWR is presented. This patch antenna is designed on FR-4 substrate with permittivity value equal to 4.4 and thickness equal to 1.6 mm.FR-4 material is cheaper and easily available.This patch antenna with improved parameters can be used for WiMAX application. The Bandwidth required for band with centre frequency 3.5GHz is 200 MHz. And the bandwidth of proposed patch antenna is 274 GHz . The proposed antenna is fabricated to obtain experimental parameters. Conventional antenna and proposed patch antenna are simulated, fabricated

tested analysed and reported for performance comparison of its parameters[99] [100].

9.2 Lefthanded and Mu negative Metamaterial Design

9.2.1 Double Negative Metamaterials

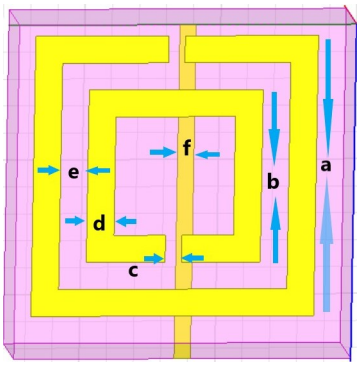


Figure 9.1: Square split ring resonators with strip (SSRR)

The SSRR Structure is designed using MATLAB code. In this way metal surface is obtained, as shown in (Fig.9.1) The SSRRs and conductor strip on ground plane create negative$\mu$and negative ϵ respectively near resonance frequency file.[40].

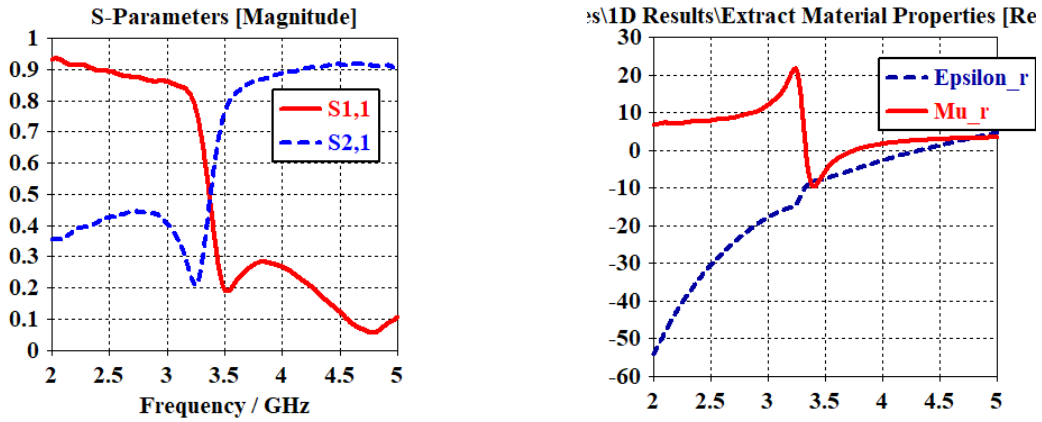
9.2.2 Design of SSRR Cell

The SSRR with strip are designed on FR-4 substrate with permittivity value equal to 4.4 and thickness equal to 1.6 mm The dimensions of 6.8 mm x 6.8 mm SSRR are, a= 5.8 mm, b=4 mm, c=0.34 mm, d=0.4 mm, and e=0.5 mm. Strip width f = 0.44 mm and strip length= 6.8 mm.

9.2.3 Parameters of SSRR Metamaterial Cell

S_{11} and S_{21} of SSRR cell depicted in (Fig.9.2a). The lowest magnitude of S_{11} indicates that the cell resonates at 3.5 GHz frequency. The Magnitude of S_{11} and S_{21} at 3.5 GHz frequency is 0.2 and 0.79 respectively. which shows that return loss is low at the resonance frequency. Both S parameters are important

to calculate epsilon and mu of the cell. Frequency v/s epsilon and mu is plotted using MATLAB software.



(a) S_{11} and S_{21} of SSRR cell (b) Permittivity and permeability of SSRR

Figure 9.2: Parameters of antenna

(Fig.9.2b)shows the real part of the epsilon and mu of SSRR, which are negative. The negative epsilon and mu appears in the frequencies between 3.3 GHz to 3.7 GHz. There for the antenna on metamaterial must be designed to operate within the range of frequencies. At 3.5 GHz permeability is -7.1, permittivity is -8.6. (Fig.9.3)shows the real and imaginary refractive index and impedance of SSRR. It is observed that real refractive index is negative near resonance frequency. Imaginary impedance equal to almost zero and real impedance equal to 50 ohms at the resonance frequency.

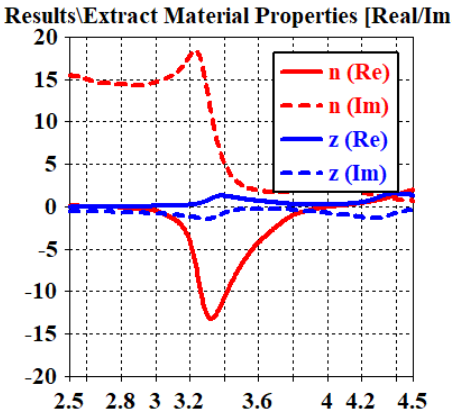


Figure 9.3: Refractive index and impedance of SSRR

Our proposed cell is 6.8 mm x 6.8 mm, If the cell is designed with smaller

dimensions then it will show the negative value of permittivity and permeability at a higher frequency.

9.2.4 Single Negative Metamaterial cell

Cells which shows negative permeability are called a mu negative metamaterial cell. The SSRR designed on FR-4 substrate with a permittivity value equal to 4.4 and thickness equal to 1.6 mm. The dimensions of 6.8 mm x 6.8 mm SSRR are, a =5.8 mm, b=4 mm, c=0.4 mm, d=0.4 mm, and e=0.5 mm. Real and imaginary values of Mu of SSRR are shown in (Fig.9.4). The negative mu appears in the frequencies between 3.35 GHz to 3.8 GHz. Therefor the antenna on metamaterial must be designed to operate within the range of frequencies. Hence, in this project we considered a resonance frequency of 3.5 GHz. which is one of the frequency band used for WiMAX applications in India.

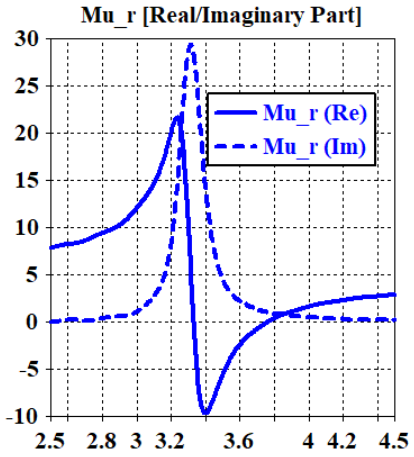


Figure 9.4: mu of SSRR at frequency 3.5 GHz

9.3 Metamaterial based Rectangular Microstrip Patch Antenna

Rectangular microstrip patch antenna is fabricated using SNG Metamaterial cells. Which are used to increase the performance of the system. This cells could substantially increase the gain and radiated power efficiency bandwidth of an antenna[101].

9.3.1 RMPA Design on Substrate without Metamaterial

RMPA has been designed at resonance frequency 3.5 GHz.For design equation refer section 6.1.5. The design of RMPA without metamaterial is depicted in(Fig.9.5).

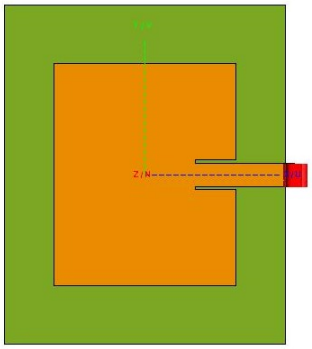


Figure 9.5: RMPA without metamaterial substrate

Table 9.1 presents dimensions of a RMPA without metamaterial cells. Resonance freq. 3.5 GHz.$Substrate : FR4$, $\epsilon_r = 4.4$, height of substrate(h) =1.6 mm Graph of reflection coefficient v/s frequency of RMPA is depicted in (Fig.9.6). It resonates at 3.5 GHz. The BW of RMPA is 123.6 MHz and Return loss = -39.6 dB.

Table 9.1: Design of RMPA

Patch dimensions	**Calculated dimensions of patch antenna (mm)**	**Optimized dimensions of Patch antenna without metamaterial(mm)**
Width of patch(W)	26.08	24
Length of patch (L)	19.98	18.8
Sub. width (Ws)	35.68	35
Sub. length (Ls)	29.66	29
Feed length		9.3

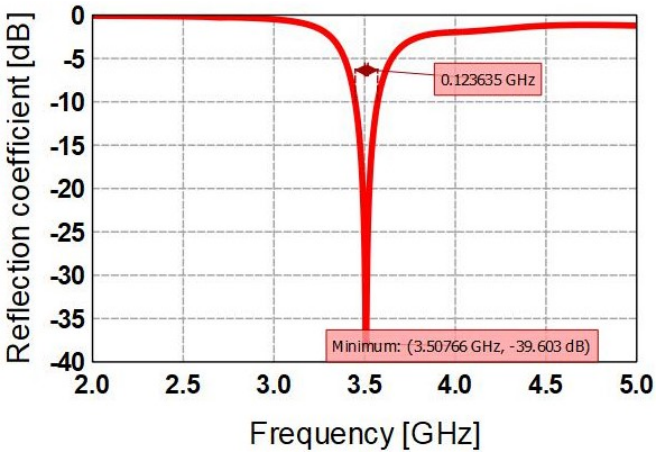


Figure 9.6: Reflection coefficient v/s frequency of RMPA without metamaterial

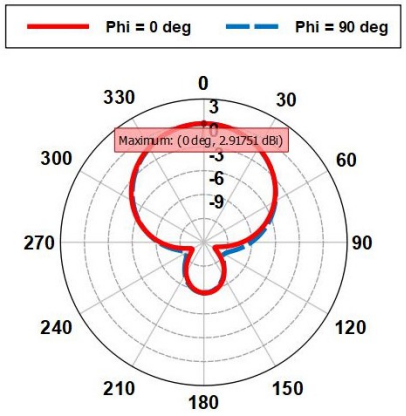


Figure 9.7: Gain of patch antenna without metamaterial

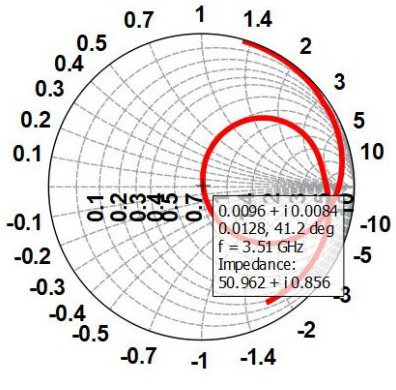


Figure 9.8: Smith chart showing impedance matching of RMPA at 3.5 GHz

The smith chart showing impedance matching at 3.5 GHz of RMPA without metamaterial is presented in(Fig.9.8). At 3.5 GHz the impedance is almost 50 ohms. without metamaterial.

9.3.2 Rectangular Microstrip Patch Antenna (RMPA) Design on Metamaterial Substrate

RMPA with metamaterial substrate has been designed at resonance frequency of 3.5 GHz .Used for WiMAX application.The dimensions of antenna are shown in Table 9.2. The FR-4 substrate with $\epsilon_r = 4.4$ and Loss tangent =0.01 is used for designing antenna . (Fig.9.9) Shows cells of SSRR on ground plane of RMPA.

Table 9.2: Design of RMPA with metamaterial

Patch dimensions	**Optimized dimensions of Patch antenna with metamaterial(mm)**
Width of patch(W)	23.5
Length of patch (L)	17.6
Sub. width (Ws)	35
Sub. length (Ls)	30
Feed length	10.4

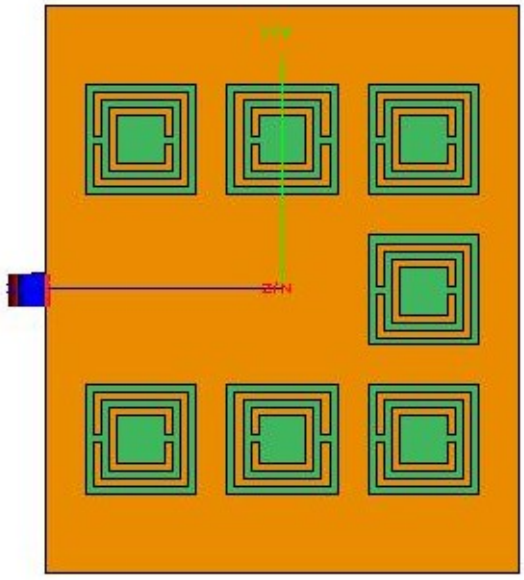


Figure 9.9: SSRR cells on ground plane of RMPA.

(Fig.9.10) presents graph of reflection coefficient v/s frequency of RMPA with a metamaterial. The RMPA resonates at 3.5 GHz . The BW of RMPA is 274 GHz. The reflection coefficient is -30 dB.

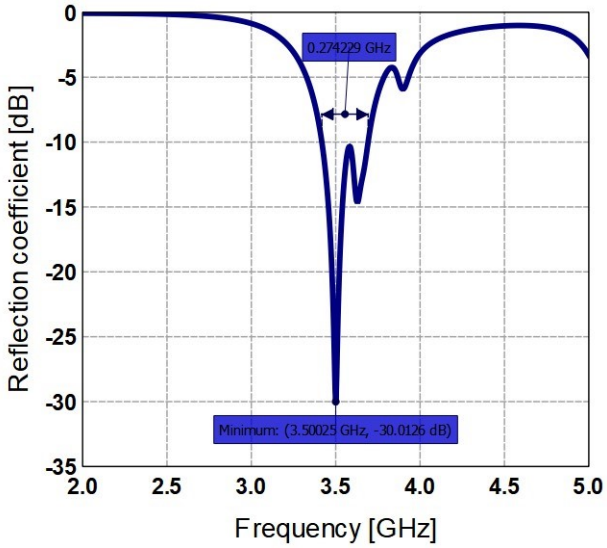


Figure 9.10: Reflection coefficient v/s frequency of RMPA with metamaterial

Impedance matching of RMPA with SSRR at 3.5 GHz is shown in smith chart(Fig.9.11) Impedance at 3.5GHz is 50 ohms.

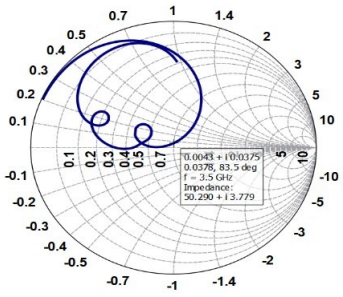
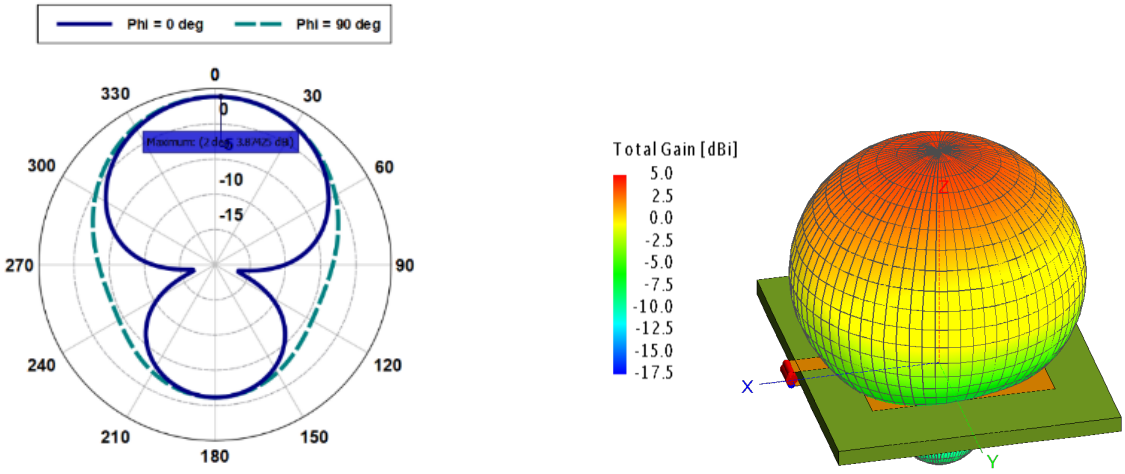
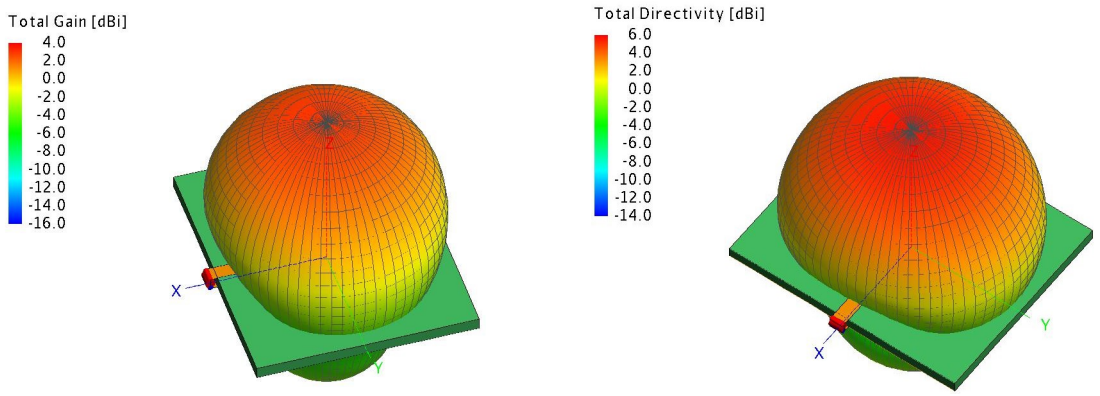


Figure 9.11: Smith chart showing impedance matching of RMPA with metamaterial at 3.5 GHz.



(a) 2D cut view of E-Field at phi=0 and phi=90 degrees (Dotted curve) (b) 3D far field total E-Field distribution at 3.5 GHz,

Figure 9.12: Parameters of antenna



(a) 3D view of far field at 3.9 GHz.

(b) Total Directivity at 3.5GHz.

Figure 9.13: Far field E-plane radiation patterns for a metamaterial loaded RMPA.

(Fig.9.12a) depicts 2D cut view of E-Field at $\phi = 0°$ and $\phi = 180°$ (Dotted curve), show a maximum antenna gain of 4 dBi with a main lobe in the direction of $\theta = 0°$ and$\phi = 0°$.(Fig.9.12b) shows 3D far field total E-Field distribution at 3.5 GHz. (Fig.9.13a) shows 3D view of far field at 3.9 GHz. Total Directivity at 3.5GHz is depicted in (Fig.9.13b) From this results we infer that a microstrip patch antenna mainly radiates in the vertical direction. This is in agreement with the theoretical radiation pattern for these structures. Gain remains almost constant over total bandwidth. The directivity of antenna is 6 dBi.

9.4 Fabrication and experimental parameters of metamaterial-based rectangular microstrip patch antenna

9.4.1 Experimental Parameters of Metamaterial loaded Rectangular Microstrip Patch Antenna.(RMPA) from Vector Network Analyser(VNA)

Practical graph of Reflection coefficient v/s frequency of RMPA with metamaterial obtained from VNA is depicted in(Fig.9.14) The fabricated antenna resonates at 3.5 GHz which is exactly same as simulated frequency. The bandwidth is 210 MHz and return loss is -40 dB.

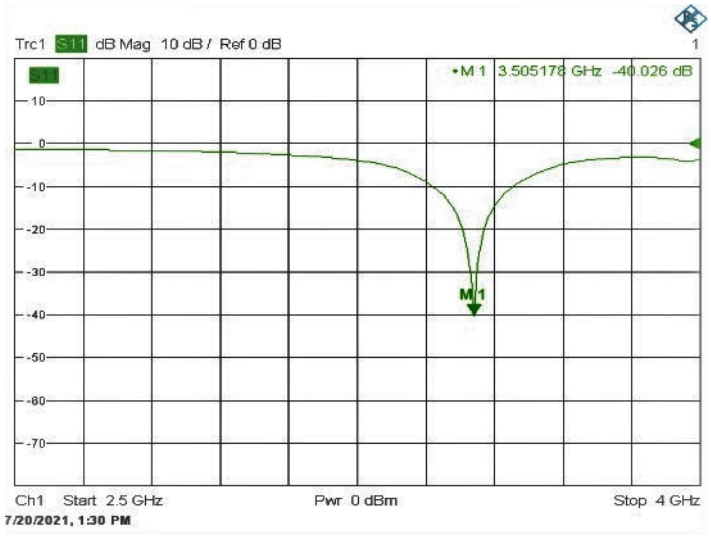


Figure 9.14: Reflection coefficient v/s frequency of RMPA with metamaterial obtained from VNA

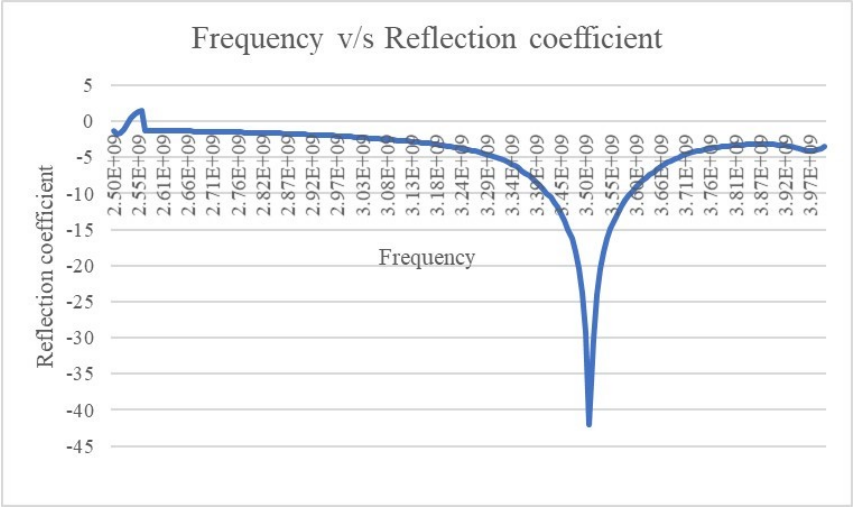


Figure 9.15: Reflection coefficient v/s frequency of metamaterial loaded RMPA generated using .csv file obtained from VNA

This graph presented in Fig.9.15 is plotted by converting real and imaginary values of S_{11} into magnitude in dB. The resonance frequency obtained using this procedure is 3.5 GHZ. Smith chart is shown in (Fig.9.16), The impedance at 3.5 GHz is 49.21 ohms. Which is almost equal to design impedance of 50 ohms.

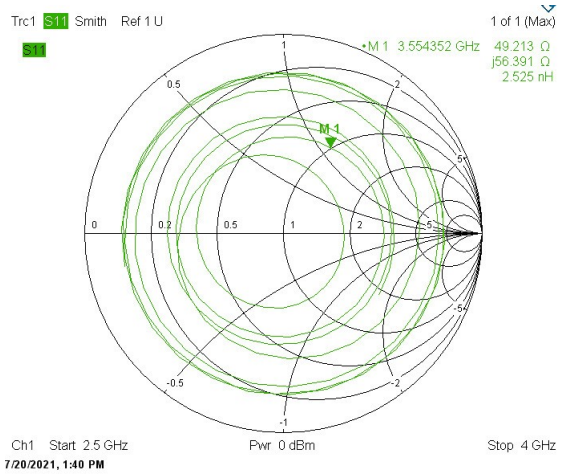
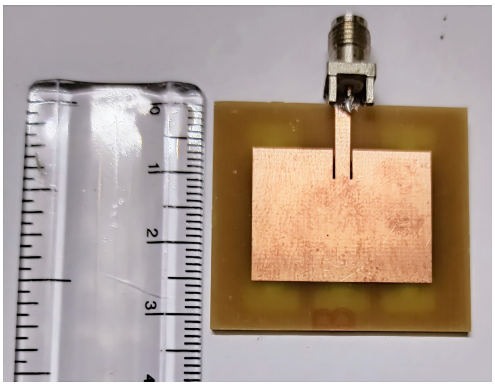


Figure 9.16: Smith chart showing impedance matching obtained from VNA



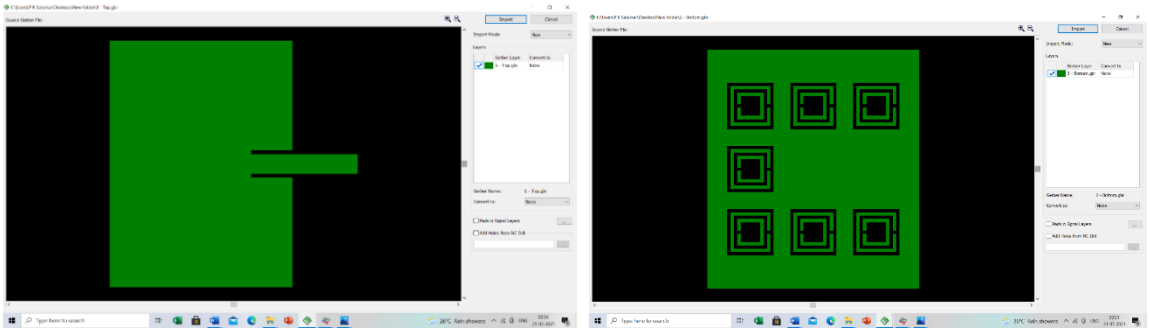
(a) Fabricated top view of RMPA.



(b) Fabricated bottom view of RMPA.

Figure 9.17: Fabricated top and bottom view of RMPA

Top view and bottom view (metamaterial loaded) of RMPA is presented in (Fig.9.17a) and (Fig.9.17b respectively. Double sided copper clad with 1.6 mm thick FR4 substrate is used for fabrication. Fabrication is done using .gbr file. Figures 9.18a and 9.18b are used for fabrication of microstrip patch antenna.



(a) Top view (b) Bottom view

Figure 9.18: Figures used for fabrication .gbr file

9.5 Results and Discussion

The metamaterial cell comprising of SSRR and copper strip on a ground plane of substrate. And metamaterial cell comprising of SSRR, are designed and simulated using MATLAB software, it has been found that the cell with combination of SSRR and copper strip on ground plane is double negative cell with negative permittivity, permeability and refractive index, while the other cell with only SSRR is a single or mu negative cell that shows negative permeability. The comparison of the parameters of RMPA with and without metamaterial is listed in Table 9.3. Metamaterial based RMPA is fabricated using double sided copper clad with 1.6 mm thick FR4 dielectric substrate. It is observed that practical value of resonance frequency is equal to design frequency.

RMPA loaded with metamaterial and without metamaterial are simulated , It has been found that the bandwidth of antenna loaded with metamaterial cells increases considerably in comparison to RMPA without cell. RMPA without cells return loss and bandwidth are –35.84 dB and 122.9 MHz respectively. Whereas RMPA with metamaterial the return loss and bandwidth are -30 dB and 274.2 MHz respectively. Gain of RMPA without cells is found to be equal to 2.74 dBi and with cells it is 5 dBi . So the bandwidth is increased by 151.3 MHz. And gain is increased by 2.23 dBi based on simulated results it has been found that the bandwidth and gain of RMPA has improved. VSWR of the conventional antenna

Table 9.3: Different parameters of RMPA.

Parameters	**RMPA without metamaterial**	**RMPA with metamaterial**	**Experimental parameters of RMPA**
Reflection coefficient	-35.84 dB	-30 dB	-40dB
Bandwidth (10dB)	122.9 MHz GHz	274.2 MHz	210.2 MHz
Gain	2.74 dBi	5 dBi	
VSWR	1.1	1.04	

is 1.1 and that of the antenna with metamaterial is 1.04.Smaller the value better is impedance matching.

Chapter 10

Conclusions And Future Scope

10.1 Conclusions

In this research work various metamaterial cells like square split ring resonator (SSRR) comprising SSRR and copper strip on a ground plane of the substrate. And metamaterial cell comprising of only SSRR, Circular split ring resonator and complementary circular split ring resonators are designed and simulated. Also various types of patch antennas like rectangular microstrip patch antenna, Circular patch antenna, covered various design concepts for unique bioinspired microstrip antennas in this thesis. The Hibiscus leaf-shaped and Kaju leaf-shaped bio-inspired conventional and metamaterial- based antennas are designed and simulated.The following are some of key observations and conclusion extracted from the simulation, testing and measurement of proposed metamaterial and patch antenna design.

• By observing simulated results, it has been found that the permeability, permittivity, and refractive index are negative in case of metamaterial cell with strip on ground plane and permeability is negative in the latter case that is only split ring resonator cell, which implies that the former one is a double negative cell and the latter one is mu negative cell or also called as single negative cell.

• From the simulated results of RMPA, it has been found that the RMPA resonates at 3.5 GHz and the parameters of antenna have improved considerably by

loading the proposed mu negative metamaterial structure at the ground plane of the antenna. That reduces surface wave propagation. The simulated results show a considerable increase in BW, low return loss, increase in gain, and decrease in VSWR. and the antenna has miniaturized in size compared to antenna without metamaterials.

• This proposed metamaterial based microstrip patch antenna designs are simulated fabricated and practically tested for validation of the design and proper functioning for WiMAX application. The fabricated antenna resonates at 3.5 GHz, which is the same as its design frequency. The center frequency of one of the WiMAX bands in India is 3.5 GHz and with improved antenna parameters, The proposed antenna can be used for WiMAX application

• We have covered various design concepts for unique bioinspired microstrip antennas in this chapter. The Hibiscus leaf-shaped and Kaju leaf-shaped bio-inspired conventional and metamaterial- based antennas are designed and simulated using FEKO software. Both antennas are multi-band. The HLMPA resonate at 5.8 GHz, 10 GHz,13.4 GHz, and Kaju leaf shape MPA resonates at 5.8 GHz and 9.67 GHz, both antennas have considerable bandwidth and gain so that can be used for WiMAX and other wireless applications. The Metamaterial-loaded antenna has shown considerable improvement in parameters. And also, it has shown a reduction in dimensions. Based on the output, it can be stated that the hibiscus leaf shape antenna has shown better performance than the Kaju leaf shape antenna. In comparison to other conventional designs, bio-inspired antennas depict a higher concentration of surface current in a smaller area.

• Along with the fundamental modeTM_{mn} of microstrip patch antenna, second order mode can be excited by loading either a slot or split ring resonator on the surface of patch antenna.

• This thesis presents an edge port fed rectangular microstrip patch antenna without and with metamaterial with resonating frequency 26GHz. Design and simulated results indicate that the RMPA gain and bandwidth have improved

considerably by loading metamaterial on it. Also, the dimensions of the patch antenna have been decreased.

• Also square split ring resonator has been mathematically modeled and simulated at 26 GHz resonance frequency . The calculated frequency was found to be almost equal to simulated frequency.

10.2 Future Scope

In this Thesis metamaterial-based patch antenna design for various frequencies have been presented. Metamaterial inspired structures like antenna designs are very interesting and useful on-going open research topics in the present scenario. Thus, the future research directions various planer antenna design based on different metamaterials structures are as follows.

• Design and develop novel metamaterial cell structure with negative epsilon and mu values and apply them to design higher frequency 5G antennas.

• Design phased array with metamaterial structure for electronically controlled beam steering function.

• Implementation of metamaterial inspired microstrip patch antenna or MIMO antenna on flexible substrate for specific applications like 5G communication.

References

[1] Yongmin Liu and Xiang Zhang. Metamaterials: a new frontier of science and technology. *Chemical Society Reviews*, 40(5):2494–2507, 2011.

[2] Marek S Wartak, Kosmas L Tsakmakidis, and Ortwin Hess. Introduction to metamaterials. *Physics in Canada*, 67(1):30–34, 2011.

[3] Ricardo Marqués, Francisco Mesa, Jesus Martel, and Francisco Medina. Comparative analysis of edge-and broadside-coupled split ring resonators for metamaterial design-theory and experiments. *IEEE Transactions on antennas and propagation*, 51(10):2572–2581, 2003.

[4] V. G. Veselago. The electrodynamics of substances with simultaneously negative values of mu,and epsilon. *Sov. Phys. Uspekhi*, 10(4), 1968.

[5] David R Smith, John B Pendry, and Mike CK Wiltshire. Metamaterials and negative refractive index. *Science*, 305(5685):788–792, 2004.

[6] Anisha Susan Thomas and AK Prakash. A survey on microstrip patch antenna using metamaterial. *International Journal of Advanced Research in Electrical, Electronics and Instrumentation Engineering*, 2:6289–6294, 2013.

[7] K Sumathi, Sunil Lavadiya, PengZhi Yin, Juveriya Parmar, and Shobhit K Patel. High gain multiband and frequency reconfigurable metamaterial superstrate microstrip patch antenna for c/x/ku-band wireless network applications. *Wireless Networks*, 27:2131–2146, 2021.

[8] Yahong Liu, Xiaojing Guo, Shuai Gu, and Xiaopeng Zhao. Zero index metamaterial for designing high-gain patch antenna. *International Journal of Antennas and Propagation*, 2013, 2013.

[9] Ari Sihvola. Metamaterials in electromagnetics. *Metamaterials*, 1(1):2–11, 2007.

[10] Wei E. I. Liu, Zhi Ning Chen, and Xianming Qing. Metamaterial-based low-profile broadband mushroom antenna. *IEEE Transactions on Antennas and Propagation*, 62:1165–1172, 2014.

[11] Chun Xu Bai, Yu Jian Cheng, Yan Ran Ding, and Jin Fan Zhang. A metamaterial-based s/x-band shared-aperture phased-array antenna with wide beam scanning coverage. *IEEE Transactions on Antennas and Propagation*, 68(6):4283–4292, 2020.

[12] Hugo F Pues and Antoine R Van De Capelle. An impedance-matching technique for increasing the bandwidth of microstrip antennas. *IEEE transactions on antennas and propagation*, 37(11):1345–1354, 1989.

[13] Juan Domingo Baena, Jordi Bonache, Ferran Martín, R Marqués Sillero, Francisco Falcone, Txema Lopetegi, Miguel AG Laso, Joan Garcia-Garcia, Ignacio Gil, M Flores Portillo, et al. Equivalent-circuit models for split-ring resonators and complementary split-ring resonators coupled to planar transmission lines. *IEEE transactions on microwave theory and techniques*, 53(4):1451–1461, 2005.

[14] Moataza A Hindy, Ragab M ElSagheer, and MS Yasseen. A circular split ringe resonator (csrr) left handed metamaterial (lhm) having simultaneous negative permeability and permittivity. *International Journal of Hybrid Information Technology*, 10(1):171–178, 2017.

[15] Nancy Gupta, Jyoti Saxena, Kamaljit Singh Bhatia, and Naveen Dadwal.

Design of metamaterial-loaded rectangular patch antenna for satellite communication applications. *Iranian Journal of Science and Technology, Transactions of Electrical Engineering*, 43:39–49, 2019.

[16] Shridhar E Mendhe and Yogeshwar Prasad Kosta. Metamaterial properties and applications. *International Journal of Information Technology and Knowledge Management*, 4(1):85–89, 2011.

[17] Eric Weisstein. Mathworld wolfram mathematical resources the complete elliptic integral of the first kind. *https://mathworld.wolfram.com/EllipticIntegraloftheFirstKind.html*, 2021.

[18] Pandharinath R Satarkar and Rajesh Basant Lohani. Characterization of metamaterial based patch antenna for worldwide interoperability for microwave access application. *Bulletin of Electrical Engineering and Informatics*, 11(5):2687–2695, 2022.

[19] Ahmad B Numan and Mohammad S Sharawi. Extraction of material parameters for metamaterials using a full-wave simulator [education column]. *IEEE antennas and propagation magazine*, 55(5):202–211, 2013.

[20] Kaushal Gangwar, RPS Gangwar, et al. Metamaterials: Characteristics, process and applications. *Advance in Electronic and Electric Engineering*, 4(1):97–106, 2014.

[21] Farhad Bin Ashraf, Touhidul Alam, Md Tarikul Islam, Mandeep Jit Singh, Norbahiah Binti Misran, and Mohammad Tariqul Islam. Inkjet printed metamaterial loaded antenna for wlan/wimax applications. *Comput. Mater. Contin*, 71:2271–2284, 2022.

[22] JG Joshi, Shyam S Pattnaik, and S Devi. Metamaterial embedded wearable rectangular microstrip patch antenna. *International Journal of Antennas and Propagation*, 2012, 2012.

[23] Marin Tadic, Matjaz Panjan, Biljana Vucetic Tadic, Jelena Lazovic, Vesna Damnjanovic, Martin Kopani, and Lazar Kopanja. Magnetic properties of hematite (- feo) nanoparticles synthesized by sol-gel synthesis method: The influence of particle size and particle size distribution. *Journal of Electrical Engineering*, 70(7):71–76, 2019.

[24] Suman Nelaturi and NVSN Sarma. Csrr based patch antenna for wi-fi and wimax applications. *Advanced Electromagnetics*, 7(3):40–45, 2018.

[25] Jeremiah O Abolade, Dominic BO Konditi, and Vasant M Dharmadhikary. Bio-inspired wideband antenna for wireless applications based on perturbation technique. *Heliyon*, 6(7):e04282, 2020.

[26] Alexandre Jean René Serres, Georgina Karla de Freitas Serres, Paulo Fernandes da Silva Júnior, Raimundo Carlos Silvério Freire, Josiel do Nascimento Cruz, Tulio Chaves de Albuquerque, Maciel Alves Oliveira, and Paulo Henrique da Fonseca Silva. Bio-inspired microstrip antenna. *Trends in Research on Microstrip Antennas*, 10.

[27] Kapil Jairath, Navdeep Singh, Mohammad Shabaz, Vishal Jagota, and Bhupesh Kumar Singh. Performance analysis of metamaterial-inspired structure loaded antennas for narrow range wireless communication. *scientific programming*, 2022, 2022.

[28] John Colaco and Rajesh Lohani. Multi-band microstrip square patch antenna design for iot based rfid technology and its various applications. In *2021 6th International Conference for Convergence in Technology (I2CT)*, pages 1–7. IEEE, 2021.

[29] Saimoom Ferdous, Ababil Hossain, Shah Mahmud Hasan Chowdhury, Mahdy Rahman Chowdhury Mahdy, and Matin Abdul. Reduced and conventional size multi-band circular patch antennas loaded with metamaterials. *IET Microwaves, Antennas & Propagation*, 7(9):768–776, 2013.

[30] David R Smith, Willie J Padilla, DC Vier, Syrus C Nemat-Nasser, and Seldon Schultz. Composite medium with simultaneously negative permeability and permittivity. *Physical review letters*, 84(18):4184, 2000.

[31] Moh. Danil HendryGamal DediIrawan Emansa Hasri Putra SaktiotoYan-Soerbakti, Romi FadliSyahputra. Improvement of low-profile microstrip antenna performance by hexagonal-shaped srr structure with dng metamaterial characteristic as uwb application. *Alexandria Engineering Journal*, 61:4241–4252, 2022.

[32] Tatjana Asenov, Nebojša Dončov, and Bratislav Milovanović. Application of metamaterials for the microwave antenna realizations. *Serbian Journal of Electrical Engineering*, 9(1):1–7, 2012.

[33] Prof. A K Prakash2 Anisha Susan Thomas1. A survey on microstrip patch antenna using metamaterial. *International Journal of Advanced Research in Electrical, Electronics and Instrumentation Engineering*, 2, 2007.

[34] Han Xiong, Jing-Song Hong, and Yue-Hong Peng. Impedance bandwidth and gain improvement for microstrip antenna using metamaterials. *Radioengineering*, 21(4):993–998, 2012.

[35] Yoonjae Lee and Yang Hao. Characterization of microstrip patch antennas on metamaterial substrates loaded with complementary split-ring resonators. *Microwave and Optical Technology Letters*, 50(8):2131–2135, 2008.

[36] R Stevenson, M Sazegar, A Bily, M Johnson, and N Kundtz. Metamaterial surface antenna technology: Commercialization through diffractive metamaterials and liquid crystal display manufacturing. In *2016 10th International Congress on Advanced Electromagnetic Materials in Microwaves and Optics (METAMATERIALS)*, pages 349–351. IEEE, 2016.

[37] Yuting Zhao, Kai Yu, and Yingsong Li. A high gain patch antenna using

negative permeability metamaterial structures. In *2017 Progress in Electromagnetics Research Symposium-Fall (PIERS-FALL)*, pages 119–123. IEEE, 2017.

[38] George V Eleftheriades and Nader Engheta. Metamaterials: Fundamentals and applications in the microwaveandopticalregimes. *Proceedings of the IEEE*, 99(10), 2011.

[39] Pushpendra Singh, Kanad Ray, and Sanyog Rawat. Nature inspired sunflower shaped microstrip antenna for wideband performance. *International Journal of Computer Information System and Industrial management Applications (IJCISM)*, 8:364–371, 2016.

[40] Hassan.B.Monk MD Nazmul. Matlab to cst interfacing method, 2000.

[41] John B Pendry, AJ Holden, DJ Robbins, and WJ Stewart. Low frequency plasmons in thin-wire structures. *Journal of Physics: Condensed Matter*, 10(22):4785, 1998.

[42] Christopher L Holloway, Edward F Kuester, James Baker-Jarvis, and Pavel Kabos. A double negative (dng) composite medium composed of magnetodielectric spherical particles embedded in a matrix. *IEEE Transactions on Antennas and Propagation*, 51(10):2596–2603, 2003.

[43] Yingsong Li and Wenhua Yu. A miniaturized triple band monopole antenna for wlan and wimax applications. *International Journal of Antennas and Propagation*, 2015, 2015.

[44] Nader Engheta and Richard W Ziolkowski. *Metamaterials: physics and engineering explorations*. 2006.

[45] Anne F D Bass. *Nanostructured metamaterial-Exchange between experts in electromagnetics and science*, volume 9.

[46] Francisco Falcone, Txema Lopetegi, MAG Laso, JD Baena, Jordi Bonache, Miguel Beruete, R Marqués, Ferran Martín, and M Sorolla. Babinet principle applied to the design of metasurfaces and metamaterials. *Physical review letters*, 93(19):197401, 2004.

[47] Tusharkumar Pravinchandra Dave and Jagdish M Rathod. Design and analysis of compact microstrip patch antenna for lte applications using metamaterials. pages 12–25.

[48] Shubham Singh and Jaswant Kumar. Design and analysis of compact microstrip patch antenna for lte applications using metamaterials with artificial intelligence in special use. Technical report, EasyChair, 2022.

[49] George V Eleftheriades and Keith G Balmain. *Negative-refraction metamaterials: fundamental principles and applications*. John Wiley & Sons, 2005.

[50] AK Iyer. Negative refractive index media using periodically lc loaded transmission lines. In *IEEE-MTT Int'l Symp. Digest, 2002*, pages 1067–1070, 2002.

[51] Christophe Caloz and Tatsuo Itoh. Transmission line approach of left-handed (lh) materials and microstrip implementation of an artificial lh transmission line. *IEEE Transactions on Antennas and propagation*, 52(5):1159–1166, 2004.

[52] Uğur Cem Hasar, Gül Buldu, Musa Bute, and A Muratoglu. Calibration-free extraction of constitutive parameters of magnetically coupled anisotropic metamaterials using waveguide measurements. *Review of Scientific Instruments*, 88(10):104702, 2017.

[53] DR Smith, DC Vier, Th Koschny, and CM Soukoulis. Electromagnetic parameter retrieval from inhomogeneous metamaterials. *Physical review E*, 71(3):036617, 2005.

[54] A Castanié, J-F Mercier, Simon Félix, and Agnes Maurel. Generalized method for retrieving effective parameters of anisotropic metamaterials. *Optics Express*, 22(24):29937–29953, 2014.

[55] Xudong Chen, Tomasz M Grzegorczyk, Bae-Ian Wu, Joe Pacheco Jr, and Jin Au Kong. Robust method to retrieve the constitutive effective parameters of metamaterials. *Physical review E*, 70(1):016608, 2004.

[56] Abdullah Alburaikan, Mohammed Aqeeli, Xianjun Huang, and Zhirun Hu. Low phase noise free-running oscillator based on high selectivity bandpass filter using composite right/left-handed transmission line. *IEEE Microwave and Wireless Components Letters*, 26(4):273–275, 2016.

[57] Filiberto Bilotti, Alessandro Toscano, and Lucio Vegni. Design of spiral and multiple split-ring resonators for the realization of miniaturized metamaterial samples. *IEEE transactions on antennas and propagation*, 55(8):2258–2267, 2007.

[58] Iryna A Buriak, VO Zhurba, GS Vorobjov, VR Kulizhko, OK Kononov, and Oleksandr Rybalko. Metamaterials: Theory, classification and application strategies. *Journal of Nano-and electronic Physics*, 8(4):4088–1, 2016.

[59] Ouail Ouchetto, Brahim Essakhi, Said Jai-Andaloussi, and Saad Zaamoun. Homogenization of bi-isotropic multilayered metamaterials. In *2017 IEEE MTT-S International Conference on Numerical Electromagnetic and Multiphysics Modeling and Optimization for RF, Microwave, and Terahertz Applications (NEMO)*, pages 91–93. IEEE, 2017.

[60] Davoud Zarifi, Mohammad Soleimani, and Ali Abdolali. Parameter retrieval of chiral metamaterials based on the state-space approach. *Physical Review E*, 88(2):023204, 2013.

[61] Cheng Xu, Zhihao Ren, Jingxuan Wei, and Chengkuo Lee. Reconfigurable

terahertz metamaterials: From fundamental principles to advanced 6g applications. *Iscience*, 2022.

[62] Masanobu Iwanaga. Photonic metamaterials: a new class of materials for manipulating light waves. *Science and Technology of Advanced Materials*, 2012.

[63] Jingping Zhong, Yongjun Huang, Guangjun Wen, Haibin Sun, and Weiren Zhu. The design and applications of tunable metamaterials. *Procedia Engineering*, 29:802–807, 2012.

[64] Rana Sadaf Anwar, Lingfeng Mao, and Huansheng Ning. Frequency selective surfaces: A review. *Applied Sciences*, 8(9):1689, 2018.

[65] CA Balanis. A.,"antenna theory analysis and design," 3rd ed., johnwiley& sons. *Inc., Publication*, pages 811–870.

[66] Ahmed Fatthi Alsager. Design and analysis of microstrip patch antenna arrays, 2011.

[67] I Bahl A Litpiboon R.Garg, P Bhartia. Introduction to microstrip patch antenna. 2000.

[68] Sunil Thakur. design and analysis of patch antenna using metamaterials. *Thesis*, 2017.

[69] SS Islam, MRI Faruque, MT Islam, and T Alam. A new mu-negative metamaterial. In *2015 2nd International Conference on Electrical Information and Communication Technologies (EICT)*, pages 269–272. IEEE, 2015.

[70] Pandharinath R Satarkar and Rajesh B Lohani. Edge port excited metamaterial based patch antennas for 5g application. *Communications and Network*, 13(3):111–129, 2021.

[71] PR Satarkar and RB Lohani. Design and characterization of coaxial feed circular patch antenna on a metamaterial substrate. In *2020 Fourth*

World Conference on Smart Trends in Systems, Security and Sustainability (WorldS4), pages 424–427. IEEE, 2020.

[72] David Ellstein, Bingnan Wang, and Koon Hoo Teo. Accurate models for spiral resonators. In *2012 9th European Radar Conference*. IEEE, 2012.

[73] K Mydhili, P Parvathi, and K Prasanthi. Design and simulation of edge fed microstrip patch antenna array. In *2018 2nd International Conference on I-SMAC (IoT in Social, Mobile, Analytics and Cloud)(I-SMAC) I-SMAC (IoT in Social, Mobile, Analytics and Cloud)(I-SMAC), 2018 2nd International Conference on*, pages 356–360. IEEE, 2018.

[74] Ahmed Boutejdar and Bishoy I Halim. Design of multiband microstrip antenna using two parasitic ring resonators for wlan/wimax and c/x/ku-band applications. In *2019 IEEE International Electromagnetics and Antenna Conference (IEMANTENNA)*, pages 046–050. IEEE, 2019.

[75] Kai Yu, Yingsong Li, and Yanyan Wang. Multi-band metamaterial-based microstrip antenna for wlan and wimax applications. In *2017 International Applied Computational Electromagnetics Society Symposium-Italy (ACES)*, pages 1–2. IEEE, 2017.

[76] Jin-Dong Zhang, Lei Zhu, Qiong-Sen Wu, Neng-Wu Liu, and Wen Wu. A compact microstrip-fed patch antenna with enhanced bandwidth and harmonic suppression. *IEEE Transactions on Antennas and Propagation*, 64(12):5030–5037, 2016.

[77] Ming-Hsuan Chang, Bo-Yu Chen, et al. Microstrip-fed ring slot antenna design with wideband harmonic suppression. *IEEE Transactions on Antennas and Propagation*, 62(9):4828–4832, 2014.

[78] Udayabhaskar Pattapu, Sonika Priyadarsini Biswal, and Sushrut Das. A 2.45 ghz dgs based harmonic rejection antenna for rectenna application. In

2017 USNC-URSI Radio Science Meeting (Joint with AP-S Symposium), pages 123–124. IEEE, 2017.

[79] Udayabhaskar Pattapu and Sushrut Das. A spurious-free 5.8 ghz circular patch antenna for rectenna applications. *IETE Technical review*, 36(5):510–516, 2019.

[80] Haiwen Liu, Zhengfan Li, Xiaowei Sun, and Junfa Mao. Harmonic suppression with photonic bandgap and defected ground structure for a microstrip patch antenna. *IEEE microwave and wireless components letters*, 15(2):55–56, 2005.

[81] Ramesh Garg and VS Reddy. Edge feeding of microstrip ring antennas. *IEEE Transactions on Antennas and Propagation*, 51(8):1941–1946, 2003.

[82] Atinder Pal Singh, Ravinder Kumar, and Hartej Singh Dadhwal. Design of edge fed rectangular microstrip patch antenna for wlan applications using ansoft-hfss. *VSRD-IJEECE*, 2(4):160–167, 2012.

[83] Md Maruf Ahamed, Kishore Bhowmik, and Abdulla Al Suman. Analysis and design of rectangular microstrip patch antenna on different resonant frequencies for pervasive wireless communication. *International journal of scientific & technology research*, 1(5):2010–2013, 2012.

[84] Nazish Irfan, Mustapha CE Yagoub, and Khelifa Hettak. Design of a microstrip-line-fed inset patch antenna for rfid applications. *International Journal of Engineering and Technology*, 4(5):558, 2012.

[85] Yuehe Ge, Karu P Esselle, and Trevor S Bird. E-shaped patch antennas for high-speed wireless networks. *IEEE Transactions on Antennas and Propagation*, 52(12):3213–3219, 2004.

[86] Valjean Elizabeth Elander. Mathematical modeling of metamaterials. *UNLV Theses, Dissertations, Professional Papers, and Capstones.*

[87] Anupma Marwaha et al. An accurate approach of mathematical modeling of srr and sr for metamaterials. *Journal of Engineering Science & Technology Review*, 9(6), 2016.

[88] Gurwinder Singh et al. A review of metamaterials and its applications. *International Journal of Engineering Trends and Technology*, 19(6):305–310, 2015.

[89] R.B.Lohani P.R.Satarkar. Mathematical modelling of metamaterial cell and its application in design of microstrip patch antenna.

[90] Prasan Kumar Mishra, Tapan Kumar Patnaik, Bhavani Prasad Panda, Rabindra Kumar Mishra, and Kailash Chandra Rout. Design and simulating of a compact antenna for wimax and lte application. In *2020 International Conference on Computer Science, Engineering and Applications (ICCSEA)*, pages 1–4. IEEE, 2020.

[91] Amit A Deshmukh and KP Ray. Compact broadband slotted rectangular microstrip antenna. *IEEE antennas and wireless propagation letters*, 8:1410–1413, 2009.

[92] Sachin Agrawal, Manoj Singh Parihar, and Pravin N Kondekar. Exact performance evaluation of rf energy harvesting with different circuit's elements. *IETE Technical review*, 35(5):514–522, 2018.

[93] R. Kiruthika L. Reshma V. Latha, Divya Rajagopal. Bioinspired red bay leaf shaped antenna for narrowband application. *International Journal of Applied Engineering Research ISSN 0973-4562*, 2019.

[94] Sujoy Biswas, Debatosh Guha, and Chandrakanta Kumar. Control of higher harmonics and their radiations in microstrip antennas using compact defected ground structures. *IEEE transactions on antennas and propagation*, 61(6):3349–3353, 2013.

[95] PR Satarkar and Rajesh B Lohani. Effects of metamaterial on bioinspired microstrip patch antenna. In *Printed Antennas*, pages 167–185. CRC Press, 2022.

[96] Rakhi Rani, Preet Kaur, and Neha Verma. Metamaterials and their applications in patch antenna: A. *International Journal of Hybrid Information Technology*, 8(11):199–212, 2015.

[97] Dhawan Singh, Aditi Thakur, and Viranjay M Srivastava. Miniaturization and gain enhancement of microstrip patch antenna using defected ground with ebg. *J. Commun.*, 13(12):730–736, 2018.

[98] M Saravanan, SM Umarani, et al. Gain enhancement of patch antenna integrated with metamaterial inspired superstrate. *Journal of Electrical Systems and Information Technology*, 5(3):263–270, 2018.

[99] Zhi Ning Chen, Xianming Qing, Jin Shi, Wei Liu, et al. Metamaterial-based antennas: Engineering designs. In *2015 Asia-Pacific Microwave Conference (APMC)*, volume 1, pages 1–3. IEEE, 2015.

[100] Wojciech Jan Krzysztofik and Thanh Nghia Cao. Metamaterials in application to improve antenna parameters. *Metamaterials and Metasurfaces*, 12(2):63–85, 2018.

[101] Rasha Mahdi Salih and Ali Khalid Jassim. Microstrip patch antenna with metamaterial using superstrate technique for wireless communication. *Bulletin of Electrical Engineering and Informatics*, 10(4):2055–2061, 2021.

Publications (Journals)

[1] Pandharinath R. Satarkar, Rajesh B. Lohani," Characterization of metamaterial-based patch antenna for worldwide interoperability for microwave access application",Bulletin of Electrical Engineering and Informatics,Vol. 11, No. 5, October2022, pp. 2687-2695ISSN: 2302-9285, DOI: 10.11591/eei.v11i5.4149.

[2] P.R.Satarkar, R.B. Lohani, " Microstrip patch antenna design using mathematically modeled metamaterial cell",IOP Conference Series: Materials Science and Engineering.

[3] P.R.Satarkar, R.B. Lohani, "Metamaterial : Fundamental and engineering exploration." Kala Sarovar , UGC care Group 1 Journal, Vol 23 ,No 02 (V), pp 381-384, July Sept. 2020.ISSN : 0975-4520.

[4] Pandharinath R. Satarkar, Rajesh B. Lohani," Edge Port Excited Metamaterial based Patch Antenna for 5G Application", Communications and Network, Vol 13,pp 111-129, 2021.DOI 10.4236/cn.2021.133009.

Publications (Conferences)

[1] P..R.Satarkar, R.B. Lohani, " Design and Characterization of Coaxial Feed Circular Patch Antenna on a Metamaterial Substrate"',2020 Fourth World Conference on Smart Trends in Systems, Security and Sustainability (WorldS4) London,UK, IEEE Xplore:pp-424-428,October 2020,Publisher: IEEE, DOI: 10.1109/WorldS450073.2020.9210420.

[2] P.R.Satarkar, R.B. Lohani, " Design and extraction of parameters of metamaterial cell and its application to enhance the performance of patch antenna",International Science Exhibition Congress Symposium (SECS-2020) organized by IETE and ISVE at Advanced Regional Telecom Training Centre, BSNL, Hazaribag Road, Ranchi-835217, Jharkhand, India ,Sept. 12 -13th , 2020.

[3] P.R.Satarkar, R.B. Lohani, " Design of capacitive coupled circular patch antenna for band suppression and gain improvement by loading circular slot on coupling", International Web Conference on "Innovative Engineering Technologies - 2020 (IWC-IET 2020.Organised by Sri Ramakrishna institute of technology(An Autonomous Institution) (Accredited by NACC with 'A' Grade, Approved by AICTE, Anna University, Chennai)

[4] P.R.Satarkar, R.B. Lohani, " Edge port excited patch antenna with rectangular slot for 5G application", AICTE sponsored international conference on

Antenna Innovation, 5G communication and Network Technology (ICA5NT 2020). Organized by Department of Electronics and Communication Engineering Velammal Institute of Technology, India.

[5] P.R.Satarkar, R.B. Lohani, " Mathematical Modelling of Metamaterial Cell and its Application in Design of Microstrip Patch Antenna", Presented and published in IC-CCDS 2022 conference, MULTICON-W 2022.Thakur college of Engineering and Technology.

Publications (Book Chapters)

[1] P.R.Satarkar, R.B. Lohani, " Effects of metamaterial on bio inspired microstrip patch antenna", (Book Chapter) Taylor and Francis Group, CRC press, London. Printed Antennas Design and challenges, DOI :10.1201/9781003347057-12.